THREE-DIMENSIONAL LINEAR ELASTIC FRACTURE MECHANICS ANALYSIS BY A DISPLACEMENT HYBRID FINITE ELEMENT MODEL

A THESIS

Presented to

The Faculty of the Division of Graduate Studies

By

K. Kathiresan

In Partial Fulfillment

of the Requirements for Degree of

Doctor of Philosophy in the School

of Engineering Science and Mechanics

Georgia Institute of Technology

September 1976

THREE-DIMENSIONAL LINEAR ELASTIC FRACTURE

MECHANICS ANALYSIS BY A DISPLACEMENT HYBRID

FINITE ELEMENT MODEL

Approved:

S. Atluri, Chairman

M. P. Stallybrass

G. J. Simitses

J. M. Anderson

C. V. Smith

Date approved by Chairman 11/19/76

This Dissertation

is dedicated to my mother

K. Dhanalakshmi

ACKNOWLEDGMENTS

The author wishes to express his sincere gratitude and appreciation to Dr. S. N. Atluri for his suggestion of the problem and knowledgeable guidance throughout this work. The author's appreciation is also extended to Dr. C. V. Smith and Dr. M. Stallybrass, members of the reading committee, for their valuable suggestions. The author's thanks go also to Dr. J. M. Anderson and Dr. G. J. Simitses for their interest in the research. The author is very thankful to Dr. M. E. Raville, Director of School of Engineering Science and Mechanics, for his encouragement and financial support during the course of study. The author also appreciates Dr. M. Nakagaki for valuable discussions and suggestions at various stages of the research. The author's thanks also go to Mrs. Jackie Van Hook for typing the final manuscript.

The author's deep appreciation goes to his mother, Mrs. K. Dhanalakshmi, for her utmost sacrifice and ordeals in bringing the author to his present attainment. The author also would like to commend his wife, Bagyalakshmi, for her patience during the author's absence.

TABLE OF CONTENTS

Page

LIST OF ILLUSTRATIONS

Figure Page

SUMMARY

During the past decade fracture mechanics has been successfully used to analyze failure of structural components and to certify a structure for its intended use. In applying fracture mechanics to problems, the analyst must know the stress-intensity factors of the flaw as well as material characteristics like fracture toughness in order to assess the situation. Unfortunately, only limited solutions of stress-intensity factors are available for idealized flaws of simple geometries and loading conditions and thus considerable engineering judgement is required before they can be used to estimate stress-intensity factors of complex flaws which exist in actual problems.

This dissertation deals with a finite-element procedure for the calculation of Modes I, II and III stress-intensity factors which vary along an arbitrarily curved three-dimensional crack front in a structural component. The finite-element model is based on a modified variational principle of potential energy with relaxed continuity requirements for displacements at the inter-element boundary. The variational principle is a three field principle, with arbitrary interior displacements for the element, inter-element boundary displacements, and element boundary tractions as variables. The unknowns in the final algebraic system of equations, in the present displacement-hybrid finite element model, are the nodal displacements and the three elastic stress-intensity factors along the crack front. Special elements, which contain proper square root and inverse square root

crack front variations in displacements and stresses, respectively, are used in a fixed region near the crack front. Inter-element displacement compatibility is satisfied by assuming an independent inter-element boundary displacement field, and using a Lagrange Multiplier technique to enforce such interelement compatibility. These Lagrangean Multipliers, which are physically the boundary tractions, are assumed from an equilibrated stress field derived from three-dimensional Maxwell stress functions. The geometry of the "basic element" used presently is a 20 node isoparametric brick element, with 60 degrees of freedom per element.

The utility of the formulation is demonstrated through numerical solutions of several crack problems. Most of these problems have either been hitherto unsolved, or for which widely varying estimated solutions exist in the literature. The problems solved by this procedure can be enumerated as: through-the-thickness edge and central cracks in finite sized specimens; buried, surface and corner elliptical cracks in finite specimens; outer and inner (pressurized and unpressurized) semi-elliptical surface flaws in internally pressurized thick-walled cylinders; central crack specimens subjected to mixed mode (I, II and III) loading; quarter-elliptical corner cracks near fastener holes in a finite specimen subjected to tension; and plates with semi-elliptical surface flaws subjected to bending and tension.

LIST OF SYMBOLS*

a,b,c	- Dimensions of the Crack
E	- Young's Modulus
[E],Eijkl	- Elastic Constant Matrix
J	- Rice's Path Independent J-integral
$\mathcal{G}$	- Strain Energy Release Rate
k_1,k_2,k_3	- Elastic Stress Intensity Factors for Modes I, II, and III respectively
ν	- Poisson's Ratio
r	- Radial distance from the Crack Tip (Figure 2)
ξ,η,ζ	- Isoparametric co-ordinates
μ	- Shear Modulus
ϵ_{ij}	- Strain Tensor
σ_{ij}	- Stress Tensor
n,t,z	- Orthogonal Co-ordinate System (Figure 2)
γ	- Surface Energy per unit area
N	- Total Number of Elements in Finite Element Breakdown
p	- Total Number of Singular Elements in Finite Element Breakdown
π_{HD}	- Total Potential Energy of the Hybrid Displacement Model
$\sum$	- Summation over the Total Number of Elements
dV	- Elemental Volume
dS	- Elemental Surface Area

*The symbols which are not found here are explained wherever they first appear.

$\vec{n}$, n_j - Outward Normal Vector at the Boundary and its components

$[\ _s]$,$[\ ]_s$ - (subscript s) Refers to Singular Fields (from Asymptotic Solution)

$[\ _R]$,$[\ ]_R$ - (subscript R) Refers to Regular Fields (Polynomial Assumption)

$\{\alpha\}$,$\{\beta\}$ - Unknown Independent Parameters

$\{q\}$ - Nodal Displacements of an Element

$\{q^*\}$ - Generalized Global Displacements

$\{k_s\}$ - Stress Intensity Factors of a Segment

$\{k_s^*\}$ - Stress Intensity Factors of all the Segments Along the Crack Front

x,y,z - Cartesian Coordinates

[J] - Jacobian Matrix

χ_1, χ_2, χ_3 - Maxwell's Stress Functions

θ - Angle as defined in Figure 2 (also Elliptical Angle in Figures 34 thru 44)

Φ - Elliptical Angle (defined in Figure 22)

GLOSSARY OF ABBREVIATIONS

COD - Crack Opening Displacement

SIF - Stress-Intensity Factor(s)

BIE - Boundary Integral Equation

ELL - Ellipse

CIR - Circle

COR - Corner

SUR - Surface

BUR - Buried

FEM - Finite Element Method

CHAPTER I

INTRODUCTION AND SOME COMMENTS ON LINEAR ELASTIC FRACTURE MECHANICS

Introduction

Structural components are often found to fail under stresses well below the ultimate or even the yield stresses. The reason for failure of such components can be attributed to the presence of some flaw or imperfections such as micro and macro cracks. Such an imperfection behaves like a notch and causes elevated stresses at that region. Such serious and detrimental fracture problems in structures, which cause damage to the structure, human life and financial loss, are encountered in the fields of aerospace, ships, pressure vessels, storage tanks, pipelines, large rotors, etc. A conventional strength analysis alone would not suffice to predict the strength and operating conditions of structural components with flaws or imperfections. So, in the last decade, many structural engineers and scientists have focused their attention to fracture problems so that the structural components can be analysed and designed for their intended purpose without catastrophic failure due to the presence of flaws or imperfections.

The study of crack extension behavior in a structural component as a function of applied loads is called "fracture mechanics". If the region very close to the crack tip or boundary does not experience large plastic yielding, then such a study is called linear fracture mechanics. The main objective of the mathematical theory of fracture mechanics is

the assessment of the theoretical strength of a cracked structural component. The theory of linear elastic fracture mechanics is based on the idea of Griffith's [1,2]* energy criterion which states that the increase in potential energy due to the surface tension of the crack must be balanced by a decrease in the strain energy and the potential of the applied forces. This energy balance concept is utilized to determine whether the crack will grow or not for a particular geometry of the structure, loading condition and material properties. It was shown by Irwin [3] that Griffith's energy criterion of the cracked structure can be characterized by the singular stress distribution around the crack tip. In other words, the presence of a crack in a structure is essentially a problem of mathematical singularity of stresses at the crack tip. Irwin also showed that the stress distribution in the neighborhood of the crack tip is proportional to the inverse square root of the distance from the crack tip and is also characterized by a set of parameters called stress intensity factors, which represent the strength of the singularity. These parameters are found to be functions of the geometry of the crack and of the structure, and the boundary conditions. But for a real material the stresses are bounded by the plastic yielding in the elevated stress region and the plastic yielding redistributes the high stresses in the vicinity of the crack tip. Because of this the validity of application of linear elastic fracture mechanics is in question. Even though the stresses near the crack tip are high, they decrease very rapidly away from the crack tip.

*Numbers indicated in parenthesis refer to references at the end of this dissertation.

Thus the plastic zone is generally very small and the contribution of the strain energy of this zone is relatively small when compared with the total strain energy of the structure. Irwin [3] concluded that as long as this plastic zone is small compared with crack length, linear elastic fracture mechanics can be used with sufficient accuracy.

Unfortunately, the application of continuum mechanics theory to seek the exact solution for the stress intensity factors for fracture problems is extremely cumbersome and difficult for real crack problems which are encountered in practice; there are, though, limited solutions available for idealized cracks with simple geometries and loading conditions. The problem becomes manifold in the case of three-dimensional continuum problems with cracks. But, because of the tremendous progress in computer technology and various numerical techniques, methods are now being developed which can solve crack problems with complicated geometries and loading conditions. Several approximate methods have been formulated and developed to solve accurately two-dimensional problems in recent years as summarized by Rice [4]. Even though a considerable amount of research has been done on two-dimensional problems, the work on three-dimensional fracture problems is very limited. This necessitates a considerable amount of engineering judgement on the part of the designer to estimate the stress intensity factors for practical crack problems in three-dimensions.

Among all the approximate methods, the finite element method offers the advantage of being able to solve continuum problems with complex geometries, non-homogeneous material properties, combined mechanical and thermal loading, etc. It is the main objective and purpose of

the present investigation to develop a finite element method using the hybrid-displacement model for the analysis and solution of three-dimensional fracture mechanics problems with arbitrarily curved crack fronts. The present study is limited to linearly elastic problems. The development of efficient "singular elements" for the treatment of crack problems requiring large scale three-dimensional finite element computation is presented. Using the special singular elements, solutions of stress intensity factors for several three-dimensional problems are presented. Comparison of the present results by the hybrid displacement finite element model with other numerical results proves the efficiency and effectiveness of the present model. Several of the solutions presented in this thesis are for problems that have hitherto been unsolved.

The rest of this chapter is devoted to some of the basic concepts of linear elastic fracture mechanics. Chapter II deals with a detailed survey of different numerical techniques that have been already developed to determine the stress intensity factors for two and three-dimensional problems.

In Chapter III a brief description of the method of approach and the formulation of the finite element model are presented. Complete mathematical details of field functions and other numerical details are presented in Chapter IV. The results and discussions of the problems solved by the above hybrid displacement finite element model are given in Chapter V. Conclusions and recommendations for future work are presented in Chapter VI.

Basic Modes of Crack Extension

The presence of cracks in structural components are considered as discontinuities of displacement field $\underset{\sim}{u}$ in the continuum mechanics theory. Due to the presence of the cracks all the spatial displacements u_x, u_y and u_z may suffer discontinuities across the crack. It was first recognized by Irwin [3] that there are three independent kinds of kinematic movements of crack surfaces, upper and lower, with respect to each other. These are called the basic types or more commonly referred to as modes of deformation of crack extension. Figure 1 illustrates the three modes of deformations namely opening, sliding and tearing modes and also shows the displacements of an element containing the crack front. Irwin also observed that these three basic modes of deformations are necessary and sufficient to describe the general state of elastic stresses and deformations of a continuum containing cracks by proper superposition. The three modes of deformation can be described as follows [9]:

Opening Mode

The opening mode, Figure 1a, is characterized by the motions of the crack surfaces that tend to separate symmetrically with respect to the plane occupied by the crack prior to deformation.

Sliding Mode

The sliding mode, Figure 1b, concerns local deformation in which the crack surfaces glide over one another in opposite directions but in the same plane.

Tearing Mode

The movement of the crack surfaces, associated with the tearing

mode of fracture, Figure 1c, can be related to the warping action of noncircular cylinders under torsion in which the material points, initially in the same plane, occupy different planes after deformation.

Asymptotic Solution and Stress Intensity Factors

It was observed by Irwin that each of the three crack movements mentioned above is connected with a set of stress and displacement fields in the immediate neighborhood of the crack tip. Sneddon [5,6] found the solution for displacements and stresses around a penny shaped crack by using Hankel transforms. The solutions for displacements and stresses around the crack tip were derived by Irwin [3] by using the method of Williams [7]. The solutions obtained by him for an isotropic material are given below and the nomenclature near the crack front is given in Figure 2.

Mode I. Symmetric Case

$$\sigma_n = \frac{k_1}{(2r)^{1/2}} \cos\frac{\theta}{2}\left\{1 - \sin\frac{\theta}{2}\cdot\sin\frac{3\theta}{2}\right\} + \cdots$$

$$\sigma_z = \frac{k_1}{(2r)^{1/2}} \cos\frac{\theta}{2}\left\{1 + \sin\frac{\theta}{2}\cdot\sin\frac{3\theta}{2}\right\} + \cdots$$

$$\sigma_{nz} = \frac{k_1}{(2r)^{1/2}} \cos\frac{\theta}{2}\cdot\sin\frac{\theta}{2}\cdot\cos\frac{3\theta}{2} + \cdots \qquad (1.1)$$

and

$$u_n = \frac{k_1(2r)^{1/2}}{8\mu}\left\{(2K - 1)\cos\frac{\theta}{2} - \cos\frac{3\theta}{2}\right\} + \cdots$$

$$u_z = \frac{k_1 (2r)^{1/2}}{8\mu} \left\{ (2K + 1) \sin \frac{\theta}{2} - \sin \frac{3\theta}{2} \right\} + \cdots \qquad (1.2)$$

Mode II. Skew-Symmetric Case

$$\sigma_n = - \frac{k_2}{(2r)^{1/2}} \sin \frac{\theta}{2} \left\{ 2 + \cos \frac{\theta}{2} \cdot \cos \frac{3\theta}{2} \right\} + \cdots$$

$$\sigma_z = \frac{k_2}{(2r)^{1/2}} \sin \frac{\theta}{2} \cdot \cos \frac{\theta}{2} \cdot \cos \frac{3\theta}{2} + \cdots$$

$$\sigma_{nz} = \frac{k_2}{(2r)^{1/2}} \cos \frac{\theta}{2} \left\{ 1 - \sin \frac{\theta}{2} \cdot \sin \frac{3\theta}{2} \right\} + \cdots \qquad (1.3)$$

and

$$u_n = \frac{k_2 (2r)^{1/2}}{8\mu} \left\{ (2K + 3) \sin \frac{\theta}{2} + \sin \frac{3\theta}{2} \right\} + \cdots$$

$$u_z = - \frac{k_2 (2r)^{1/2}}{8\mu} \left\{ (2K - 3) \cos \frac{\theta}{2} + \cos \frac{3\theta}{2} \right\} + \cdots \qquad (1.4)$$

where

$K = 3 - 4\nu$ for plane strain

$= (3 - 4\nu)/(1 + \nu)$ for plane stress

It should also be noted that for plane strain conditions

$$\sigma_t = \nu(\sigma_n + \sigma_z)$$

$$= \frac{k_1}{(2r)^{1/2}} 2\nu \cos \frac{\theta}{2} - \frac{k_2}{(2r)^{1/2}} \sin \frac{\theta}{2} + \cdots \qquad (1.5)$$

Mode III. Antiplane Case

$$\sigma_{nt} = -\frac{k_3}{(2r)^{1/2}} \sin\frac{\theta}{2} + \cdots$$

$$\sigma_{zt} = \frac{k_3}{(2r)^{1/2}} \cos\frac{\theta}{2} + \cdots \tag{1.6}$$

and

$$u_t = \frac{k_3(2r)^{1/2}}{\mu} \sin\frac{\theta}{2} + \cdots \tag{1.7}$$

Higher order terms like $O(r^{n/2}, n \geq 0)$ in stresses and $O(r^{n/2}, n \geq 2)$ in displacements are neglected.

For a general three-dimensional crack bounded by a smooth curve, with a continuous tangent, in an isotropic material the solution for displacements and stresses near the crack front was obtained by Kassir and Sih [8,9] and is given below.

$$\sigma_n = \frac{k_1}{4(2r)^{1/2}} \left\{3\cos\frac{\theta}{2} + \cos\frac{5\theta}{2}\right\} - \frac{k_2}{4(2r)^{1/2}} \left\{7\sin\frac{\theta}{2} + \sin\frac{5\theta}{2}\right\} + \cdots$$

$$\sigma_t = \frac{k_1}{(2r)^{1/2}} 2\nu\cos\frac{\theta}{2} - \frac{k_2}{(2r)^{1/2}} 2\nu\sin\frac{\theta}{2} + \cdots$$

$$\sigma_z = \frac{k_1}{4(2r)^{1/2}} \left\{5\cos\frac{\theta}{2} - \cos\frac{5\theta}{2}\right\}$$

$$- \frac{k_2}{4(2r)^{1/2}} \left\{ \sin \frac{\theta}{2} - \sin \frac{5\theta}{2} \right\} + \cdots$$

$$\sigma_{tz} = \frac{k_3}{(2r)^{1/2}} \cos \frac{\theta}{2} + \cdots$$

$$\sigma_{zn} = - \frac{k_1}{4(2r)^{1/2}} \left\{ \sin \frac{\theta}{2} - \sin \frac{5\theta}{2} \right\}$$

$$+ \frac{k_2}{4(2r)^{1/2}} \left\{ 3 \cos \frac{\theta}{2} + \cos \frac{5\theta}{2} \right\} + \cdots$$

$$\sigma_{nt} = - \frac{k_3}{(2r)^{1/2}} \sin \frac{\theta}{2} + \cdots \qquad (1.8)$$

and

$$u_n = \frac{k_1 (2r)^{1/2}}{2\mu} \cos \frac{\theta}{2} \left\{ 1 - 2\nu + \sin^2 \frac{\theta}{2} \right\}$$

$$+ \frac{k_2 (2r)^{1/2}}{2\mu} \sin \frac{\theta}{2} \left\{ 2 - 2\nu + \cos^2 \frac{\theta}{2} \right\} + \cdots$$

$$u_t = \frac{k_3 (2r)^{1/2}}{\mu} \sin \frac{\theta}{2} + \cdots$$

$$u_z = \frac{k_1 (2r)^{1/2}}{2\mu} \sin \frac{\theta}{2} \left\{ 2 - 2\nu - \cos^2 \frac{\theta}{2} \right\}$$

$$- \frac{k_2 (2r)^{1/2}}{2\mu} \cos \frac{\theta}{2} \left\{ 1 - 2\nu - \sin^2 \frac{\theta}{2} \right\} + \cdots \qquad (1.9)$$

It is to be noted here that the displacement solution for three-dimensional case can be obtained by the superposition of all the three modes for the plane strain case with $k = 3 - 4\nu$. But in three-dimensional problems, the parameters k_1, k_2 and k_3 depend on the curvature of the crack edge.

The parameters k_1, k_2 and k_3^* are called Irwin's stress intensity factors corresponding to opening, sliding and tearing modes of fracture respectively. These parameters play a very important role in the computation of brittle strength of the structures with cracks as they govern the magnitude and intensity of the stresses in the vicinity of cracks. These parameters are found to be functions of structural geometry, crack geometry and boundary conditions. From Griffith's criterion (for pure mode I case) when the k value reaches a critical value k_c, the crack becomes unstable and the onset of fracture initiates. k_c, which is called fracture toughness, is a material constant and can be determined experimentally for brittle materials. Other fracture criteria for pure and mixed mode problems are discussed later in this chapter.

The three stress intensity factors can be defined as follows:

---

*In some literature, they are denoted by K_I, K_{II} and K_{III} and the relationships between them are $(k_1, k_2, k_3) = (1/\sqrt{\pi})(K_I, K_{II}, K_{III})$.

$$k_1 = \lim_{r \to o} \sigma_z \cdot (2r)^{1/2} \Big|_{\theta = 0}$$

$$k_2 = \lim_{r \to o} \sigma_{zn} \cdot (2r)^{1/2} \Big|_{\theta = 0}$$

$$k_3 = \lim_{r \to o} \sigma_{tz} \cdot (2r)^{1/2} \Big|_{\theta = 0} \qquad (1.10)$$

Strain Energy Release Rate

Griffith [1,2] considered the fracture problem from the point of view of energy, which forms the foundation of fracture mechanics today. In his theory of energy balance for a cracked body of brittle material, he introduced the concept of strain energy release rate, denoted by $\mathcal{G}$. The mathematical statement of his theory is

$$- dU = dU^S \qquad (1.11)$$

where -dU is the decrease in the strain energy and the potential of applied loads and dU^S is the increase in the surface energy. The strain energy release rate is defined as the rate of change of strain energy with respect to the crack length (for unit thickness of plate)

$$\mathcal{G} = - \frac{dU}{d(2a)} \qquad (1.12)$$

where 2a is the crack length.

The above equation is obtained for "fixed grip" condition during crack extension and the corresponding equation for "constant external forces" during crack extension is

$$\mathcal{G} = \frac{dV}{d(2a)} \tag{1.13}$$

where V is the work done by the external forces.

The strain energy release rate is also related to γ, the surface energy per unit area by

$$\mathcal{G} = 2\gamma \tag{1.14}$$

By using Griffith's theory Irwin [3,10,11] computed the work done by the stresses near the crack tip during mixed mode crack extension which is a function of stress intensity factors as shown below.

$$\mathcal{G} = \frac{\pi(1-\nu^2)}{E}(k_1^2 + k_2^2) + \frac{\pi}{2\mu} k_3^2 \qquad \text{(plane strain)}$$

$$= \frac{\pi}{E}(k_1^2 + k_2^2) + \frac{\pi}{2\mu} k_3^2 \qquad \text{(plane stress)} \tag{1.15}$$

$\mathcal{G}$ is also referred as crack extension force by Irwin.

Since the onset of fracture takes place when k_1 reaches the critical value k_{1c}, there is also a critical value for $\mathcal{G}_I$ denoted by $\mathcal{G}_{Ic}$ for the crack to extend, where subscript I refers to pure Mode I case only. $\mathcal{G}_{Ic}$ is a material property and is also referred to as fracture toughness. The concept of strain energy release rate is not only suitable for numerical calculation of stress intensity factors, but also for experimental determination of stress intensity factors, and such experiments are often called compliance calibration tests.

Path Independent J-Integral

It is a well known fact that for real materials, the region around the crack tip undergoes plastic yielding. In this plastically yielded region, the stresses are uncertain and the stress intensity factors no longer govern and characterize the stresses and displacements. Rice [4] and Eshelby [12] introduced a parameter called the J-integral for evaluation of the strain energy release rate for two-dimensional problems (plane stress and plane strain). This parameter J is evaluated without the direct use of the uncertain state of stress in the plastically yielded region and provides us with a more practical criterion for fracture. This parameter J was arrived at by considering the energy variation and also found to be independent of the path (contour Γ in Figure 3). The J-integral for two-dimensional linear or nonlinear elastic material behavior is given by

$$J = \int_{\Gamma} \left(w \, dx_2 - \vec{T} \frac{\partial \vec{u}}{\partial x_1} \, ds \right) \tag{1.16}$$

Referring to Figure 3, Γ is an arbitrary curve surrounding the crack tip, x_1 and x_2 are the cartesian coordinates, and W is the strain energy density function defined by

$$W = W(x_1, x_2) = \int_{o}^{\epsilon_{k\ell}} \sigma_{ij} \, d \, \epsilon_{ij} \tag{1.17}$$

where ϵ_{ij} and σ_{ij} are strain and stress tensors respectively.

$\vec{T}$ is the surface traction along the boundary Γ defined by $\vec{T} = \sigma_{ij} n_j$ where n_j are the components of outward normal $\vec{n}$. $\vec{u}$ is the

displacement vector and s is the arc length along Γ.

The J-integral represents the flow of strain energy towards the crack tip as the crack elongates and Rice [4] proved that the J-integral is an alternative method to find the strain energy release rate for two-dimensional linear elastic problems leading to

$$J = \mathcal{G} = -\frac{dU}{d(2a)} = \begin{cases} \frac{\pi(1-\nu^2)}{E}\left(k_1^2 + k_2^2\right) + \frac{\pi}{2\mu} k_3^2 & \text{(plane strain)} \\ \frac{\pi}{E}\left(k_1^2 + k_2^2\right) + \frac{\pi}{2\mu} k_3^2 & \text{(plane stress)} \end{cases} \tag{1.18}$$

Fracture Criteria

In the macroscopic (continuum) theories of fracture mechanics there are generally three types of problems which are: (1) the solution of the mechanics problems for the given geometry and applied loads to determine the "stress-intensity factors" representing the severity of applied loads and corresponding to the conjectured modes of fracture such as brittle or ductile fracture, (2) experimental work to determine the resistance of materials to fracture, quantified by parameters such as the "characteristic strength parameters" and (3) development of an appropriate fracture criterion which is nothing but the direct comparison of "characteristic strength parameters" to the calculated "stress-intensity factors" or a function of these stress-intensity factors. In other words, one of the most important problems in fracture mechanics is to determine the critical crack size in structural components. Critical crack size means the size of the crack for which final failure is initiated for a certain structural component with

certain boundary conditions.

A brief discussion of the most commonly used fracture criteria pertaining to linear elastic fracture is presented below. For pure Mode I linear elastic fracture problems, the fracture criteria are well established and as mentioned before, the failure is initiated when the stress-intensity factor k or the strain energy release rate $\mathcal{G}$ (or Rice's J-integral) reaches a critical value of k_c (fracture toughness) or $\mathcal{G}_c$ (also denoted as fracture toughness) respectively.

For general mixed mode three-dimensional problems, it can be stated that the formulation of fracture criteria is still an open subject. A fracture criterion for mixed mode problems was proposed by Sih [13] based on the strain energy density concept. From the asymptotic solution, the strain energy density (per unit volume) near the crack front may be written as

$$\frac{16\mu\, s(\theta)}{r} = \pi(a_{11}k_1^2 + a_{22}k_2^2 + 2a_{12}k_1k_2 + a_{33}k_3^2)/r \qquad (1.19)$$

where

$$a_{11} = (3 - 4\nu - \cos\theta)(1 + \cos\theta)$$

$$a_{22} = 4(1 - \nu)(1 - \cos\theta) + (1 + \cos\theta)(3\cos\theta - 1)$$

$$a_{12} = 2\sin\theta\,(\cos\theta - 1 + 2\nu)$$

$$a_{33} = 4$$

The fracture criterion is stated as (1) the crack grows in a direction, $\theta = \theta_c$ for which $s(\theta)$ reaches a relative minimum, (2) the crack growth begins when the value of $S(k_1,k_2,k_3)$ at $\theta = \theta_c$ reaches a

critical value S_c, which is a material parameter.

Another fracture criterion which is in use is to find the angle θ for which the stress σ_θ is maximum. According to this criterion the stress σ_θ can be expressed as

$$\sigma_\theta = \frac{k_\theta}{(2r)^{1/2}} f(\theta) \tag{1.20}$$

and the fracture initiates when the value of k_θ reaches the critical value k_c and the crack grows in the direction of θ. This critical angle θ for pure mode II problems was found to be a constant ($= -70.5^\circ$) for all materials. But the criterion based on strain energy density yields that θ_c is a function of Poisson's ratio (ν) making θ_c material dependent. It is interesting to note that $\theta_c = -70.5^\circ$ predicted by σ_θ maximum criterion corresponds to the material of zero Poisson ratio by the strain energy density concept.

All the above mentioned fracture criteria pertain to linear problems and when the plastically yielded region near the crack tip and the energy dissipated in that region are no longer small and negligible, these fracture criteria fail to predict the crack initiation and crack growth. In the past decade, several ductile fracture criteria have been proposed to investigate such nonlinear problems. One of the criteria which deserves mentioning for the investigation of critical crack sizes, is the path-independent J-integral. J-integral, which is equal to the crack driving force $\mathcal{G}$, proved to be an important tool for linear elastic materials. For nonlinear elastic body, J is interpreted as the energy available for unit crack extension. For a deformation

theory of plasticity, J-integral is still equal to $-\frac{dU}{d(2a)}$ provided that no unloading occurs. Thus, the concept of J-integral can still be utilized for elastic-plastic fracture problems based on the deformation theory of plasticity. If the crack has been subjected to cyclic loading and the crack has grown due to fatigue, the J-integral concept cannot be used. Furthermore, the J-integral concept can be used only for two-dimensional plane-stress and plane-strain problems and not for a general three-dimensional problem.

Another attractive criterion which can be applied to both, linear and nonlinear problems, is the crack opening displacements (COD). The crack opening displacement can be defined as the relative movement (opening) of the two crack surfaces at the crack tip and is denoted by δ. For a Dugdale model of crack tip yielding, Burdekin and Stone [14] found the expression for δ for an infinite plate with a crack subjected to uniform stress σ is given by

$$\delta = \frac{8\sigma_{ys}\,\sigma}{\pi E} \log\left[\sec\frac{\pi\sigma}{2\sigma_{ys}}\right] \tag{1.21}$$

The critical value of δ of fracture denoted by δ_c can be obtained from experiments and can be used as a fracture criterion.

Several other concepts like maximum radius of the plastic zone and maximum strain, and plastic stress intensity factor K_σ and plastic strain intensity factor K_ε, have been proposed as ductile fracture criteria. But no definite conclusions have been reached as to which method is the best. However, the COD method and J-integral concept seem to be attractive for ductile fracture problems.

CHAPTER II

COMPUTATIONAL METHODS FOR FRACTURE MECHANICS PROBLEMS

Need for Computational Methods

It has been well established already that the stresses, displacements and strain energy release rate for a structural component containing cracks are functions of stress-intensity factors. The importance of determining the stress-intensity factors for the investigation of fracture can not be overemphasized. As mentioned in the previous chapter, exact and closed form solutions are available for some fracture problems and can be found in references like [15-16]; but they are limited to problems with simple geometries of structure and cracks, and simple loading conditions. Even in the case of two-dimensional problems when the geometries of structure and crack are no longer simple, the closed form solution becomes extremely tedious forcing the investigator to make simplifying assumptions which only approximate the actual conditions. In the case of three-dimensional problems with arbitrarily curved crack front, the closed form solution is almost impossible.

The alternative way to solve these complicated problems is to seek solutions through numerical procedures. In aircraft and pressure vessel industries, where fracture problems are of main concern, solutions of stress intensity factors within 5 to 10 percent errors are acceptable. A most feasible and widely accepted numerical method,

in industry, is the finite element method. During the past four or five years finite element methods have been extensively used and proved to be very efficient engineering tools in solving two as well as three-dimensional fracture mechanics problems.

Depending upon the unknowns the finite element method can be broadly classified into three different methods namely displacement method, force method, and mixed method. The most commonly used formulation today is the displacement method. The displacement method relates the generalized nodal displacements and nodal forces through element stiffness matrices and is often referred to as the stiffness method. The compatible displacement model and the hybrid model come under the category of stiffness methods. The compatible displacement model is based on the principle of minimum potential energy and assumes a continuous displacement field over the entire body. The hybrid model may be subdivided into hybrid stress model and hybrid displacement model. In the hybrid stress mode, a modified complementary energy principle is used, and the field variables are compatible displacements along the inter-element boundaries and equilibrated stresses within each element. The hybrid displacement model uses a modified potential energy principle and the field variables are compatible displacements along the inter-element boundaries, a displacement field within each element and an equilibrated surface traction field on the element boundary for each element. In the present investigation, the hybrid displacement model is used.

Finite Element Methods in Fracture Mechanics

The primary objective of the finite element method in fracture mechanics is to obtain the stress intensity factors for cracked structures. There have been many investigators who looked into problems with singularities, like cracks in structural components using finite element method. Survey papers were written by Gallagher [17], Rowe [18], Hilton and Sih [19], Rich and Tracey [20], and Oglesby and Lomacky [21]. The most recent survey was done by Pian [22]. A survey on existing computer programs for fracture problems was made by Benzley and Park [23]. A brief discussion on the various methods and techniques already used to solve two and three-dimensional crack problems is presented below.

Finite element methods for solving stress-intensity factors for two-dimensional problems may be categorized as follows

(1) Using conventional elements

  (a) direct methods

    (i) based on stresses

    (ii) based on displacements

    (iii) based on calibrated stress and displacement

  (b) based on energy

    (i) strain energy release rate $\mathcal{G}$

    (ii) Rice's J-integral

    (iii) local strain energy

(2) Special singular elements at crack tip

  (a) using interpolation functions which yield $r^{-\frac{1}{2}}$ stress singularity

(b) special elements which contain only asymptotic solution;

(c) special elements which contain the asymptotic solution along with regular polynomials;

(d) method of superposition.

Descriptions of the above methods which have so far been used, mostly for two-dimensional problems, are reviewed in the following sections. Comments on three-dimensional crack problems follow them.

Methods Using Conventional Elements

These methods are completely based on the fact that displacements, stresses, strain energy, and other parameters are directly related to the stress-intensity factors. Once these parameters are determined by the finite element method, it is very simple to compute the corresponding stress-intensity factors. The six different possibilities of accomplishing this are explained here.

(a) Direct Methods

(i) Based on Stresses

Christensen and Denke [24,25] used the force method to investigate the stress distribution at the crack tip. They did not directly compute the stress intensity factors; but instead, they compare their solution with the Westergaard solution. Watwood [26] analysed a rectangular plate with central crack and computed the stress-intensity factors by considering two stress components at a point or two stress values at two different locations in the vicinity of the crack tip and using the asymptotic solution. This method was found unreliable. Cylindrical panels and pressurized cylindrical shells with through-wall cracks were analyzed by Ando et al. [27] by using shell elements,

they compared their results with a rectangular plate with a central crack and concluded that the curvature effects were quite significant.

(ii) Based on Displacements

An effective method of computing the stress-intensity factors from the crack surface displacement called crack opening displacement (COD) was pioneered by Kobayashi et al [28]. Chan, Tuba and Wilson [29] used the concept of COD and conventional constant strain triangular elements for the investigation of stress-intensity factors. They found that the stress-intensity factor obtained through COD was good as long as the reference points are not too close to the crack tip. They also found that the values of the stress-intensity factor vary with the element size in the finite element analysis. The same approach with eight-node isoparametric elements was carried out by Henshell and Shaw [30].

(iii) Based on Calibrated Stress and Displacement

Based on the fact that the average stresses in a given area near the crack tip is also a function of SIF, Miyata et al. [31] developed a FEM to calculate SIF using a constant strain triangular element. Initially their results had considerable discrepancies with the correct value, but by using a group of triangular elements at the crack tip, they discovered some regular correlation between stress components and the corresponding average values in the same area due to exact singular term. This technique has been applied successfully by Miyata for pure mode I problems and a mixed mode problem of a rectangular panel with a slanted crack and the results have been found to be very good. They also extended the technique for three-dimensional problems using

tetrahedron elements at crack tip.

(b) Based on Energy

(i) Strain Energy Release Rate $\mathcal{G}$

The strain energy release rate $\mathcal{G}$ can be computed by considering two finite element solutions of two crack problems with slightly different crack lengths and taking the difference in the strain energies. This method was successfully used by Dixon and Pook [32], Mowbray [33], and Anderson et al. [34] and is also referred to as the compliance method. This method is strictly applicable to pure mode I or mode II cases in which the crack is assumed to propagate along the original crack plane. The disadvantage of this method is that it demands two separate finite element solutions of the structure. Parks [35], keeping this disadvantage in mind, came up with an excellent idea that the rate of change of total potential energy with respect to crack length can be expressed in terms of the rate of change of global stiffness matrix. Thus by considering the change of very few element stiffness matrices at the crack tip, the strain energy release rate can be estimated. Hellen [36] also used the same idea and named it method of virtual crack extension. He also pointed out that this method can be used to determine the direction of maximum energy release rate in the case of mixed mode problems.

(ii) Rice's J-Integral

As mentioned before, another method of computing the strain energy release rate for two-dimensional problems is using path independent J-integral. The attractive advantage of this method is that it requires only one finite element solution to determine the strain energy release

rate. This method was employed by Chan et al [29].

(iii) Local Strain Energy

The local strain energy U^* for a circular region surrounding the crack tip is given by

$$U^* = \frac{5-3\nu}{16\mu(1+\nu)} r_1 K_I^2 \quad \text{(mode I plane stress)}$$

where r_1 is the radius of the circle. Miyata [31] and Deverall and Lindsey [37] estimated K_I for different reference radii and different mesh sizes using the local strain energy concept.

All the above methods using conventional finite element models require very small elemental breakdown near the crack tip in order to accurately estimate the near field displacements and stresses. Thus thousands of degrees of freedom are required to get a solution within a few percent error and this is the major disadvantage in all the methods.

Methods Using Special Singular Elements at the Crack Tip

Tong and Pian [38] proved that the rate of convergence of total strain energy for problems with stress singularities using conventional elements is directly related to the element size. In order to improve the rate of convergence, the element size near the crack tip should be comparatively small, at least several orders of magnitude less than that of the crack size. This enforces large degrees of freedom and higher computer time. Another method of improving the rate of convergence for problems with stress singularities is to embed the singular behavior at the crack tip in the finite element solution. This method may be divided into four categories which are discussed below:

(a) Using Interpolation Functions Which Yield $r^{-\frac{1}{2}}$ Stress Singularity

Triangular elements at the crack tip in which the displacements are assumed to vary as $a + b\sqrt{r} + cr$, r being the distance from the crack tip, were used by Tracey [39]. Such an assumption of displacements yields $r^{-\frac{1}{2}}$ stress singularity and the θ variation of stresses is obtained by placing a group of triangular elements around the crack tip. Henshell and Shaw [30] developed four special eight-node square elements around the crack tip. In both models, the elements are compatible.

(b) Special Elements Which Contain Only Asymptotic Solution

A circular crack element which contains only the singular stresses, given by an asymptotic solution, was used by Hilton and Hutchinson [40]. Constant strain triangular elements were used in the remainder of the structure. In this case, the SIF is related to the displacements of the nodes on the circle. This element was found to yield good results when the radius of the circle of singular element is about two percent of crack length. An element at the crack tip which contains two regions was proposed by Walsh [41]. The inner element contains asymptotic solution and the outer region is a conventional model element with equilibrium and compatibility conditions enforced.

(c) Special Elements Which Contain Asymptotic Solution Along With Regular Polynomials

Atluri et al. [42,43] used a hybrid displacement model in which the boundary displacements, interior displacements and boundary tractions are assumed independently a priori and the continuity condition is forced a posteriori. Singular behavior of the tractions and displacements is taken into account in this model. This procedure has

been successfully applied for isotropic as well as anisotropic materials. Since this procedure uses eight-node isoparametric elements, curved crack problems have been solved using parabolic shaped elements. In this procedure the SIF k_1 and k_2, are treated as additional unknowns and computed directly instead of computing them from the finite element displacement solution.

Pian et al. [44] used an assumed stress hybrid model to develop a special element at the crack tip. The assumed variables in this model are the interior stresses and the boundary displacements. It was found in this investigation that in order to get accurate solutions for SIF, the assumed stresses must satisfy the stress free condition along the crack surface whereas the hybrid displacement model does not pose such severe problems. Both the models are applicable to two-dimensional mixed mode problems and yield very good results. Wilson [45] extended the model proposed by Hilton [40] including higher order terms proportional to $r^{1/2}$, r, $r^{3/2}$ in displacements.

Byskov [46] developed a four node isosceles triangular element for treatment of crack problems. Since this element has only few nodal displacements, only a limited number of stress terms could be incorporated. Even though this element is not compatible with the neighboring element, it proved to be an efficient method. A multi-sided superelement was proposed by Rao et al. [47]. Aberson et al. [48] developed special elements using higher order terms in William's series of stress functions instead of regular polynomials. Expressing the stress functions in a power series, Tong et al. [49] developed a special element which contains the crack along an axis of symmetry.

(d) Method of Superposition

The method of superposition of analytical and finite element solution for two-dimensional and axisymmetric problems was used by Yamamoto, et al., [50,51]. This method proved to be an effective method and SIF are computed directly. By using a slightly different approach, Yagawa et al. [52] solved the problem of a rectangular panel with central cracks of different sizes.

Three-Dimensional Problems

Some of the approaches which were used successfully to treat two-dimensional crack problems have been extended to three-dimensional crack problems. A through-the-thickness crack in a plate subjected to out of plane bending was solved by Wilson and Thompson [53] by using conventional elements and crack surface displacements. By using COD, a semi-eiliptical surface flaw in a rectangular plate was solved by Miyamota [54]. Tracey [55,56] extended his two-dimensional approach and solved three-dimensional problems of through-the-thickness straight crack and buried, surface and corner (circular) cracks. Bergan and Aamodt [57,58] used the concept of strain energy release rate to compute the SIF. An elastic-plastic analysis of a plate with two edge cracks was also carried out by them. Three-dimensional stress analysis of a finite slab containing a transverse central crack for mode I problems was carried by Sih et al. [59]. Several circular and elliptical crack problems were solved by Cruse [60] by using boundary-integral equation method. Miyata and Kusumota [61] determined the calibration constants needed for the computation of three-dimensional SIF. They used tetrahedron elements

in the vicinity of the crack tip. Solutions for SIF for semicircular crack in a semi-infinite solid for axial, bending and thermal loads were presented by Smith et al. [62].

It is seen from the above discussion that the development of finite element methods for three-dimensional fracture analysis is in its infant stage. Currently, for analyzing practically significant problems of practical use such as surface flaws in plates, and cracks near fastener holes, etc., only highly approximate solutions are available. These solutions involve Schwarz-Neumann alternating method and various ad hoc "correction factors". More discussion on the shortcomings of such methods is presented in later chapters.

The present investigation is an extension and application of the assumed displacement hybrid finite element model, employed by Atluri, et al. [42,43] for two-dimensional problems, to three-dimensional problems. This finite element procedure is used for the calculation of modes I, II and III SIF, which vary along an arbitrarily curved three-dimensional crack front in a structural component. The finite element model is based on a modified variational principle of potential energy with relaxed continuity requirements for displacements at the interelement boundary. The variational principle is a three-field principle, with arbitrary interior displacements for the element, interelement boundary displacements, and element boundary tractions as variables. The unknowns in the final algebraic system of equations in the present model, are the nodal displacements and the three elastic SIF. Special elements, which contain proper square root and inverse square root crack front variations in displacement and stresses,

respectively, are used in a fixed region near the crack front. Interelement displacement compatibility is satisfied by assuming an independent interelement boundary displacement field and using Lagrange multipliers. These multipliers, are physically the boundary tractions. These are assumed from an equilibrated stress field derived from three-dimensional Maxwell stress functions. Since the method is based on a rigorous variational principle, which enforces, at least on an average the condition of interelement displacement continuity when $\sqrt{r}$ type displacements are included in the near-tip region, the convergence of the finite element solution for nodal displacements as well as SIF can be established mathematically [38]. The geometry of the basic element used is a twenty node isoparametric brick element, with sixty degrees of freedom per element.

CHAPTER III

METHOD OF APPROACH

Formulation of an Embedded Singularity Three-Dimensional Finite Element Hybrid Displacement Model

In as much as the most commonly used compatible displacement finite element model with polynomial basis functions in each element cannot represent the asymptotic singular stress and strain fields in the vicinity of the crack boundary, an alternative finite element formulation is needed. In such a formulation, one should be able to incorporate the exact asymptotic form of solution for singular stresses and strains in elements in a fixed region near the crack boundary and use only regular polynomial type basis functions in elements in the far field. Interelement continuity of displacements and tractions must also be maintained between the near field elements with singular basis functions and the far field elements with regular polynomial basis functions. One such formulation is the assumed displacement hybrid finite element model. The solid is considered to be discretized into a union of finite number of finite sized three-dimensional elements which have piecewise continuous boundaries at which neighboring elements join.

The variational principle which governs the assumed displacement hybrid finite element model is the stationary condition of a modified variational principle of potential energy for which the

functional to be varied is

$$\pi_{HD} = \sum_{m=1}^{N} \left\{ \int_{V_m} \left(\frac{1}{2} E_{ijk\ell}\, \epsilon_{ij} \epsilon_{k\ell} - \bar{F}_i u_i \right) dV \right.$$

$$\left. + \int_{\partial V_m} T_{Li}(v_i - u_i) dS - \int_{S_{\sigma_m}} \bar{T}_i v_i \, dS \right\} \qquad (3.1)$$

V_m = Volume of the m^{th} element ($m = 1,2,\ldots,N$)

N = total number of finite elements

∂V_m = entire boundary of m^{th} element

S_{σ_m} = that portion of ∂V_m where $\bar{T}_i$ are actually prescribed

u_i = independently assumed interior displacements for each element

ϵ_{ij} = $\frac{1}{2}(u_{i,j} + u_{j,i})$ within each element V_m

v_i = independently assumed interelement boundary displacements which are inherently compatible

T_{Li} = Lagrangian multiplier terms which are physically the independently assumed arbitrary interelement boundary tractions

$\bar{F}_i$ = body forces

$\bar{T}_i$ = Specified surface tractions on $S\sigma_m$

$E_{ijk\ell}$ = elasticity tensor

dV = elemental volume

dS = elemental surface area

v_i is continuous and assumed independently on ∂V_m and subjected

to the condition that $v_i = \bar{u}_i$ on S_{um} where S_{um} is that portion of ∂V_m over which the displacements $\bar{u}_i$ is prescribed.

This is a three-field variational principle and the three unknown variables are u_i, v_i and T_{Li}. The first variation of the functional π_{HD} for arbitrary δu_i in V_m, for arbitrary δT_{Li} on ∂V_m and for arbitrary admissible δv_i on ∂V_m such that $\delta v_i = 0$ on S_{um} yields the following equation

$$\delta\pi_{HD} = \sum_{m=1}^{N} \Big\{ -\int_{V_m} [(E_{ijk\ell}\epsilon_{k\ell})_{,j} + \bar{F}_i]\delta u_i dV + \int_{\partial V_m} T_{Li}\delta v_i dS + \int_{\partial V_m} (E_{ijk\ell}\epsilon_{k\ell}\, n_j - T_{Li})\delta u_i dS + \int_{\partial V_m} (v_i - u_i)\delta T_{Li}\, dS - \int_{S\sigma_m} \bar{T}_i\, \delta v_i\, dS \Big\} \tag{3.2}$$

where n_j are the direction-cosines of the outward boundary surface normal. From calculus of variations, the vanishing of $\delta\pi_{HD}$ for arbitrary δu_i, δv_i and δT_{Li} can be shown to furnish the following Euler equation and the three natural boundary conditions.

$$(E_{ijk\ell}\,\epsilon_{k\ell})_{,j} + \bar{F}_i = 0 \quad \text{in } V_m \tag{3.3}$$

$$u_i = v_i \quad \text{on } \partial V_m \tag{3.4}$$

$$E_{ijk\ell}\,\epsilon_{k\ell}\, n_j - T_{Li} = 0 \quad \text{on } \partial V_m \tag{3.5}$$

$$T_{Li} = \bar{T}_i \quad \text{on } S\sigma_m \tag{3.6}$$

Thus the stationary condition of the functional π_{HD} for arbitrary admissible variations of u_i, v_i and T_{Li}, yields equations (3.3) to (3.6). Equation (3.3) states the fact that the interior displacements u_i in V_m generates the stresses $\left\{\frac{1}{2} E_{ijk\ell}(u_{k,\ell} + u_{\ell,k})\right\} = \sigma_{ij}$ that satisfy the local equilbrium equation $\sigma_{ij,j} + \bar{F}_i = 0$ in V_m. Equation (3.4) states that the variational principle forces the interior displacements u_i on ∂V_m to coincide with the interelement boundary displacements v_i which are treated and assumed as independent unknowns. The fact that the tractions generated by the independently assumed interior displacements u_i on ∂V_m, $\frac{1}{2} E_{ijk\ell} (u_{k,\ell} + u_{\ell,k}) n_j = \sigma_{ij} n_j = T_i$ coincide with the independently assumed boundary tractions T_{Li} is displayed by equation (3.5). Equation (3.6) states that the independently assumed boundary tractions coincide with the prescribed tractions $\bar{T}_i$ on S_{σ_m}. While assuming the element boundary displacements v_i, they are assumed in such a way that they are the same for two adjacent elements at their common boundary. This, along with equation (3.3), enforces the a posteriori condition that u_i of one element is equal to u_i of its neighboring element at their common boundary. Thus, it can be easily seen that the present hybrid displacement finite element model enables one to choose element interior displacement basis functions that are completely arbitrary and need not satisfy the inter-element compatibility condition at all. The inter-element compatibility condition is enforced a posteriori by introducing the inter-element boundary displacement v_i as an independent variable and enforcing the constraint condition $u_i = v_i$ on ∂V_m. This is essentially enforced in the variational principle by the term $\int T_{Li} (v_i - u_i)\, dS$ of equation (3.1). The displacements u_i and v_i

are matched at the boundary ∂V_m through the use of the Lagrange multipliers T_{Li} which are again treated as independent variables. These Lagrangean multipliers are physically the tractions at the element boundary as can be seen from equations (3.5) and (3.6).

If one studies equation (3.6), it can be easily seen that the Lagrange multiplier tractions T_{Li} are equal to the prescribed $\bar{T}_i$ on S_{σ_m}. Considering S_σ as the physical boundary of the structure including the crack surfaces, this equation would force the Lagrange multiplier T_{Li} to be equal to the applied boundary traction on S_σ. On those portions of S_σ where no tractions are prescribed, the Lagrange multiplier would be set to zero. This also allows one to consider crack problems with prescribed tractions on the crack surface, for example, constant, linearly or quadratically varying pressure distribution on the crack surface. One such practical problem would be a pressurized thick-walled cylinder with an inner semi-elliptical surface flaw where the crack surface would be subjected to constant pressure due to the internal pressure.

Brief Mathematical Details

In the analysis of three-dimensional linear elastic fracture mechanics problems by the hybrid displacement model, the domain of the problem is divided into two distinct regions. (1) A small region near the crack front where the dominant singular behavior of strains and stresses is present and the elements in this region are referred to as "singular elements", and (2) the region away from the crack front where the effects of singularity are no longer felt and the behavior of

stresses and strains can be approximated using regular polynomial basis functions. The elements in this region are referred to as "regular elements".

The formal derivation and the properties of the finite element in the vicinity of the crack front are developed in this section. As the nature of displacement behavior near the crack front is known, it is a very simple task to incorporate the correct singular behavior of displacement in the assumed approximate basis functions for interior displacements u_i in the near crack front elements. Thus, for a singular element, the interior displacement is assumed as

$$\{u_i\}_s = [U_R]\{\beta_I\} + [U_{RB}]\{\beta_{II}\} + [U_S]\begin{Bmatrix} k_1 \\ k_2 \\ k_3 \end{Bmatrix}$$

$$= [U_R]\{\beta_I\} + [U_{RB}]\{\beta_{II}\} + [U_S]\{k_s\} \qquad (3.7)$$

where $[U_R]$ are simple polynomials which do not contain any rigid body modes and have only straining modes in displacements, $[U_{RB}]$ are simple polynomials which contain only rigid body modes; $[U_S]$ are known displacement functions for three-dimensional problems which yield the correct singular behavior for stresses and strains in linear elastic analysis; β_I and β_{II} are unknown independent parameters; k_1, k_2 and k_3 are the SIF for mode I, II and III crack extension behavior repsectively.

Next, the element boundary displacements are assumed in such a way that they are uniquely interpolated in terms of the nodal displacements $\{q\}$. Since these nodes are common for elements that share the

common boundary, the above unique interpolation ensures inter-element compatibility in an integral average sense. As the interior displacements contain $\sqrt{r}$ type of variation in displacements, the element boundary displacements also should contain $\sqrt{r}$ type of variation in displacements on the element boundary in order to obtain better accuracy. Thus, a correct $\sqrt{r}$ type displacement interpolation is built in for the element boundaries which contain the crack front, and regular isoparametric interpolation functions are assumed for the element boundaries which do not contain the crack front so that the displacements can be matched uniquely at the interface of singular element and the neighboring regular element. A detailed discussion of the boundary displacements will be presented in the next chapter. Thus for a singular element, the boundary displacements v_i are interpolated as

$$\{v_i\}_s = [L_s]\{q\} \tag{3.8}$$

where $[L_s]$ is the matrix which contains the interpolation functions and $\{q\}$ are the appropriate nodal displacements.

Finally, the element boundary tractions T_{Li} (which may be identified as Lagrangean multipliers in this formulation) for singular elements are assumed independently. As the $\sqrt{r}$ type displacement behavior generate inverse $\sqrt{r}$ type behavior in strains and stresses, the inverse $\sqrt{r}$ type behavior tractions are also included in the boundary tractions for better accuracy. Thus, for a singular element, the boundary tractions are assumed as

$$\{T_{Li}\}_S = [R_S]\ \{\alpha\} \tag{3.9}$$

where $[R_s]$ contains the regular as well as singular modes of tractions and $\{\alpha\}$ are unknown independent parameters.

The details of all the matrices in equations (3.7), (3.8) and (3.9) are given in the next chapter and by using the above three field functions, the singular element properties can be derived.

Similar assumptions for the three field functions can be assumed for regular elements. They are assumed exactly in the same pattern but without any singular terms. The corresponding assumptions for a regular element may be written as

$$\{u_i\}_R = [U_R]\{\beta_I\} + [U_{RB}]\{\beta_{II}\} \tag{3.10}$$

$$\{v_i\}_R = [L_R]\{q\} \tag{3.11}$$

$$\{T_{Li}\}_R = [R_R]\{\alpha\} \tag{3.12}$$

From the total number of elements N, the first p elements are the so-called singular elements and the rest are so-called regular elements. Then when equations (3.7) to (3.12) are substituted in equation (3.1) the equation for π_{HD} can be written as follows

$$\pi_{HD} = \sum_{m=1}^{p} \frac{1}{2}\lfloor\beta_I\rfloor[H_1]\{\beta_I\} + \lfloor\beta_I\rfloor[H_2]\{k_s\} + \frac{1}{2}\lfloor k_s\rfloor[H_3]\{k_s\}$$

$$- \lfloor\beta_I\rfloor\{F_1\} - \lfloor k_s\rfloor\{F_2\} - \lfloor\beta_{II}\rfloor\{F_4\} + \lfloor q\rfloor[G]\{\alpha\} - \lfloor\beta_I\rfloor[P_1]\{\alpha\}$$

$$- \lfloor k_s\rfloor[P_2]\{\alpha\} - \lfloor\beta_{II}\rfloor[P_3]\{\alpha\} - \lfloor q\rfloor\{F_3\}$$

$$+ \sum_{m=p+1}^{N} \frac{1}{2} \lfloor \beta_I \rfloor [H_1^*] \{\beta_I\} - \lfloor \beta_I \rfloor \{F_1^*\} - \lfloor \beta_{II} \rfloor \{F_4^*\}$$

$$+ \lfloor q \rfloor [G_1^*] \{\alpha\} - \lfloor \beta_I \rfloor [P_1^*] \{\alpha\} - \lfloor \beta_{II} \rfloor [P_3^*] \{\alpha\} - \lfloor q \rfloor \{F_3^*\} \qquad (3.13)$$

where

$$\lfloor \ \rfloor = \{ \ \}^T$$

The corresponding strains that are derived from the assumed interior displacements as in equations (3.7) and (3.10) are

$$\{\epsilon\} = \frac{1}{2} \{u_{k,\ell} + u_{\ell,k}\} = [W_R] \{\beta_I\} + [W_S] \{k_s\} \qquad (3.14)$$

for the singular elements (m = 1,2,...,p) and

$$\{\epsilon\} = [W_R] \{\beta_I\} \qquad (3.15)$$

for the regular elements (m = p+1, p+2,...,N). Note that in equations (3.14) and (3.15), the terms corresponding to $\{\beta_{II}\}$ do not appear because they are pure rigid body modes and do not produce any straining terms.

The definitions of different matrices in equation (3.13) are as follows:

For singular elements (m = 1,2,...,p)

$$[H_1] = \int_{V_m} [W_R]^T [E] [W_R] \, dV \qquad (3.16)$$

$$[H_2] = \int_{V_m} [W_R]^T [E][W_S] \, dV \tag{3.17}$$

$$[H_3] = \int_{V_m} [W_S]^T [E][W_S] \, dV \tag{3.18}$$

$$[G] = \int_{\partial V_m} [L_S]^T [R_S] \, dS \tag{3.19}$$

$$[P_1] = \int_{\partial V_m} [U_R]^T [R_S] \, dS \tag{3.20}$$

$$[P_2] = \int_{\partial V_m} [U_S]^T [R_S] \, dS \tag{3.21}$$

$$[P_3] = \int_{\partial V_m} [U_{RB}]^T [R_S] \, dS \tag{3.22}$$

$$\{F_1\} = \int_{V_m} [U_R]^T \{\bar{F}_i\} \, dV \tag{3.23}$$

$$\{F_2\} = \int_{V_m} [U_S]^T \{\bar{F}_i\} \, dV \tag{3.24}$$

$$\{F_3\} = \int_{S_{\sigma_m}} [L_S]^T [\bar{T}_i] \, dS \tag{3.25}$$

$$\{F_4\} = \int_{V_m} [U_{RB}]^T \{\bar{F}_i\} \, dV \tag{3.26}$$

For regular elements (m = p+1, p+2,...,N)

$$[H_1^*] = \int_{V_m} [W_R]^T [E][W_R] \, dV \tag{3.27}$$

$$[G^*] = \int_{\partial V_m} [L_R]^T [R_R] \, dS \tag{3.28}$$

$$[P_1^*] = \int_{\partial V_m} [U_R]^T [R_R] \, dS \tag{3.29}$$

$$[P_3^*] = \int_{\partial V_m} [U_{RB}]^T [R_R] \, dS \tag{3.30}$$

$$\{F_1^*\} = \int_{V_m} [U_R]^T \{\bar{F}_i\} \, dV \tag{3.31}$$

$$\{F_3^*\} = \int_{S_{\sigma_m}} [L_R][\bar{T}_i] \, dS \tag{3.32}$$

$$\{F_4^*\} = \int_{V_m} [U_{RB}]\{\bar{F}_i\} \, dV \tag{3.33}$$

where [E] is the elasticity constant matrix.

Now consider the potentials which correspond to the terms $- \lfloor \beta_{II} \rfloor \cdot \{F_4\} - \cdot \lfloor \beta_{II} \rfloor [P_3] \{\alpha\}$. Since body forces are not going to be considered in the present work, $\{F_4\}$ would be zero. $\lfloor \beta_{II} \rfloor [P_3]\{\alpha\}$ can be represented symbolically as

$$- \lfloor \beta_{II} \rfloor [P_3]\{\alpha\} = - \int_{\partial V_m} u_{iRB} \, T_{Li}^S \, dS \tag{3.34}$$

where u_{iRB} are the rigid body displacements, and T^s_{Li} are the assumed surface tractions ($= \{T_{Li}\}_s$). Using the divergence theorem, Equation (3.34) can be written as

$$- \int_{\partial V_m} u_{iRB}\, T^s_{Li}\, dS = - \int_{V_m} (u_{iRB}\sigma^{sp}_{ij})_{,j}\, dV \qquad (3.35)$$

where σ^{sp}_{ij} are the pseudo stresses which contain the asymptotic solution for stresses and the stresses derived from three-dimensional stress functions. σ^{sp}_{Li} are called "pseudo" stresses because the Lagrange multipliers T^s_{Li} are not assumed directly, instead they are assumed indirectly in terms of stress function (see section 5 of Chapter IV). The RHS of equation (3.35) can be written as

$$- \int_{V_m} u_{iRB}\, \sigma^{sp}_{ij,j}\, dV - \int_{V_m} u_{(iRB,j)}\sigma^{sp}_{ij}\, dV \qquad (3.36)$$

The second term in the above expression is zero because u_{iRB} are rigid body displacements. Thus the RHS in Equation (3.36) can be written as

$$= \int_{V_m} u_{iRB}\, (\sigma^{sp}_{ij,j})\, dV \qquad (3.37)$$

Because the expression in the bracket in Equation (3.37) is the equation of equilibrium for the asymptotic stresses and stresses derived from three-dimensional stress functions, which are inherently satisfied, and thus in the absence of body forces, $- [\beta_{II}]\{F_4\} - [\beta_{II}][P_3]\{\alpha\}$ can be set to zero.

Now the equation (3.13) may be rewritten as

$$\pi_{HD} = \sum_{m=1}^{p} \frac{1}{2} \lfloor \beta \rfloor [H_1] \{\beta\} + \lfloor \beta \rfloor [H_2] \{k_s\} + \frac{1}{2} \lfloor k_s \rfloor [H_3] \{k_3\} - \lfloor \beta \rfloor \{F_1\}$$

$$- \lfloor k_s \rfloor \{F_2\} + \lfloor q \rfloor [G] \{\alpha\} - \lfloor \beta \rfloor [P_1] \{\alpha\} - \lfloor k_s \rfloor [P_2] \{\alpha\} - \lfloor q \rfloor \{F_3\}$$

$$+ \sum_{m=p+1}^{N} \frac{1}{2} \lfloor \beta \rfloor [H_1^*] \{\beta\} - \lfloor \beta \rfloor \{F_1^*\} + \lfloor q \rfloor [G^*] \{\alpha\}$$

$$- \lfloor \beta \rfloor [P_1^*] \{\alpha\} - \lfloor q \rfloor \{F_3^*\} \qquad (3.38)$$

where $\lfloor \beta_I \rfloor$ is now represented by $\lfloor \beta \rfloor$ and the definitions for different matrices are still given by Equations (3.16) to (3.33).

In Equation (3.38), the unknown parameters $\lfloor \beta \rfloor$ and $\lfloor \alpha \rfloor$ are independent for each of the elements whereas the parameters $\lfloor q \rfloor$ (nodal displacements) are associated with the entire system of elements and $\lfloor k_s \rfloor$ (stress intensity factors) are associated with segments along the crack front. Now taking the first variation of π_{HD} of Equation (3.38) with respect to $\lfloor \beta \rfloor$ and $\lfloor \alpha \rfloor$ and equating them to zero, the following equations can be attained.

For singular elements (m = 1,2,...,p)

$$[H_1] \{\beta\} + [H_2] \{k_s\} - \{F_1\} - [P_1] \{\alpha\} = 0 \qquad (3.39)$$

$$[G]^T \{q\} - [P_1]^T \{\beta\} - [P_2]^T \{k_s\} = 0 \qquad (3.40)$$

For regular elements (m = p+1, p+2,...,N)

$$[H_1^*] \{\beta\} - \{F_1^*\} - [P_1^*] \{\alpha\} = 0 \qquad (3.41)$$

$$[G_1^*]^T\{q\} - [P_1^*]^T\{\beta\} = 0 \tag{3.42}$$

From the above equations, the parameters $[\beta]$ and $[\alpha]$ can be expressed in terms of the nodal displacements $[q]$ and stress intensity factors $[k_s]$ as follows

For singular elements ($m = 1,2,\ldots,p$)

$$\{\beta\} = [P_1]^{-T}\left\{[G]^T\{q\} - [P_2]^T\{k_s\}\right\} \tag{3.43}$$

$$\{\alpha\} = [P_1]^{-1}\left\{[H_1][P_1]^{-T}[G]^T\{q\} - [H_1][P_1]^{-T}[P_2]^T\{k_s\} + [H_2]\{k_s\} - \{F_1\}\right\} \tag{3.44}$$

For regular elements ($m = p+1, p+2,\ldots,N$)

$$\{\beta\} = [P_1^*]^{-T}[G^*]^T\{q\} \tag{3.45}$$

$$\{\alpha\} = [P_1^*]^{-1}\left\{[H_1^*][P_1^*]^{-T}[G^*]^T\{q\} - \{F_1^*\}\right\} \tag{3.46}$$

In Equations (3.43) to (3.46) the matrices $[P_1]$ and $[P_1^*]$ are assumed to be square and invertible. Substituting Equations (3.43) to (3.46) in Equation (3.38), the following equation can be obtained for the total potential energy:

$$\pi_{HD} = \sum_{m=1}^{p} \tfrac{1}{2}[q][K_{m1}]\{q\} + \tfrac{1}{2}[k_s][K_{m3}]\{k_s\} + [k_s][K_{m2}]\{q\} - [q]\{R_1\} - [k_s]\{R_2\} + \sum_{m=p+1}^{N} \tfrac{1}{2}[q][K_m]\{q\} - [q]\{R\} \tag{3.47}$$

which is a function of $[q]$ and $[k_s]$ only. For singular elements

$(m = 1,2,\ldots,p)$

$$[K_{m1}] = [G][P_1]^{-1}[H_1][P_1]^{-T}[G]^T \tag{3.48}$$

$$[K_{m2}] = [H_2]^T[P_1]^{-T}[G]^T - [P_2][P_1]^{-1}[H_1][P_1]^{-T}[G]^T \tag{3.49}$$

$$[K_{m3}] = [P_2][P_1]^{-1}[H_1][P_1]^{-T}[P_2]^T + [H_3] - 2[P_2][P_1]^{-1}[H_2] \tag{3.50}$$

$$\{R_1\} = [G][P_1]^{-1}\{F_1\} + \{F_3\} \tag{3.51}$$

$$\{R_2\} = \{F_2\} - [P_2][P_1]^{-1}\{F_1\} \tag{3.52}$$

For regular elements $(m = p+1, p+2,\ldots,N)$

$$[K_m] = [G^*][P_1^*]^{-1}[H_1^*][P_1^*]^{-T}[G^*]^T \tag{3.53}$$

$$\{R\} = [G^*][P_1^*]^{-1}\{F_1^*\} + \{F_3^*\} \tag{3.54}$$

Now by expressing the element nodal displacements $\{q\}$ in terms of independent generalized global displacements $\{q^*\}$ (the transformation from $\{q\}$ to $\{q^*\}$ might involve a co-ordinate rotation because the matrix properties are evaluated in local co-ordinate system which are shown in Figure 19b) and by realizing that the SIF are common for segments along the crack front, the expression for π_{HD} becomes,

$$\pi_{HD} = \frac{1}{2}\lfloor q^*\rfloor[K_1]\{q^*\} + \lfloor k_s^*\rfloor[K_2]\{q^*\} + \frac{1}{2}\lfloor k_s^*\rfloor[K_3]\{k_s^*\} - \lfloor q^*\rfloor\{Q_1\} - \lfloor k_s^*\rfloor\{Q_2\} \tag{3.55}$$

where $[k_s^*]$ is the vector representing the SIF of singular elements along the crack front and $[K_1]$, $[K_2]$, $[K_3]$, $\{Q_1\}$ and $\{Q_2\}$ are the global matrices which we get after the assembly of element matrices. Now the stationary condition of π_{HD} in Equation (3.55) with respect to $[q^*]$ and $[k_s^*]$ yields the final form of the equation as

$$[K_1]\{q^*\} + [K_2]^T\{k_s^*\} = \{Q_1\} \tag{3.56}$$

$$[K_2]\{q^*\} + [K_3]\{k_s^*\} = \{Q_2\} \tag{3.57}$$

The solution for the generalized global displacements $\{q^*\}$ and the SIF $\{k_s^*\}$ for singular elements along the crack front for mixed mode behavior of cracks can be obtained by solving the system of simultaneous Equations (3.56) and (3.57).

For a general three-dimensional crack problem, with an arbitrarily curved crack front, the SIF's vary along the crack front. In the present formulation, two versions of SIF variation are assumed within each singular element; one, a constant within each element and the other with a quadratic variation within each element.

Singularity "Super-Element" Stiffness Matrix by a Static Condensation Procedure

The direct result for the present formulation is the final system of algebraic Equations (3.56) and (3.57). Although one can solve for $\{q^*\}$ and $\{k_s^*\}$, the procedure is not immediately adaptable to the widely used general purpose computer codes (such as NASTRAN, STRUDL, NONSAP, and TEXGAP) using the well known direct stiffness method based on a compatible displacement finite element model. These general purpose

computer codes are capable of incorporating new and special formulation of element stiffness matrices to solve special kinds of problems such as fracture mechanics problems. The present formulation is not easily adaptable because of the nature of the final system of algebraic Equations (3.56) and (3.57). The nature of the arrangement of these equations is displayed by Figure 4. The presence of $[K_2]$ and $[K_2]^T$ spoil the bandwidth property of the global stiffness matrix. This calls for either a special solution procedure or the bandwidth has to be considered as the total number unknowns. As the present three-dimensional formulation is a large-scale computer code, considering the total number of unknowns as the bandwidth is practically impossible and highly inefficient. Although special solution procedures may be developed to solve the algebraic equations as such, it was not carried out because the algebraic equations can be reduced to the standard form of those of general purpose computer codes.

This is done by using a static condensation procedure to derive a "super-element" stiffness matrix for elements in the immediate vicinity of the crack tip, that will be compatible with the stiffness matrix for the rest of the structure generated by the above mentioned general purpose programs. In the singular element, one can treat k_1, k_2 and k_3 as "internal" degrees of freedom. The assembly of four singular elements near a segment of the crack boundary is shown in Figure 5. The nodal displacements of this four element assembly are labelled as $\{q'\}$ and are partitioned as

$$\{q'\} = \begin{Bmatrix} q_1' \\ q_2' \end{Bmatrix} \tag{3.58}$$

where $\{q_1'\}$ and $\{q_2'\}$ are displacements on the boundary and interior of the assembly, respectively. The present hybrid-displacement method as applied to only this four-element assembly leads to the algebraic equations in matrix form,

$$\begin{bmatrix} K_{011} & K_{012} & K_{11}^T \\ K_{021} & K_{022} & K_{12}^T \\ K_{11} & K_{12} & K_2 \end{bmatrix} \begin{Bmatrix} q_1' \\ q_2' \\ k_s' \end{Bmatrix} = \begin{Bmatrix} Q_{11}' \\ Q_{12}' \\ Q_2' \end{Bmatrix} \tag{3.59}$$

where $K_{021} = K_{012}^T$ and k_s' are the SIF for the segment of the crack boundary considered.

Since body forces are zero, then $Q_2' = 0$. If, in addition, $Q_{12}' = 0$ (which depends upon the specified $\bar{T}_i$ on S_{σ_m}), then in Equation (3.59), $\{q_2'\}$ and $\{k_s'\}$ can be eliminated and the modified equation may be written as

$$K'q_1' = Q_{11}' \tag{3.60}$$

where

$$K' = K_{011} - [K_{012}\ K_{11}^T] \begin{bmatrix} K_{022} & K_{12}^T \\ K_{12} & K_2 \end{bmatrix}^{-1} \begin{bmatrix} K_{021} \\ K_{11} \end{bmatrix}$$

Thus K' given by Equation (3.61) becomes the "stiffness-matrix" of the super-element. Provided the boundary displacement assumptions built into this super-element coincide with the boundary displacements of the surrounding far-field regular elements, one can, without loss

of any mathematical rigor, use the super-element stiffness matrix in conjunction with the stiffness matrix of the rest of the structure generated from the existing finite element programs.

The above method of finding the super-element stiffness matrices requires that all the relevant matrices for the four singular elements should be computed and assembled first to evaluate K'. This may not be simple or feasible for some of the codes. An alternative method which is still simpler but evaluates only the stiffness matrix of each singular element is also presented here.

Consider the present hybrid displacement model applied to any one of the singular elements. At the singular element level, Equations (3.56) and (3.57) would look like

$$[K_{m1}]\{q\} + [K_{m2}]^T\{k_s\} = \{Q_1'\} \tag{3.62}$$

$$[K_{m2}]\{q\} + [K_{m3}]\{k_s\} = \{Q_2'\} \tag{3.63}$$

Here again since there are no body forces $\{Q_2'\} = 0$, so that we can express $\{k_s\}$ in terms of $[K_{m2}]$, $[K_{m3}]$, and q.

$$\{k_s\} = -[K_{m3}]^{-1}[K_{m2}]\{q\} \tag{3.64}$$

Substituting Equation (3.64) into Equation (3.62), one obtains

$$\left[[K_{m1}] - [K_{m2}]^T[K_{m3}]^{-1}[K_{m2}]\right]\{q\} = \{Q_1'\} \tag{3.65}$$

i.e.

$$[K_m]\{q\} = \{Q_1'\} \tag{3.66}$$

$[K_m]$ in Equation (3.66) is the condensed stiffness matrix of the singular element and can be very easily used in almost all general purpose computer codes.

Once the static condensation of stiffness matrix is done and the finite element solution for the global generalized displacements is carried out, then the SIF k_1, k_2, and k_3 can be obtained by post-processing the finite element displacement solution. Using the corresponding $[K_{m2}]$, $[K_{m3}]$, $\{q\}$ and Equation (3.64), the SIF can be evaluated.

Some of the basic results pertaining to the singular elements using the method of static condensation will be presented in Chapter V. The second method of static condensation of stiffness matrix mentioned here is used in the investigation of three-dimensional crack problems.

Some details of the procedure used for the solution of simultaneous equations obtained after assembling the stiffness matrices are given in Appendix I.

CHAPTER IV

ASSUMED SHAPE FUNCTIONS AND HYBRID DISPLACEMENT FINITE ELEMENT PROCEDURE

Introduction

In the preceding chapter the basic formulation of a hybrid-displacement finite element model to analyze the linear elastic three-dimensional fracture problems was presented. This chapter is devoted to the detailed description of all the field functions and interpolation functions for both the singular as well as regular elements. The basic element design, the numerical procedure to evaluate the volume and the area integral and the related quantities such as the Jacobian, Hessian, etc. are also presented here. Though the present formulation is capable of computing the stress intensity factors directly, they can also be calculated by the method of crack opening displacement which is also described here.

Geometry of the Finite Element

The basic element used in the present three-dimensional investigation is the twenty-node isoparametric hexahedral or "brick" element. The total number of degrees of freedom per element is 60. This family of the isoparametric hexahedron elements was first introduced by Irons [65] (also Reference [66]) and has proven to be very well suited for linear stress analysis. The term "isoparametric" means that the geometry of the element and the interior displacement field

function are described by the same interpolation functions.

If x, y and z are the global cartesian coordinates, we introduce three local curvilinear coordinates ξ, η and ζ such that the relation between the two co-ordinate systems is given by

$$x = N_1x_1 + N_2x_2 + \cdots + N_{20}x_{20} = \sum_{i=1}^{20} N_i(\xi,\eta,\zeta)x_i$$

$$y = N_1y_1 + N_2y_2 + \cdots + N_{20}y_{20} = \sum_{i=1}^{20} N_i(\xi,\eta,\zeta)y_i$$

$$z = N_1z_1 + N_2z_2 + \cdots + N_{20}z_{20} = \sum_{i=1}^{20} N_i(\xi,\eta,\zeta)z_i \qquad (4.1)$$

where $N_i (i = 1,2,\ldots 20)$ are called the shape functions which are expressed in terms of local coordinates ξ, η and ζ; x_i, y_i and z_i $(i = 1,2,\ldots,20)$ are the cartesian coordinates of the ith node of the element. In the case of regular elements, the displacement of any point within the element can also be expressed as

$$u = N_1u_1 + N_2u_2 + \cdots + N_{20}u_{20} = \sum_{i=1}^{20} N_i(\xi,\eta,\zeta)u_i$$

$$v = N_1v_1 + N_2v_2 + \cdots + N_{20}v_{20} = \sum_{i=1}^{20} N_i(\xi,\eta,\zeta)v_i$$

$$w = N_1w_1 + N_2w_2 + \cdots + N_{20}w_{20} = \sum_{i=1}^{20} N_i(\xi,\eta,\zeta)w_i \qquad (4.2)$$

where N_i are the same shape functions as in Equation (4.1) and u_i, v_i and w_i are the nodal displacements of the element.

Essentially, a general quadratic curvilinear element having eight-corner nodes and twelve midside nodes which have physical cartesian co-ordinates is transformed into a cubic element whose non-dimensional co-ordinates ξ, η and ζ are such that $-1 \leq \xi, \eta, \zeta \leq 1$. This transformation is schematically shown in Figure 6a. This isoparametric transformation is very useful in evaluating the element properties which can be done by numerical integration with respect to non-dimensional coordinates ξ, η and ζ. For this element, the interpolation functions assumed for the interior displacement field and the geometry of the element are of parabolic type. Referring to Figure 6b, the shape functions for the twenty-node isoparametric element can be written as

corner nodes:

$$N_i(\xi,\eta,\zeta) = \frac{1}{8}(1 + \xi_o)(1 + \eta_o)(1 + \zeta_o)(\xi_o + \eta_o + \zeta_o - 2)$$

for i = 1,3,5,7,13,15,17,19

Mid-side node where $\xi_i = 0$:

$$= \frac{1}{4}(1 - \xi^2)(1 + \eta_o)(1 + \zeta_o)$$

for i = 2,6,14,18

Mid-side node where $\eta_i = 0$:

$$= \frac{1}{4}(1 + \xi_o)(1 - \eta^2)(1 + \zeta_o)$$

for i = 9,10,11,12

Mid-side nodes where $\zeta_i = 0$:

$$= \frac{1}{4}(1 + \xi_o)(1 + \eta_o)(1 - \zeta^2)$$

$$\text{for } i = 4,8,16,20 \qquad (4.3)$$

where $\xi_o = \xi\xi_i$; $\eta_o = \eta\eta_i$; $\zeta_o = \zeta\zeta_i$

and ξ_i, η_i and ζ_i denote the nodal values of ξ, η and ζ respectively, i.e. + 1 or -1.

As we need the partial derivatives of the shape functions in evaluating the element properties, they can be obtained from Equation (4.3) and are given below.

Corner nodes:

$$\frac{\partial N_i}{\partial \xi} = \frac{1}{8}\xi_i(1 + \eta_o)(1 + \zeta_o)(2\xi_o + \eta_o + \zeta_o - 1)$$

$$\frac{\partial N}{\partial \eta} = \frac{1}{8}\eta_i(1 + \xi_o)(1 + \zeta_o)(\xi_o + 2\eta_o + \zeta_o - 1)$$

$$\frac{\partial N}{\partial \zeta} = \frac{1}{8}\zeta_i(1 + \xi_o)(1 + \eta_o)(\xi_o + \eta_o + 2\zeta_o - 1)$$

$$\text{for } i = 1,3,5,7,13,15,17,19$$

Mid-side nodes where $\xi_i = 0$:

$$\frac{\partial N_i}{\partial \xi} = -\frac{1}{2}\xi(1 + \eta_o)(1 + \zeta_o)$$

$$\frac{\partial N_i}{\partial \eta} = \frac{1}{4}\eta_i(1 - \xi^2)(1 + \zeta_o)$$

$$\frac{\partial N_i}{\partial \zeta} = \frac{1}{4}\,\zeta_i(1 - \xi^2)(1 + \eta_o)$$

for i = 2,6,14,18

Mid-side nodes where $\eta_i = 0$:

$$\frac{\partial N_i}{\partial \xi} = \frac{1}{4}\,\xi_i(1 - \eta^2)(1 + \zeta_o)$$

$$\frac{\partial N_i}{\partial \eta} = -\frac{1}{2}\,\eta(1 + \xi_o)(1 + \zeta_o)$$

$$\frac{\partial N_i}{\partial \zeta} = \frac{1}{4}\,\zeta_i(1 + \xi_o)(1 - \eta^2)$$

for i = 9,10,11,12

Mid-side nodes where $\zeta_i = 0$:

$$\frac{\partial N_i}{\partial \xi} = \frac{1}{4}\,\xi_i(1 + \eta_o)(1 - \zeta^2)$$

$$\frac{\partial N_i}{\partial \eta} = \frac{1}{4}\,\eta_i(1 + \xi_o)(1 - \zeta^2)$$

$$\frac{\partial N}{\partial \zeta} = -\frac{1}{2}\,\zeta(1 + \xi_o)(1 + \eta_o)$$

for i = 4,8,16,20 (4.4)

In the present finite element procedure, in order to obtain the strains and stresses, we need the derivatives of the shape functions with respect to physical coordinate system. As most of the shape

functions are assumed in terms of non-dimensional coordinates ξ, η and ζ, we need to establish the following relationship between derivatives with respect to physical coordinate system and the curvilinear coordinate system.

$$\begin{Bmatrix} \frac{\partial}{\partial \xi} \\ \frac{\partial}{\partial \eta} \\ \frac{\partial}{\partial \zeta} \end{Bmatrix} = \begin{bmatrix} \frac{\partial x}{\partial \xi} & \frac{\partial y}{\partial \xi} & \frac{\partial z}{\partial \xi} \\ \frac{\partial x}{\partial \eta} & \frac{\partial y}{\partial \eta} & \frac{\partial z}{\partial \eta} \\ \frac{\partial x}{\partial \zeta} & \frac{\partial y}{\partial \zeta} & \frac{\partial z}{\partial \zeta} \end{bmatrix} \begin{Bmatrix} \frac{\partial}{\partial x} \\ \frac{\partial}{\partial y} \\ \frac{\partial}{\partial z} \end{Bmatrix} = [J] \begin{Bmatrix} \frac{\partial}{\partial x} \\ \frac{\partial}{\partial y} \\ \frac{\partial}{\partial z} \end{Bmatrix} \tag{4.5}$$

where [J] is the Jacobian matrix.

Thus we have

$$\begin{Bmatrix} \frac{\partial}{\partial x} \\ \frac{\partial}{\partial y} \\ \frac{\partial}{\partial z} \end{Bmatrix} = [J]^{-1} \begin{Bmatrix} \frac{\partial}{\partial \xi} \\ \frac{\partial}{\partial \eta} \\ \frac{\partial}{\partial \zeta} \end{Bmatrix} \tag{4.6}$$

The elemental volume is now given by the relation

$$dV = dxdydz = \det [J] \, d\xi d\eta d\zeta \quad . \tag{4.7}$$

The differential area on the boundary of the element can be computed as follows. The elemental area dS can be combined with unit outward normal $\vec{n}$ and written as $d\vec{S}$. For a three-dimensional isoparametric element, there are six different surfaces and each of them has to

be computed separately. For example, the elemental vector area on the ξ = constant ($+$ 1) surface is given by the cross product of the base vectors $\vec{\eta}$ and $\vec{\zeta}$ and can be expressed as

$$d\vec{S} = \vec{n}dS = \vec{\eta}x\vec{\zeta}\, d\eta d\zeta = \left(\hat{i}\frac{\partial x}{\partial \eta} + \hat{j}\frac{\partial y}{\partial \eta} + \hat{k}\frac{\partial z}{\partial \eta}\right)$$

$$x \left(\hat{i}\frac{\partial x}{\partial \zeta} + \hat{j}\frac{\partial y}{\partial \zeta} + \hat{k}\frac{\partial z}{\partial \zeta}\right) d\eta d\zeta$$

Similar relations can be obtained for the other five surfaces.

In the present formulation we need to establish the relation between the second derivatives of the physical coordinate and non-dimensional coordinate systems as the derivations of stresses and thus the tractions involve the second derivatives of the stress functions with respect to the physical coordinate system. We can write the relation between second derivatives of a function in the physical and non-dimensional coordinate systems in index notation as follows:

$$\frac{\partial^2 \varphi}{\partial a_i \partial a_j} = \frac{\partial \varphi}{\partial b_k}\frac{\partial^2 b_k}{\partial a_i \partial a_j} + \frac{\partial^2 \varphi}{\partial b_k \partial b_\ell}\frac{\partial b_k}{\partial a_i}\frac{\partial b_\ell}{\partial a_j} \qquad (4.8)$$

where

$$a_1 = \xi \qquad b_1 = x$$
$$a_2 = \eta \qquad b_2 = y$$
$$a_3 = \zeta \qquad b_3 = z$$

Equation (4.8) can be written in matrix form as

$$[\xi\eta\zeta - H_\varphi] = \frac{\partial\varphi}{\partial x}[\xi\eta\zeta - H_x] + \frac{\partial\varphi}{\partial y}[\xi\eta\zeta - H_y] + \frac{\partial\varphi}{\partial z}[\xi\eta\zeta - H_z]$$

$$+ [J][xyz - H_\varphi][J]^T \qquad (4.9)$$

With the following notation utilized.

$$\begin{bmatrix} \frac{\partial^2\varphi}{\partial x^2} & \frac{\partial^2\varphi}{\partial x\partial y} & \frac{\partial^2\varphi}{\partial x\partial z} \\ \frac{\partial^2\varphi}{\partial y\partial x} & \frac{\partial^2\varphi}{\partial y^2} & \frac{\partial^2\varphi}{\partial y\partial z} \\ \frac{\partial^2\varphi}{\partial z\partial x} & \frac{\partial^2\varphi}{\partial z\partial y} & \frac{\partial^2\varphi}{\partial z^2} \end{bmatrix} = [xyz - H_\varphi]$$

$$\begin{bmatrix} \frac{\partial^2\varphi}{\partial\xi^2} & \frac{\partial^2\varphi}{\partial\xi\partial\eta} & \frac{\partial^2\varphi}{\partial\xi\partial\zeta} \\ \frac{\partial^2\varphi}{\partial\eta\partial\xi} & \frac{\partial^2\varphi}{\partial\eta^2} & \frac{\partial^2\varphi}{\partial\eta\partial\zeta} \\ \frac{\partial^2\varphi}{\partial\zeta\partial\xi} & \frac{\partial^2\varphi}{\partial\zeta\partial\eta} & \frac{\partial^2\varphi}{\partial\zeta^2} \end{bmatrix} = [\xi\eta\zeta - H_\varphi] \qquad (4.10)$$

Noting that [J] is the Jacobian matrix in Equation (4.9), we can rewrite it as

$$[xyz - H_\varphi] = [J]^{-1}\left\{[\xi\eta\zeta - H_\varphi] - \frac{\partial\varphi}{\partial x}[\xi\eta\zeta - H_x]\right.$$

$$\left. - \frac{\partial\varphi}{\partial y}[\xi\eta\zeta - H_y] - \frac{\partial\varphi}{\partial z}[\xi\eta\zeta - H_z]\right\}[J]^{-T} \qquad (4.11)$$

$[xyz - H_\varphi]$ is called the xyz-Hessian of φ.

Assumed Interior Displacements

For a near field singular element, the interior displacement is assumed as

$$\{u_i\}_s = [U_R]\{\beta_I\} + [U_{RB}]\{\beta_{II}\} + [U_s]\{k_s\} \tag{4.12}$$

where

$$\{u_i\}_s = \begin{Bmatrix} u \\ v \\ w \end{Bmatrix} \tag{4.13}$$

and

$$\{k_s\} = \begin{Bmatrix} k_1 \\ k_2 \\ k_3 \end{Bmatrix} \tag{4.14}$$

are the three stress-intensity factors as mentioned previously. In Equation (4.13) u, v and w denote the displacements in x, y and z directions respectively.

The regular field function $[U_R]$ which contains pure straining modes is assumed in terms of isoparametric coordinate system and cartesian coordinates system. $[U_R]\{\beta_I\}$ is then written in component form as

$$\begin{aligned} u_R = {} & \beta_1 x + \beta_2 y + \beta_3 z + \beta_4 \xi\eta + \beta_5 \eta\zeta + \beta_6 \zeta\xi + \beta_7 \xi^2 + \beta_8 \eta^2 + \beta_9 \zeta^2 + \beta_{10} \xi^3 \\ & + \beta_{11} \xi\eta^2 + \beta_{12} \xi\zeta^2 + \beta_{13} \xi^2\eta + \beta_{14} \eta^3 + \beta_{15} \xi^4 + \beta_{16} \xi^2\zeta \\ & + \beta_{17} \xi^2\zeta^2 + \beta_{18} \zeta^3 + \beta_{19} \xi\eta\zeta \end{aligned}$$

$$v_R = \beta_2 x + \beta_{20} y + \beta_{21} z + \beta_{22}\xi\eta + \beta_{23}\eta\zeta + \beta_{24}\zeta\xi + \beta_{25}\xi^2 + \beta_{26}\eta^2 + \beta_{27}\zeta^2$$
$$+ \beta_{28}\xi^3 + \beta_{29}\xi\eta^2 + \beta_{30}\eta^4 + \beta_{31}\xi^2\eta + \beta_{32}\eta^3 + \beta_{33}\eta\zeta^2 + \beta_{34}\xi^2\eta^2$$
$$+ \beta_{35}\eta^2\zeta + \beta_{36}\zeta^3 + \beta_{37}\xi\eta\zeta$$

$$w_R = \beta_3 x + \beta_{21} y + \beta_{38} z + \beta_{39}\xi\eta + \beta_{40}\eta\zeta + \beta_{41}\zeta\xi + \beta_{42}\xi^2 + \beta_{43}\eta^2 + \beta_{44}\zeta^2$$
$$+ \beta_{45}\xi^3 + \beta_{46}\zeta^4 + \beta_{47}\xi\zeta^2 + \beta_{48}\eta^2\zeta^2 + \beta_{49}\eta^3 + \beta_{50}\eta\zeta^2 + \beta_{51}\xi^2\zeta$$
$$+ \beta_{52}\eta^2\zeta + \beta_{53}\zeta^3 + \beta_{54}\xi\eta\zeta \qquad (4.15)$$

It is to be noted here that $[U_R]$ contains only pure straining modes and not rigid body modes. Such a restriction forces one to assume the terms corresponding to β_1, β_2, β_3, β_{20}, β_{21} and β_{38} in terms of physical co-ordinate system so that all the three rotational rigid body freedoms are suppressed completely.

The regular field function $[U_{RB}]$ which contains pure rigid body modes is assumed in terms of cartesian coordinate system and can be written in component form as

$$u_{RB} = \beta_{55} - \beta_{56} y + \beta_{57} z$$
$$v_{RB} = \beta_{56} x + \beta_{58} - \beta_{59} z$$
$$w_{RB} = -\beta_{57} x + \beta_{59} y + \beta_{60} \qquad (4.16)$$

Thus a total of 60 polynomial basis functions are assumed for the displacements, out of which 54 produce strains and the other six are rigid body modes. Care has been exercised to see that even in the

limiting cases, any of the 54 straining modes do not degenerate to rigid body modes.

The singular displacement field function $[U_s]$, which plays the predominant role in the singular element, has the identical form as the asymptotically correct near field displacement solution given by Equation (1.9), with the stress intensity factors being used directly as undetermined parameters.

For a three-dimensional solid containing an arbitrarily curved crack front, the stress intensity factors are found to be functions of the coordinate t (see Figure 2). Thus, the asymptotic solution for displacement at any point along the crack front can be written as

$$\{u_i^a\} = \{u_i^a(r,\theta)\} = [\tilde{u}_i^a(\sqrt{r},\theta)]\begin{Bmatrix} k_1 \\ k_2 \\ k_3 \end{Bmatrix} \tag{4.17}$$

$$= \{u_i^a(r,\theta,t)\} = [\tilde{u}_i^a(\sqrt{r},\theta)]\begin{Bmatrix} k_1(t) \\ k_2(t) \\ k_3(t) \end{Bmatrix} \tag{4.18}$$

where $[\tilde{u}_i^a(\sqrt{r},\theta)] = [U_s^{ntz}]$, superscript ntz denotes that the displacements are given in n,t,z coordinate system (see Figure 2) and is given by

$$[U_s^{ntz}] = \frac{(2r)^{1/2}}{\mu}\begin{bmatrix} \frac{1}{2}\cos\frac{\theta}{2}\left\{1-2\nu+\sin^2\frac{\theta}{2}\right\} & \frac{1}{2}\sin\frac{\theta}{2}\left\{2-2\nu+\cos^2\frac{\theta}{2}\right\} & 0 \\ 0 & 0 & \sin\frac{\theta}{2} \\ \frac{1}{2}\sin\frac{\theta}{2}\left\{2-2\nu-\cos^2\frac{\theta}{2}\right\} & -\frac{1}{2}\cos\frac{\theta}{2}\left\{1-2\nu-\sin^2\frac{\theta}{2}\right\} & 0 \end{bmatrix} \tag{4.19}$$

The singular field function $[U_s]$ can be obtained from $[U_s^{ntz}]$ after establishing the relation between the n, t and z and cartesian coordinate systems.

In the finite element approximation, the stress intensity factors can be written as

$$\begin{Bmatrix} k_1(t) \\ k_2(t) \\ k_3(t) \end{Bmatrix} = [F(t)] \begin{Bmatrix} k_1^j \\ k_2^j \\ k_3^j \end{Bmatrix} \tag{4.20}$$

where superscript j denotes the jth node at crack front of the elements along the crack front and $[F(t)]$ is a polynomial interpolation function for the stress-intensity factors along the crack front. For example, for a 20 node isoparametric brick element, there are three nodes which lie on the crack front and the stress-intensity factors can be interpolated quadratically. In other words, the stress-intensity factors can be interpolated quadratically along the crack front within an element. After non-dimensionalizing the coordinate t, which happens to be the coordinate η with the present notation, $[F(t)]$ can be written as

$$F(t) = \begin{bmatrix} \eta(\eta-1)/2 & (1-\eta^2) & \eta(\eta+1)/2 & 0 & 0 & 0 & 0 & 0 & 0 \\ 0 & 0 & 0 & \eta(\eta-1) & (1-\eta^2) & \eta(\eta+1)/2 & 0 & 0 & 0 \\ 0 & 0 & 0 & 0 & 0 & 0 & \eta(\eta-1)/2 & (1-\eta^2) & \eta(\eta+1)/2 \end{bmatrix} \tag{4.21}$$

and

$$\begin{Bmatrix} k_1^j \\ k_2^j \\ k_3^j \end{Bmatrix} = \begin{Bmatrix} k_1^1 \\ k_1^2 \\ k_1^3 \\ k_2^1 \\ k_2^2 \\ k_2^3 \\ k_3^1 \\ k_3^2 \\ k_3^3 \end{Bmatrix} \tag{4.22}$$

Denoting the three nodes along the crack front of an element by 1, 2 and 3, the Equations (4.21) and (4.22) assume the following relations

$$\begin{aligned} &\text{at node 1} \quad \eta = -1 \\ &\text{at node 2} \quad \eta = 0 \\ &\text{at node 3} \quad \eta = +1 \end{aligned} \tag{4.23}$$

It is also to be noted here that all the three stress intensity factors are interpolated using the same quadratic interpolation functions.

Though the above general procedure of varying the stress-intensity factors within an element may be used, in the present procedure, they are assumed constant within an element but vary from element to element along the crack front because of limitations of computational time. This would reduce the Equation (4.20) as follows:

$$\begin{Bmatrix} k_1(t) \\ k_2(t) \\ k_3(t) \end{Bmatrix} = \begin{Bmatrix} k_1^m \\ k_2^m \\ k_3^m \end{Bmatrix} \tag{4.24}$$

where superscript m denotes the mth element along the crack front.

For a regular element, the element interior displacement field function is assumed as

$$\{U_i\}_R = [U_R]\{\beta_I\} + [U_{RB}]\{\beta_{II}\} \tag{4.25}$$

and the matrices $[U_R]$ and $[U_{RB}]$ are exactly the same as those of the singular element as given by Equations (4.15) and (4.16).

Assumed Boundary Displacements

As discussed in the previous chapter, the boundary displacements $\{v_i\}_s$ should be same at common boundaries of neighboring element (the common boundaries of neighboring elements are denoted by the symbol ρ_m). This is accomplished by interpolating for $\{v_i\}_s$ on a segment of ρ_m in terms of nodal displacements on the particular segment of ρ_m only. Thus, referring to Figure 6b, the following boundary displacements are assumed for singular element, followed by regular element

assumptions. The element is described by nodes ABCDEFGH as shown in Figure 6b.

Face ABFE ($\zeta = -1$)

for singular element

$$u = a_1 + a_2\sqrt{r} + a_3\eta + a_4 r + a_5\eta^2 + a_6\sqrt{r}\eta + a_7 r\eta + a_8\sqrt{r}\eta^2 \qquad (4.26)$$

where r is the radius (dimensional) measured normal to the crack boundary. It can thus be seen that the displacements on face ABEF (plane of the crack) has the asymptotically correct $\sqrt{r}$ so that better matching condition can be obtained between interior and boundary displacements. The above interpolation function essentially interpolates the displacements as functions of $\sqrt{r}$ in the direction normal to the crack front and as η (non-dimensional) in the direction parallel to the crack front. The parameters $(a_1, a_2, \ldots, a_8)$ are determined uniquely in terms of the relevant u-displacement coordinates on ABFE, viz., q_1, q_2, q_3, q_9, q_{10}, q_{13}, q_{14} and q_{15}. Thus, the boundary displacement would be the same for two singular elements joining at face ABFE.

for regular elements

$$\begin{aligned} u = {} & q_1(1 - \xi)(1 - \eta)(-\xi - \eta - 1)/4 + q_2(1 - \xi^2)(1 - \eta)/2 \\ & + q_3(1 + \xi)(1 - \eta)(\xi - \eta - 1)/4 + q_9(1 - \xi)(1 - \eta^2)/2 \\ & + q_{10}(1 + \xi)(1 - \eta^2)/2 + q_{13}(1 - \xi)(1 + \eta)(-\xi + \eta - 1)/4 \\ & + q_{14}(1 - \xi^2)(1 + \eta)/2 + q_{15}(1 + \xi)(1 + \eta)(\xi + \eta - 1)/4 \end{aligned} \qquad (4.27)$$

The above equation represents a unique quadratic interpolation

for displacements on face ABFE of a regular element. All the other interpolation functions for the remaining five faces are also uniquely interpolated. It should be noted here that similar interpolates are used for the other two displacements, v and w correspondingly for all six faces of the cube.

Face CDHG ($\zeta = +1$)

Since this face is remote from the crack boundary, the displacements on this segment of the boundary can be regular polynomials. Thus for instance, the displacement u on this face is interpolated uniquely in terms of the relevant nodal displacements q_5, q_6, q_7, q_{11}, q_{12}, q_{17}, q_{18} and q_{19} as

$$u = q_5(1 + \xi)(1 - \eta)(\xi - \eta - 1)/4 + q_6(1 - \xi^2)(1 - \eta)/2$$
$$+ q_7(1 - \xi)(1 - \eta)(-\xi - \eta - 1)/4 + q_{11}(1 + \xi)(1 - \eta^2)/2$$
$$+ q_{12}(1 - \xi)(1 - \eta^2)/2 + q_{17}(1 + \xi)(1 + \eta)(\xi + \eta - 1)/4$$
$$+ q_{18}(1 - \xi^2)(1 + \eta)/2 + q_{18}(1 - \xi)(1 + \eta)(-\xi + \eta - 1)/4 \quad (4.28)$$

Exactly the same interpolation function, as in Equation (4.28), is also used for a regular element and hence is automatically compatible with the boundary displacements of the regular element that adjoins the present face CDHG of singular element.

Faces ABCD ($\eta = -1$) and EFGH ($\eta = +1$)

On these faces, which are perpendicular to the crack front, the asymptotic solution for displacements indicates not only a $\sqrt{r}$ variation, but also a rapid variation with θ. To reflect this for instance, the displacements on face ABCD are assumed as,

$$u = a_1 + a_2\xi + a_3\zeta + a_4 r + a_5\sqrt{r}\sin\frac{\theta}{2}\left(2 - 2\nu - \cos^2\frac{\theta}{2}\right)$$

$$+ a_6\sqrt{r}\cos\frac{\theta}{2}\left(1 - 2\nu - \sin^2\frac{\theta}{2}\right) + a_7\sqrt{r}\cos\frac{\theta}{2}\left(1 - 2\nu + \sin^2\frac{\theta}{2}\right)$$

$$+ a_8\sqrt{r}\sin\frac{\theta}{2}\left(2 - 2\nu + \cos^2\frac{\theta}{2}\right) \qquad (4.29)$$

and identical displacements v and w, with $(a_1,\ldots,a_8)$ above, being replaced by $(b_1,\ldots,b_8)$ and $(c_1,\ldots,c_8)$ respectively. The parameters $(a_1,\ldots,a_8)$ are uniquely found from $(q_1,\ldots,q_8)$; $(b_1,\ldots,b_8)$ are found from $(q_{21},\ldots,q_{28})$; and $(c_1,\ldots,c_8)$ are found from $(q_{41},\ldots,q_{48})$ with the notation (q_1 thru q_{20}), (q_{21} thru q_{40}) and (q_{41} thru q_{60}) are the nodal displacements u, v and w of nodes (1 thru 20) respectively. An interpolate similar to that in Equation (4.29) is likewise used for each of the three displacements on face EFGH. It is clear that when other singular elements adjoin the present element at faces ABCD and EFGH, the interelement displacements are compatible. For a regular element for face ABCD the interpolation function can be written as

$$u = q_1(1 - \xi)(1 - \zeta)(-\xi - \zeta - 1)/4 + q_2(1 - \xi^2)(1 - \zeta)/2$$

$$+ q_3(1 + \xi)(1 - \zeta)(\xi - \zeta - 1)/4 + q_4(1 + \xi)(1 - \zeta^2)/2$$

$$+ q_5(1 + \xi)(1 + \zeta)(\xi + \zeta - 1)/4 + q_6(1 - \xi^2)(1 + \zeta)/2$$

$$+ q_7(1 - \xi)(1 + \zeta)(-\xi + \zeta - 1)/4 + q_8(1 - \xi)(1 - \zeta^2)/2 \qquad (4.30)$$

and for face EFGH

$$u = q_{13}(1 - \xi)(1 - \zeta)(-\xi - \zeta - 1)/4 + q_{14}(1 - \xi^2)(1 - \zeta)/2$$

$$+ q_{15}(1 + \xi)(1 - \zeta)(\xi - \zeta - 1)/4 + q_{16}(1 + \xi)(1 - \zeta^2)/2$$

$$+ q_{17}(1 + \xi)(1 + \zeta)(\xi + \zeta - 1)/4 + q_{18}(1 - \xi^2)(1 + \zeta)/2$$

$$+ q_{19}(1 - \xi)(1 + \zeta)(-\xi + \zeta - 1)/4$$

$$+ q_{20}(1 - \xi)(1 - \zeta^2)/2 \qquad (4.31)$$

Face ADHE ($\xi = -1$)

Similar to the interpolate on face ABFE, we assume for face ADHE

$$u = a_1 + a_2 \sqrt{r} + a_3\eta + a_4 r + a_5\eta^2 + a_6 \sqrt{r}\,\eta + a_7 r\eta + a_8 \sqrt{r}\,\eta^2 \qquad (4.32)$$

where the constants $(a_1,\ldots,a_8)$ are now evaluated in terms of (q_1, q_7, q_8, q_9, q_{12}, q_{13}, q_{19} and q_{20}). For faces ABFE and ADHE, the values of θ are constants, i.e. 0 and $\bar{\Lambda}/2$ respectively, and thus it is not necessary to incorporate any θ variation in the interpolate. For a regular element the interpolate would be

$$u = q_1(1 - \eta)(1 - \zeta)(-\eta - \zeta - 1)/4 + q_8(1 - \eta)(1 - \zeta^2)/2$$

$$+ q_7(1 - \eta)(1 + \zeta)(-\eta + \zeta - 1)/4 + q_{12}(1 - \eta^2)(1 + \zeta)/2$$

$$+ q_{19}(1 + \eta)(1 + \zeta)(\eta + \zeta - 1)/4 + q_{20}(1 + \eta)(1 - \zeta^2)/2$$

$$+ q_{13}(1 + \eta)(1 - \zeta)(\eta - \zeta - 1)/4 + q_9(1 - \eta^2)(1 - \zeta)/2 \qquad (4.33)$$

Face BCGF ($\xi = +1$)

Similar to that of face CDHG, the interpolate for this face would be

$$u = q_3(1 - \eta)(1 - \zeta)(-\eta - \zeta - 1)/4 + q_4(1 - \eta)(1 - \zeta^2)/2$$

$$+ q_5(1 - \eta)(1 + \zeta)(-\eta + \zeta - 1)/4 + q_{11}(1 - \eta^2)(1 + \zeta)/2$$

$$+ q_{17}(1 + \eta)(1 + \zeta)(\eta + \zeta - 1)/4 + q_{16}(1 + \eta)(1 - \zeta^2)/2$$

$$+ q_{15}(1 + \eta)(1 - \zeta)(\eta - \zeta - 1)/4 + q_{10}(1 - \eta^2)(1 - \zeta)/2 \quad (4.34)$$

The interpolate for a regular element is also the same as given by Equation (4.34).

In the preceding discussion, the interpolation functions corresponding to a singular element where θ varying from (0 to $\bar{\Lambda}/2$) are given. For the other three singular elements where the θ variations are ($\bar{\Lambda}/2$ to $\bar{\Lambda}$), (0 to $-\bar{\Lambda}/2$) and ($-\bar{\Lambda}/2$ to $-\bar{\Lambda}$), similar ideas of assuming proper interpolates are used accordingly.

Assumed Boundary Tractions

The boundary tractions $\{T_{Li}\}_s$, mathematically interpreted as Lagrangean multipliers in the assumed displacement hybrid finite element method, as such can be assumed in any convenient form. However, we first note one of the relevant natural boundary conditions of the present variational principle, which states that the boundary tractions generated by the assumed element interior displacements $\{u_i\}_s$ must match the independently assumed boundary tractions $\{T_{Li}\}_s$ at ρ_m. This can be stated precisely as

$$\{T_{Li}\}_s = \frac{1}{2} E_{ijkl} (u_{k,\ell} + u_{\ell,k}) \cdot n_j \quad (4.35)$$

Thus, since the assumed $\{u_i\}_s$ includes a $\sqrt{r}$ variation in displacements for the singular element, the boundary tractions generated by these $\{u_i\}_s$ would have a $1/\sqrt{r}$ variations. Thus, it can be seen that for better numerical accuracy, the assumed tractions $\{T_{Li}\}_s$ for

the singular element must also contain a $1/\sqrt{r}$ behavior. From a purely mathematical point of view when $\{T_{Li}\}_s$ are Lagrangean multipliers, this condition is not immediately apparent. The singular stresses and thus the singular tractions actually dominate the regular stresses for a singular element. This fact was established in the two-dimensional analysis of linear fracture mechanics problems by the hybrid displacement model (see Reference [67]). After subsequent numerical experimentation, it was shown that it was necessary to assume the asymptotically correct singular boundary traction field in the singular elements for better matching condition of $\{T_{Li}\}_s$ and the tractions generated by the displacement $\{u_i\}_s$. Incidentally these singular tractions would also satisfy the traction free conditions on the crack surface.

Since the displacement field $\{u_i\}_s$, in addition to satisfying Equation (4.35), is also forced to satisfy the equilibrium equations through the variational principle, it can be seen that better accuracy in the formulation is achieved if the assumed $\{T_{Li}\}_s$ are obtained from a equilibrated stress field. Since, in the present finite element model, the body forces are not considered, such a stress field can be obtained from the three-dimensional stress functions. To this regard, three stress functions namely Maxwell, Morera and Beltrami can be introduced. The relationships between the Maxwell's stress functions and the stresses are given as follows

$$\sigma_x = \frac{\partial^2 \chi_3}{\partial y^2} + \frac{\partial^2 \chi_2}{\partial z^2} \; ; \qquad \sigma_{yz} = - \frac{\partial^2 \chi_1}{\partial y \partial z}$$

$$\sigma_y = \frac{\partial^2 \chi_1}{\partial z^2} + \frac{\partial^2 \chi_3}{\partial x^2} \quad ; \qquad \sigma_{zx} = - \frac{\partial^2 \chi_2}{\partial z \partial x}$$

$$\sigma_z = \frac{\partial^2 \chi_2}{\partial x^2} + \frac{\partial^2 \chi_1}{\partial y^2} \quad ; \qquad \sigma_{xy} = - \frac{\partial^2 \chi_3}{\partial x \partial y} \tag{4.36}$$

where (χ_1, χ_2 and χ_3) are Maxwell's stress functions. The relationships between Morera's stress function and the stresses can be found in Reference [101]. Beltrami's stress functions are merely a particular linear combination of Maxwell's and Morera's stress functions [102].

For simplicity and computational ease, in the actual computation, only the stress function based on Maxwell's representation are used. Since the tractions generated from the above stress field have to be evaluated on the faces of the singular element, it is convenient to assume the stress functions in terms of curvilinear coordinates ξ, η and ζ. For reasons discussed in previous chapter, the stress functions (χ_1, χ_2 and χ_3) were assumed with a total of 54 undetermined parameters in them. Out of these, 51 basis functions were of regular polynomial nature and the other three had a $1/\sqrt{r}$ variation in them. Each of these 54 basis functions in the three stress function assumptions should be such that it does not produce a stress tensor that is linearly dependent on the stress tensor produced by the other 53 basis functions. Another necessary condition in the proper choice of these stress functions is that the matrix $[P_1]$ represented in the scalar

$$\lfloor \beta \rfloor [P_1] \{\alpha\} = \int_{\partial V_m} \lfloor \beta \rfloor [U_R]^T [R_s] \{\alpha\} dS \tag{4.37}$$

(where $\{\alpha\}$ are parameters in boundary tractions $\{T_{Li}\} = [R_s]\ \{\alpha\}$) be non-singular. Thus, considerable care had to be exercised in properly choosing the stress functions such that they produce the needed stress modes, and these are given below.

$$\chi_1 = \alpha_1\eta^2 + \alpha_2\eta\zeta + \alpha_3\xi\eta^2 + \alpha_4\xi\zeta^2 + \alpha_5\eta\zeta^2 + \alpha_6\eta^2\zeta + \alpha_7\xi\eta\zeta + \alpha_8\eta^3\zeta^2$$
$$+ \alpha_9\xi\eta^2\zeta + \alpha_{10}\xi\eta\zeta^2 + \alpha_{11}\eta^3\zeta + \alpha_{12}\eta\zeta^3 + \alpha_{13}\xi\zeta^3 + \alpha_{14}\xi^2\eta^2$$
$$+ \alpha_{15}\eta^2\zeta^2 + \alpha_{16}\xi^2\zeta^2 + \alpha_{17}\eta^4\zeta$$

$$\chi_2 = \alpha_{18}\zeta^2 + \alpha_{19}\xi\zeta + \alpha_{20}\eta\zeta^2 + \alpha_{21}\xi^2\eta + \alpha_{22}\xi^2\zeta + \alpha_{23}\xi\zeta^2 + \alpha_{24}\xi\eta\zeta$$
$$+ \alpha_{25}\xi^2\zeta^3 + \alpha_{26}\xi\eta\zeta^2 + \alpha_{27}\xi^2\eta\zeta + \alpha_{28}\xi\zeta^3 + \alpha_{29}\xi^3\zeta + \alpha_{30}\xi^3\eta$$
$$+ \alpha_{31}\eta^2\zeta^2 + \alpha_{32}\xi^2\zeta^2 + \alpha_{33}\xi^2\eta^2 + \alpha_{34}\xi\zeta^4$$

$$\chi_3 = \alpha_{35}\xi^2 + \alpha_{36}\xi\eta + \alpha_{37}\xi^2\zeta + \alpha_{38}\eta^2\zeta + \alpha_{39}\xi\eta^2 + \alpha_{40}\xi^2\eta + \alpha_{41}\xi\eta\zeta$$
$$+ \alpha_{42}\xi^3\eta^2 + \alpha_{43}\xi^2\eta\zeta + \alpha_{44}\xi\eta^2\zeta + \alpha_{45}\xi^3\eta + \alpha_{46}\xi\eta^3 + \alpha_{47}\eta^3\zeta$$
$$+ \alpha_{48}\xi^2\zeta^2 + \alpha_{49}\xi^2\eta^2 + \alpha_{50}\eta^2\zeta^2 + \alpha_{51}\xi^4\eta \qquad (4.38)$$

The stresses σ_{ij} can be calculated by using Equation (4.36) and the Hessian as given by Equation (4.11), from which the boundary tractions are derived as $\{T_{Li}\} = [\sigma_{ij}]\ \{n_j\}$. The remaining three traction modes are assumed from the singular stress field given in Equation (1.8) wherein k_1, k_2, k_3 are replaced by α_{52}, α_{53} and α_{54}.

Care should be taken to transform the singular stresses from (n, t and z) coordinate system to (x, y and z) coordinate system.

For a regular element also, the total number of undetermined parameters are still 54 but the singular stress terms should not be present in the assumption of stress functions. Instead α_{52}, α_{53} and α_{54} terms in the traction are now replaced by some other regular polynomial which do not generate already existing traction modes. The additional three regular terms for a regular element can be written as

$$\chi_1 = \alpha_{52}\ \eta\zeta^4$$

$$\chi_2 = \alpha_{53}\ \xi^4\zeta$$

$$\chi_3 = \alpha_{54}\ \xi\eta^4 \qquad (4.39)$$

Some Details of the Numerical Procedure

In order to obtain the element stiffness matrix for the singular element, a volume integral involving strain energy density must be evaluated. It can be seen that the strain energy involves tensor inner products of the following three types, as the assumed interior displacements involve a combination of regular polynomials and $\sqrt{r}$ type variation.

(i) Product of regular-regular polynomials tensor (Equation (3.16))

$$[H_1] = \int_{V_m} [W_R]^T [E][W_R]\, dV \quad (m = 1,\ldots,p) \qquad (4.40)$$

(ii) Product of regular-singular polynomials tensor (Equation (3.17))

$$[H_2] = \int_{V_m} [W_R]^T [E][W_s]\, dV \quad (m = 1,\ldots,p) \tag{4.41}$$

(iii) Product of singular-singular polynomials tensor (Equation (3.18))

$$[H_3] = \int_{V_m} [W_s]^T [E][W_s]\, dV \quad (m = 1,\ldots,p) \tag{4.42}$$

where the strains were obtained from displacements using the following formula

$$\{\epsilon\} = [W]\{\beta\} = \begin{Bmatrix} \epsilon_x \\ \epsilon_y \\ \epsilon_z \\ \gamma_{xy} \\ \gamma_{yz} \\ \gamma_{zx} \end{Bmatrix} = \begin{Bmatrix} u,_x \\ v,_y \\ w,_z \\ u,_y + v,_x \\ v,_z + w,_y \\ w,_x + u,_z \end{Bmatrix} \tag{4.43}$$

where

$$u,_x = \frac{\partial u}{\partial x} \; ; \quad v,_y = \frac{\partial v}{\partial y} \; ; \text{ etc.}$$

The stresses are obtained as

$$\{\sigma\} = \begin{Bmatrix} \sigma_x \\ \sigma_y \\ \sigma_z \\ \sigma_{xy} \\ \sigma_{yz} \\ \sigma_{zx} \end{Bmatrix} = [E] \begin{Bmatrix} \epsilon_x \\ \epsilon_y \\ \epsilon_z \\ \gamma_{xy} \\ \gamma_{yz} \\ \gamma_{zx} \end{Bmatrix} \tag{4.44}$$

where [E] is the elasticity matrix and is given by

$$[E] = \frac{E(1-\nu)}{(1+\nu)(1-2\nu)} \begin{bmatrix} 1 & & & & & \\ \frac{\nu}{1-\nu} & 1 & & & \text{Symmetric} & \\ \frac{\nu}{1-\nu} & \frac{\nu}{1-\nu} & 1 & & & \\ 0 & 0 & 0 & \frac{(1-2\nu)}{2(1-\nu)} & & \\ 0 & 0 & 0 & 0 & \frac{(1-2\nu)}{2(1-\nu)} & \\ 0 & 0 & 0 & 0 & 0 & \frac{(1-2\nu)}{2(1-\nu)} \end{bmatrix} \tag{4.45}$$

where E is Young's modulus and ν is Poisson's ratio.

Numerical evaluation of Equation (4.40) was carried out by using a five point product Gaussian quadrature formula and the total number of Gaussian points for this integration is 125. Appendix B gives the details of the Gaussian quadratures used for volume integration. Though the Equations (4.41) and (4.42) can be evaluated through the volume integration, they were first transformed to an area integral

by using the divergence theorem for the following reason. The strain energy corresponding to singular strains if evaluated by volume integration would contain a 1/r singularity (Equation (4.42)). By using divergence theorem the strain energy corresponding to singular strains can be written as

$$\int_{V_m} \sigma_{ij}^s \, \epsilon_{ij}^s \, dV = \int_{V_m} \sigma_{ij}^s \, u_{(i,j)}^s \, dV$$

$$= \int_{V_m} (\sigma_{ij}^s \, u_i^s)_{,j} \, dV - \int_{V_m} \sigma_{ij,j}^s \, u_i \, dV$$

The second term would be zero because the asymptotic solution for stresses is self-equilibrating, thereby yielding

$$\int_{V_m} \sigma_{ij}^s \, \epsilon_{ij}^s \, dV = \int_{\partial V_m} \sigma_{ij}^s \, n_j \, u_i^s \, dS \qquad (4.46)$$

where n_j the direction-cosines of outward normal. On the right hand side of Equation (4.46), we can see that there is no singularity as the $1/\sqrt{r}$ in stresses and $\sqrt{r}$ in displacements cancel thus yielding a regular integral for strain energy due to singular strains if the evaluation is carried out in area integral. This can be expressed in matrix form as

$$[H_3] = \int_{\partial V_m} [U_s]^T [n][E][W_s] dS \quad (m = 1,\ldots,p) \qquad (4.47)$$

Similar technique could be followed to transform the strain

energy due to singular stresses and regular strains and expressed in matrix form as

$$[H_2] = \int_{\partial V_m} [U_R]^T [n][E][W_s] dS \quad (m = 1,\ldots,p) \tag{4.48}$$

As it can be seen from Equation (4.48) the integrand still has a $1/\sqrt{r}$ singularity. During the numerical integration, another transformation could be used to eliminate this. For faces ABFE and ADHE, dS can be separated by dr and $d\eta$ after properly taking care of the Jacobian of the transformation for that particular face. Now, introducing a transformation $r = t^{*2}$, dr can be written as

$$dr = 2t^* \, dt^* = 2\sqrt{r} \, dt^*$$

$$\frac{dr}{\sqrt{r}} = 2 \, dt^* \tag{4.49}$$

From Equation (4.49), it is apparent that the singularity can be removed for the matrix. The above idea is utilized in the actual computation for faces ABFE and ADHE. For the other four surfaces isoparametric non-dimensional coordinates were used to evaluate the integral. The quadrature formula used for area integration is also given in Appendix B.

It was mentioned in section 3 of this chapter that the stress intensity factors k_1, k_2 and k_3 can be varied as quadratic functions of the crack front coordinate η. In this case, the asymptotic singular solution will not be equilibrated a priori and thus the strain energies

corresponding to singular-singular polynomials and singular-regular polynomials, i.e. $[H_3]$ and $[H_2]$ have to be evaluated by volume integral with $1/r$ and $1/\sqrt{r}$ singularities respectively.

However, such singularities can be removed by using the following idea for the faces ABCD and EFGH. The face ABCD (as well as EFGH) can be divided into two regions as a quarter circle with A as origin and A B (=AD) as radius, and the rest of that face. Now for the quarter circular region the differential area can be written as $rdrd\theta$ and the "r" in the differential area can be used to cancel either $1/r$ or $1/\sqrt{r}$ singularities making them regular integrals. As the other region is far away from the crack front, the numerical integration can be carried out without using any such special transformation.

Such an idea was used in the development of singular elements and some basic checks (similar to the one which would be discussed in the next chapter where the stress-intensity factors were assumed constant within an element) were made for these elements and they satisfied all the checks. However, this element takes more computer time than the element where the stress-intensity factors were assumed constant within an element, as the area integration is now split up into two parts on faces ABCD and EFGH.

Conventional Displacement Finite Element Model for Regular Elements

The present hybrid displacement model essentially leads to matrix displacement method. In the basic formulation, the nodal displacements as well as the stress-intensity factors along the crack front were kept as unknowns and in the final system of algebraic equation they could be

solved for directly. But the direct solution for nodal displacements and the stress intensity factors posed problems of special solution procedure and was not easily adaptable for general purpose computer codes. As discussed in section 3 of previous chapter, by using a static condensation procedure, the so-called stiffness matrix of the singular element can be obtained. This procedure is basically used in view of easy adaptability and saving of otherwise longer computer time when special solution techniques are employed. While assuming the three field functions for a singular element, the corresponding three field functions for a regular element were also presented. The stiffness matrix for a regular element could be generated by the hybrid displacement finite element model, but such a method would consume much more computer time than would be used in developing the stiffness matrix of regular element through conventional displacement model. Especially when the stiffness matrices of a large number of regular elements must be generated, the hybrid displacement model would increase computer time enormously.

For an isoparametric quadrilateral compatible displacement finite element with twenty nodes along the boundary, the boundary displacements would be interpolated quadratically. From the assumptions of boundary displacements for a singular element, it is clear that the boundary displacements along the boundaries where the singular elements join the regular elements are also interpolated quadratically. Obviously, the regular elements developed by the conventional displacement method would be compatible with the singular elements in the present formulation, which is exactly the condition we are trying to enforce. Thus,

one can develop the stiffness matrices of singular elements along the crack front separately using the hybrid displacement model and combine them with the stiffness matrices of the rest of the structure, which are developed through the conventional compatible displacement model. Thus, the introduction of conventional compatible displacement model for regular elements will reduce the cost of computer usage.

The theoretical formulation of the conventional compatible displacement finite element model can be enumerated briefly as follows: the variational principle which governs the compatible displacement model is the principle of minimum potential energy for which the functional to be varied is

$$\pi_{CD} = \sum_{m=p+1}^{N} \left\{ \int_{V_m} \left(\frac{1}{2} E_{ijk\ell} \epsilon_{ij} \epsilon_{k\ell} - \bar{F}_i u_i \right) dV - \int_{S_{\sigma_m}} \bar{T}_i u_i dS \right\} \tag{4.50}$$

where all the notations are explained in section 1 of this chapter. The first variation of the functional π_{CD} with respect to the assumed interior displacement u_i results in the following equation

$$(E_{ijk\ell}\ \epsilon_{k\ell})_{,j} + \bar{F}_i = 0 \quad \text{in} \quad V_m \tag{4.51}$$

$$E_{ijk\ell}\ \epsilon_{k\ell}\ n_j - \bar{T}_i = 0 \quad \text{on} \quad S_{\sigma_m} \tag{4.52}$$

Equation (4.51) states that the stresses generated by the assumed interior displacements satisfy the local equilibrium equation and Equation (4.52) shows that the tractions generated by the assumed interior displacements are equal to the applied traction $\bar{T}_i$ on S_{σ_m}.

The discussions on the assumption of the interior displacement at any point within the element, the corresponding derivatives and the Jacobian were already given in section 1 of this chapter. Now the interior displacement $\{u_i\}$ can be expressed in terms of nodal displacements as

$$\{u_i\} = [U]\{q\} \tag{4.53}$$

The strains can thus be obtained as

$$\{\epsilon\} = [W]\{q\} \tag{4.54}$$

Substituting in Equation (4.52),

$$\pi_{CD} = \sum_{m=p+1}^{N} \left[\frac{1}{2} \lfloor q \rfloor \left\{ \int_{V_m} [W]^T[E][W]dV \right\} \{q\} \right.$$

$$\left. - \left\{ \lfloor q \rfloor \int_{V_m} [U]^T\{\bar{F}_i\}dV \right\} + \left\{ \lfloor q \rfloor \int_{S_{\sigma_m}} [U]^T[\bar{T}_i]dS \right\} \right] \tag{4.55}$$

$$\pi_{CD} = \sum_{m=p+1}^{N} \frac{1}{2} \lfloor q \rfloor [K]\{q\} - \lfloor q \rfloor [\{F_2\} + \{F_1\}] \tag{4.56}$$

where

$$[K] = \int_{V_m} [W]^T[E][W]\, dV \tag{4.57}$$

$$\{F_1\} = \int_{V_m} [U]^T\{\bar{F}_i\}\, dV \tag{4.58}$$

$$\{F_2\} = \int_{S_{\sigma_m}} [U]^T [\bar{T}_i] \, dS \tag{4.59}$$

and [E] is the elasticity constant matrix. By expressing the element nodal displacements $\{q\}$ in terms of independent generalized global displacements $\{q^*\}$ of the structure considered, the Equation (4.56) can be written as

$$\pi_{CD} = \frac{1}{2} \lfloor q^* \rfloor [K] \{q^*\} - [q^*] \{Q\} \tag{4.60}$$

where [K] and $\{Q\}$ are the global matrices after assembling the element matrices. The condition of minimum of π_{CD} with respect to $\lfloor q^* \rfloor$ in Equation (4.60) yields the following equation

$$[K] \{q^*\} = \{Q\} \tag{4.61}$$

Optimum Singular Element Size

It is a well known fact that the effects of singular behavior of stresses near the crack front in a cracked structure are predominant in a small but finite region, about five to ten percent of the crack length, around the crack front. Thus, for a finite element solution of crack problems, the singular stress and strain terms must be included in a finite region near the crack front. For the convergence study of regular elasticity problems, the element sizes of the problem can be reduced progressively and the convergence may be established [38]. However, in the case of singular elements, which are specially developed by incorporating singular stress and strain terms for analyzing the cracks in a structure, the element size should not be made progressively

smaller finally approaching to zero, because the singularity effect of stresses and strains will completely vanish; and the finite element solution will not converge to the correct stress intensity factor.

A study on the optimum size of singular element using the same hybrid-displacement finite element model for two-dimensional fracture mechanics was carried out by Nakagaki [67]. A centrally cracked tension plate was considered for this study with two singular elements and 22 regular elements. The conclusion of the above numerical experimentation was that the optimum size of the singular element is about ten percent of the half crack size. Strictly speaking, the optimum size of the singular element is problem dependent; and any definite general conclusion about the optimum size of the singular element cannot be reached. Such a thorough study on the convergence of the finite element solution for varying singular and regular element sizes is not carried out for the present three-dimensional fracture mechanics problems because it would be very expensive and is not the aim of the present investigation. However, the conclusion that the optimum size of the singular element is about ten percent of the half crack length is arrived at in the present investigation through numerical solution for simpler problems such as through-the-thickness cracks in tension specimen. For through-the-thickness straight crack problems and circular crack problems, the size of the singular element was kept as ten percent of the half crack length. For elliptical crack problems, the size of the singular element was kept as ten percent of the minor axis length of the ellipse. For computational ease the cross-section of the singular element in the plane which is perpendicular to the crack front

is constructed to be a square. Since the variation of stresses and strains is not singular in the direction along the crack front, the thickness of the singular element along the crack front is chosen according to the problem without any restriction. Because of the computer storage limitations, the total number of degrees of freedom and the total number of elements have to be kept as small as possible. Thus, for problems with simple geometries like through-the-thickness straight crack, the sizes of the regular elements are kept fairly large as can be seen by the element breakdown for straight crack problems. For problems with complicated geometries, the sizes of regular elements are varied as necessary for better accuracies in the finite element solution. Sizes of regular elements equivalent to that of singular element sizes are used near the singular elements and they are progressively increased away from the singular elements.

Determination of Stress Intensity Factor k_1 by Crack Opening Displacement (COD)

Apart from serving as one of the fracture criteria in linear as well as nonlinear fracture problems, the crack opening displacement (COD) can be utilized to evaluate the stress intensity factor k_1 by considering the displacements at the nodes near the crack tip. This method was used to estimate the stress intensity factor from the finite element solution by Kobayashi [28] and Pian et al. [44]. Kobayashi considered a node very close to the crack tip and Pian considered two nodes close to the crack tip and estimated the value of k_1. If the finite element solution for displacements reflects the true nature of

the singular behavior of stresses and strains around the crack tip, then the crack opening displacement would provide an accurate estimation of the stress intensity factor. The finite element solution obtained by using conventional model for crack problems requires very small element sizes at the crack tip, relatively larger degrees of freedom and does not incorporate the correct displacement behavior near the crack tip. Therefore this method cannot be expected to provide accurate estimation of stress-intensity factor evaluated by the crack opening displacement even at the nodal point closest to the crack front. Thus, for a more meaningful and accurate estimation of stress intensity factor through crack opening displacement procedure, the singular nature of the stresses and strains need to be incorporated or embedded in the finite element procedure. All the methods using special singular elements at the crack tip, including the hybrid-displacement model mentioned in Chapter II, possess the true nature of the singular behavior of the stresses and strains around the crack tip. Thus, the crack opening displacement procedure can be utilized very effectively to estimate the stress intensity factor from the displacement solution of the finite element models where special singular elements with a correctly embedded singularity are used.

As the present hybrid displacement model utilizes the correct asymptotic behavior of boundary displacements, the stress intensity factor can be estimated by using the displacements of five nodes on the crack surface close to the crack front. Refer to Figure 6b and assume that the singular element corresponding to the variation of θ from $\bar{\Lambda}/2$ to $\bar{\Lambda}$. As it can be seen from section four of this chapter the

boundary displacements on the crack surface ABFE ($\theta = \bar{\Lambda}$) are interpolated quadratically with $\sqrt{r}$ and the non-dimensional coordinate η. The boundary displacement u_z on the crack surface ABFE is written as

$$u_z = a_1 + a_2\sqrt{r} + a_3\eta + a_4 r + a_5\eta^2 + a_6\sqrt{r}\,\eta + a_7 r\eta + a_8\sqrt{r}\,\eta^2 \qquad (4.62)$$

and the values of $a_1,\ldots,a_8$ can be evaluated by substituting the nodal displacements of nodes 1, 2, 3, 9, 10, 13, 14 and 15. Now considering the displacements of the nodes relative to the displacements of the crack front, Equation (4.62) can be written as

$$u_z = a_2\sqrt{r} + a_4 r + a_6\sqrt{r}\,\eta + a_7 r\eta + a_8\sqrt{r}\,\eta^2 \qquad (4.63)$$

The nodal displacements of the five nodes 1, 2, 9, 13 and 14 which are close to the crack front can be used to evaluate the constants a_2, a_4, a_6, a_7 and a_8 of Equation (4.63).

From the asymptotic near field solution for displacements (Equation 1.9), for the crack surface where $\theta = \bar{\Lambda}$, we get

$$u_z = \frac{k_1 (2r)^{1/2}}{2\mu} (2 - 2\nu) \qquad (4.64)$$

We note, from the definition of stress-intensity factors in Equation (1.10), that they are defined for r tending to zero. Now equating Equations (4.63) and (4.64) and letting $r \to 0$, we obtain

$$\frac{k_1 \sqrt{2}\,(2 - 2\nu)}{2\mu} = a_2 + a_6\eta + a_8\eta^2 \qquad (4.65)$$

where η is the non-dimensional coordinate along the crack front varying

between -1 and +1. The crack opening displacement procedure thus yields an equation in which the stress intensity factor varies quadratically within an element along the crack front as seen by Equation (4.65). This method of estimation of stress intensity factor by crack opening displacement procedure has been found to provide an accurate variation of the stress intensity factor along the crack front. However, the difference in the stress intensity factors computed directly and computed through the crack opening displacement procedure is about two percent in the case of simple geometry problems like through the thickness central and edge cracks and about four percent in the case of problems with somewhat complicated geometries like inner surface flaw in a pressurized cylinder and elliptical cracks in a cube. As the crack front is divided into finite segments in the present method, the direct computation of stress-intensity factors would not be able to estimate the stress-intensity factors at edges such as the point of intersection of the crack front and the free surface. In such cases for all the problems solved by the present procedure, the method of crack opening displacement is used. Again, to emphasize the point, determination of stress-intensity factors is more meaningful only when the boundary displacements are interpolated by the correct type of interpolating functions.

CHAPTER V

SOLUTIONS OBTAINED BY HYBRID DISPLACEMENT FINITE ELEMENT MODEL

Introduction

The displacement hybrid finite element procedure developed here was used to solve for stress-intensity factors along the crack front for different kinds of problems, and the results are compared with existing numerical or exact solutions. The problems solved by this procedure can be enumerated as through-the-thickness edge and central straight cracks; buried, surface and corner elliptical cracks in finite specimens; outer and inner (pressurized and unpressurized) semi-elliptical surface flaws in an internally pressurized thick-walled cylinder; central crack specimen subjected to mixed mode (I, II and III) load; quarter-elliptical corner cracks near fastener holes in a finite specimen subjected to tension; and plates with semi-elliptical surface flaws subjected to bending and tension.

First the "singular elements" corresponding to straight crack problems were developed using the hybrid displacement finite element model. Some of the basic results which serve as checks of the singular element are presented in the next section of this chapter. Then the program was modified for the generation of stiffness matrix of singular elements for which the crack boundary is curved (for example, circular and elliptical singular elements). The "curved singular element" which was developed and checked for its accuracy was nevertheless found to

take more computer time than the straight singular element. Because of limited computer funds and a large number of problems which were sought to be solved, it was decided to use the straight singular elements for curved crack problems by approximating the curved boundary as closely as possible by piecewise linear segments. This idealization was shown to result in negligible errors in the solution of problems with known exact solutions such as buried circular and elliptical cracks in specimens subjected to uniform axial tension. Such an idealization is also widely used in literature, as for instance, in the boundary-integral equation solution procedure by Cruse [60].

The approximation of the curved boundary of crack (for a general ellipse) by straight segments is schematically shown in Figure 19a. A quarter of the cross-sectional view of the approximated crack boundary on the crack plane with the straight singular elements is given in Figure 19b. The cross-sectional area A'B'CD is again approximated to the area ABCD. In other words the stiffness matrix of the element with cross-section A'B'CD is approximated to the stiffness matrix of the element with cross-section ABCD. Away from the crack tip, no such approximation is made and isoparametric elements are used.

The singular elements generated by the straight segmented crack front program were used to solve a problem of an embedded 1" radius circular crack in a 10" x 10" x 10" cube specimen (see Figure 20). Figure 21 shows the finite element model. The results obtained for the above-mentioned embedded circular crack problem were in excellent agreement with the exact solution of an embedded circular crack in an infinite solid (see Figure 22). This result is presented in Figure 23

corresponding to a/b = 1. The 3 percent higher value of the result could be accounted by the "finite width" effect of the specimen.

The same problem was also solved by using curved (circular) singular elements and the results obtained were very close to the results obtained by using straight segmented crack front singular elements.

Some Basic Singular Element Results

Before using the singular element stiffness matrices to solve any practical structural problem, they were checked for certain characteristics. Corresponding to the rigid body translation and rotation, the stiffness matrices of the singular elements as well as regular elements should satisfy the equilibrium conditions. Such a check proved that the singular elements and regular elements satisfy the equilibrium condition very well, and the nodal residual forces in the equilibrium check were of about 10^{12} order less than the diagonal terms in the stiffness matrix. The matrix used for the singular element check is the statically condensed stiffness matrix explained in Section 3 of Chapter III.

Next a single singular element, for instance the element with $0 \leq \theta \leq \bar{\Lambda}/2$ in Figure 2, was considered. The relevant equations for this single element under the present method, are

$$\begin{bmatrix} K_1 & K_2^T \\ K_2 & K_3 \end{bmatrix} \begin{Bmatrix} \underset{\sim}{q} \\ \underset{\sim}{k} \end{Bmatrix} = \begin{Bmatrix} \underset{\sim}{Q} \\ 0 \end{Bmatrix} \tag{5.1}$$

where $\underset{\sim}{q}$ are the 60 nodal displacements, $\underset{\sim}{k}$ the three elastic stress intensity factors and $\underset{\sim}{Q}$ the equivalent nodal forces. For this singular element, element nodal displacements were first computed from the known analytical asymptotic solution viz., Equation (1.0) corresponding

to a hypothetical mixed mode loading which generate the stress intensity factors to be $k_1 = k_2 = k_3 = 1.0$. Using these $\underset{\sim}{q}$ as input conditions, from the numerically generated matrices K_2 and K_3, the results for k_1, k_2 and k_3 were computed from the second equation of Equation (5.1). The computed results were

$$k_1 = 1.050; \quad k_2 = 0.979; \quad k_3 = 0.998 ,$$

which compare favorably with input values $k_1 = k_2 = k_3 = 1.0$. Corresponding to asymptotic stress field of Equation 1.8, with input values $k_1 = k_2 = k_3 = 1.0$, the equivalent nodal loads $\underset{\sim}{Q}$ were also computed. Using the input values of $\underset{\sim}{q}$, and the computed $\underset{\sim}{k}$'s as in second equation of Equation 5.1, the left hand side of first equation of Equation 5.1, was computed and compared with the right hand side input values of $\underset{\sim}{Q}$. This comparison was found to be good to a third digit accuracy. The above procedure was repeated for the other three singular elements ($\bar{\Lambda}/2 \leq \theta \leq \bar{\Lambda}$, $-\bar{\Lambda}/2 \leq \theta \leq 0$, $-\bar{\Lambda} \leq \theta \leq \bar{\Lambda}/2$) and the above mentioned checks were made and the corresponding results are given below (in the same order).

$k_1 = 0.960$	$k_2 = 1.026$	$k_3 = 0.995$
$k_1 = 1.047$	$k_2 = 1.016$	$k_3 = 0.998$
$k_1 = 0.996$	$k_2 = 1.027$	$k_3 = 0.995$

As another check, the four element assembly as shown in Figure 5 and discussed in section 3 of Chapter III, was considered. The displacement at the nodes on the boundary of this four element assembly were computed from the known analytical solution, Equation 1.9, with

hypothetical input values $k_1 = k_2 = k_3 = 1.0$. Using the equation similar to second equation of Equation 5.1 above for this four element assembly, the numerical solution for $\underset{\sim}{k}$ were computed, which are

$$k_1 = 0.978 \qquad k_2 = 1.005 \qquad k_3 = 0.997$$

The internal nodal forces were then computed from the left hand side of an equation similar to first equation of Equation 5.1 and were compared with the external nodal forces $\underset{\sim}{Q}$ computed from the asymptotic stress field with input values $k_1 = k_2 = k_3 = 1.0$. This comparison was also good to a third digit accuracy.

The Problems Solved by the Hybrid-Displacement Finite Element Model

Through-the-Thickness Straight Cracks in a Finite Specimen

Introduction. One of the basic problems in the field of fracture mechanics is the solution of a through-the-thickness straight crack in a finite specimen subjected to pure mode I loading. As mentioned earlier, extensive work has been carried out for two-dimensional modelling of such problems. The three-dimensional solution for through-the-thickness straight crack problem was presented by Sih et al. [59] using special elements at the crack tip. Tracey [56] also developed special elements at the crack to solve the through-the-thickness straight crack problems. The stress-intensity factor k_1 was obtained by using crack opening displacements by Tracey. The present hybrid finite element model was used to solve through-the-thickness central and edge crack problems and the results of the variation of normalized stress-intensity factors along the crack front are presented.

The Problem. The description of the geometric parameters of the four through-the-thickness straight crack problems is given below.

1. A slab of 8" x 4" x 1" (and .6") with a central crack of length 4". (Figure 7a).
2. A slab of 10" x 10" x 1" with a central crack of length 4" (Figure 7b).
3. A slab of 4" x 8" x 1" with an edge crack of length 2" (Figure 7c).
4. A slab of 1.25" x 1.2" x 0.75" (Figure 7d).

The material properties are given in the respective figures where the solutions are presented. In the first three problems, the external applied loads are uniform tension (σ_{zz} = 1 psi) and in the fourth problem, the specimen is pulled by the line load of P = 1000 lb/in. as shown in the figure. Because of symmetry, either one eighth (for central crack problems) or one fourth (for edge crack problems) of the structure needs to be considered. The finite element breakdown for the first three problems is given in Figure 8 and for the fourth problem in Figure 9. The total number of degrees of freedom and the total number of elements are 1218 and 60 for the first breakdown and 1476 and 75 for the second breakdown. By applying the boundary conditions appropriately on faces ABCD, ADHE and ABFE, either central or edge crack problems could be generated using the same configuration.

Results and Discussions. The numerical solution for the first problem was carried out and the variation of normalized stress-intensity factor along the crack front is presented in Figure 10. The computation of stress-intensity factors was done by using four different

methods. Curve 1 corresponds to the solutions obtained by using the singular elements formulated by the present hybrid displacement finite element model. Curve 2 corresponds to the solution obtained by crack opening displacement procedure described in the previous chapter. As mentioned before, this method yields an equation in which the stress-intensity factor at the crack tip (i.e., by taking lim r→0) is quadratically varying within each element. In analyzing this problem, the predictions by Sih [68], that the stress intensity factor k_1 approaches zero at the point where the crack intersects the free surface and that a thin boundary layer is expected at the free surface across which the stress-intensity factor varies rapidly, is noted.

Also, the recent prediction of Folias [89] and Benthem [90] regarding the structure of singularity near the point of intersection of the crack front with the flat free surfaces of the specimen are kept in mind. However, since the present procedure relies on building-in a known singularity in special elements, the present results cannot be expected to shed any new light on the controversy in the works of [89,90]. However, once this controversy is resolved and the structure of singularity near the free surface is resolved, it is an easy task to extend the present procedure to build in such singularities in elements near the free surface. For the above reason it cannot also be expected that the present finite element solution will naturally yield a vanishing k_1 at the free surface, but such a condition can be imposed in the present procedure. Two methods have been used to make the stress intensity factor to assume zero values at the free surface. One simple, but crude, way is to use a thin "regular" element at the

free surface, which would automatically correspond to zero k_1 since there is no embedded singularity. Strictly speaking these elements would not be compatible at the interelement boundary of neighboring element which is singular. But the computation was carried out and the result is given by the curve 3. The second method was to use the singular elements as such, but to force the stress intensity factors to be zero during the solution of algebraic equations. The result is represented by curve 4. This method of forcing stress-intensity factors to be zero at the free surface is rather unnatural. By studying the solution by first method, it could be easily noted that the stress-intensity factor has a tendency to droop down and they may go to zero as shown by the dotted line. A two-dimensional, plane strain, analysis of the identical problem geometry was carried by the program developed in [67]. The thus obtained result for normalized intensity factor of 1.95 agrees well with a corresponding result of 1.96 reported by Sih et al. [59]. The variation of the stress intensity factor across the plate thickness, for two different values of thickness reported by Sih et al. [59] are also reproduced. It is noted that the present values are about three to five percent higher than the 2-D result whereas the results of Sih et al. are about 10-11 percent higher than the 2-D result, at the center of the plate. An identical problem with 0.6" thickness was also solved and the result was so close to that of 1" thickness problem, it could not be marked in the figure. It is also noted that the SIF drops by about ten percent at the free surface of the specimen in this problem as well as the other straight crack problems.

The next problem is also a centrally cracked specimen with different dimensions as shown in Figure 7b. The result of the variation of normalized stress-intensity factor along the crack front is shown in Figure 11. The corresponding two-dimensional plane strain value of stress intensity factor was also obtained from Reference [67] and the three-dimensional value at the midsurface is about five percent higher than the 2-D value. The third problem is that of an edge crack in a finite specimen as shown in Figure 7c, and the result is presented in Figure 12 and the comparative 2-D plane strain value is also marked. The fourth problem is a problem of a compact specimen which is a typical specimen used in experimental fracture mechanics and is shown in Figure 7d. The finite element breakdown is slightly different from the previous ones and the breakdown is shown in Figure 9. The variation of the stress intensity factor across the thickness and the corresponding 2-D plane strain value computed by using Bucci's [69] empirical formula are presented in Figure 13.

Mixed Mode Problem

Introduction. Another interesting problem is the three-dimensional analysis of a finite specimen subjected to combined mode I, mode II and mode III loading conditions. Two dimensional analysis of mixed mode I and mode II loading condition has been carried out by several investigators, for example, Atluri et al. [42] and Pian et al. [44]. However, the solution of mixed mode I, mode II and mode III fracture problem does not exist in open literature. The hybrid finite element model developed in the present investigation was used to solve one such mixed mode problem and the results are presented here.

The Problem. The geometric dimension of the mixed mode problem considered here is given in Figure 14 along with the applied loads. The finite element breakdown for the present analysis is given in Figure 15. This breakdown consists of 2016 total degrees of freedom. Because of large number of degrees of freedom, the total number of elements along the crack front was limited to two and the total number of elements are 96. The Poisson's ratio was taken to be 0.3.

Results and Discussions. The variations of the three stress-intensity factors k_1, k_2 and k_3 for the mixed mode problem are given in Figure 16, 17 and 18 respectively. Since there is only one element along the crack front for half the thickness of the specimen, the three curves represent a quadratic variation of stress-intensity factors, as they were obtained from crack opening displacement procedure discussed previously. The solution of the mixed mode problem may be compared with the solution of the through-the-thickness central crack problem given in Figure 7a as they have the identical dimension. Comparing them with a two-dimensional plane strain value of 1.96, the k_1 value is of comparable accuracy in both cases. Assuming the finite width effect as same, the values of k_2 and k_3 are about 10 percent and 8.5 percent higher, respectively, at the midsurface. The qualitative feature being same as in other straight crack problem, the SIF drops by about 10 percent at the free surface as it can be seen from the figures.

Elliptical Cracks in Finite Specimen

Introduction. The problem of computing stress-intensity factors for elliptical crack in a three-dimensional finite space is a formidable

one, with analytical solutions being limited to simple embedded crack geometries in an infinite space. The problems of embedded circular or elliptical flaws near a free surface have been studied using the Schwarz-Neumann alternating technique by Smith et al. [70] and Shah et al. [71]. Part circular and semi-elliptical cracks intersecting with a free surface ("surface cracks") have also been studied by Hartranft et al. [72] and Kobayashi et al. [64] using the alternating technique. Treatment of embedded, surface and corner flaws through the boundary-integral method have been presented by Cruse [60] for mode I type problems. The procedure used by Cruse is to reduce 3-D problem to a 2-D boundary integral equation with a finer surface element breakdown near the crack front. The mode I stress intensity factors were then obtained from the computed crack opening displacements. In the present section, results of variation of stress-intensity factors along the crack for various embedded, surface and corner crack problems are presented.

The Problem. The first problem corresponds exactly to the same problem solved by Cruse [60] using the boundary-integral equation procedure. The specimen dimension is 2H x 2H x 2H, H = 5". The area of the quarter ellipse, viz., ($\bar{\Lambda}/4$ ab) is kept constant as $\bar{\Lambda}/4$, thus ab = 1 and the aspect ratio (a/b) is varied from 0.25 to 4, as shown in Figure 20. The Poisson's ratio ν is assumed to be 0.3 in all the three cases namely buried, surface and corner crack problems. Because of symmetry, only one eighth of the specimen needs to be considered and the finite element breakdown is shown in Figure 21. The number of total elements and the total number of degrees of freedom for this breakdown are 156 and 2670 respectively. The exact solution for a

buried elliptical crack in an infinite solid is displayed in Figure 22 for convenience, as we need them for comparison purposes. The present finite element procedure was also used to solve two other semi-elliptical surface flaws, a semicircular surface flaw and a part circular surface flaw problem. The dimensions of these problems are presented along with the results and the Poisson's ratio is assumed to be 0.3.

Results and Discussions.

(a) Buried Elliptical Cracks in a Finite Specimen. The numerical solutions of SIF obtained for the buried elliptical cracks in a finite specimen for aspect ratios, 1, 1.5, 2.0 and 4.0 are shown in Figure 23. We note that the normalizing factor used in Figure 23 is the exact K_I solution for buried circle of radius b, in an infinite solid, viz., $K_I = \frac{2}{\pi}\sqrt{\pi}b$. The corresponding exact solutions for an infinite-domain are also shown in Figure 23 for various (a/b) ratios. It is seen that when (a/b) = 4. (and corresponding a/H = .4 and b/H = .1) the finite width correction is about 25 percent at the ellipse major axis location ($\varphi = 0$) and this correction drops to about +5 percent near the minor axis location ($\varphi = 90^{\circ}$) where the actual stress-intensity is maximum. These finite width corrections reduce progressively as (a/b) decreases, and when (a/b) = 1 (buried circular crack) the finite width correction factor is +3 percent. We note that the boundary integral method by Cruse for the same problem yields little or no finite width corrections to the infinite domain solutions for all aspect ratios. Part of this discrepancy from Cruse's results is due to the fact that the solutions obtained by BIE method were normalized with respect to the numerical solution, obtained again through BIE method, for the buried circular crack. However, it appears that in the solutions obtained by

him, the numerical solution of the buried circular crack was eight to ten percent lower than the corresponding infinite-domain solution. The solutions for the aspect ratios 0.667, 0.5 and 0.25 are identical as the solutions for the aspect ratios 1.5, 2.0 and 4.0 respectively with the elliptical angle φ being replaced by $\bar{\Lambda}/2 - \varphi$.

(b) Semi-elliptical Surface Flaws in a Finite Specimen. The K_I variations for the semi-elliptical surface cracks, for various a/b ratios, normalized with respect to the exact solution of a buried elliptical crack of the same aspect ratio and in an infinite solid, are shown in Figure 24. Unfortunately, in varying a/b ratio, because H and ab were kept constant, the depth ratio b/H (and hence a/H) also varied continuously. It is seen that for a/b = 4 (a/H = .4 and b/H = .1) the maximum stress intensity magnification occurs near the free surface. This free surface stress intensity magnification factor decreases continuously as the ratio a/b is decreased. At a/b = 1 (semi-circular surface flaw) the obtained solution is found to agree well with Kobayashi's [64] solution. It is interesting to note that as a/b becomes less than 1, the maximum stress intensity magnification occurs at the point of deepest penetration, rather than at the free surface. It is seen from Figure 24, that for a/b = 0.25 (a/H = .1; b/H = 0.4), i.e., when the crack depth is 40 percent of the specimen thickness the stress intensity magnification at the deepest penetration is about 17 percent higher than that of the free surface. The results obtained by Cruse [60] for identical problem of semi-elliptical surface flaws using BIE method is reproduced separately in Figure 25 for comparison purposes. As it can be seen from Figure 24 and

Figure 25, the present results are significantly different from those of Cruse. To explain these discrepancies, the following checks have been made. For the case of a narrow and deep surface flaw with $a/b = 0.25$, it may be expected that the K_I value in the neighborhood of the free surface (near $\varphi = 0$) approaches that of a through the thickness central crack with problem dimension $2H \times 2H$ and the crack length $2a$. This can be treated as a two-dimensional infinite domain problem with a central crack of length $2a$ and the corresponding K_I value can be computed as $\sigma_o\sqrt{\pi a} = 1.2533$ psi $\sqrt{\text{in.}}$ for $\sigma_o = 1$ psi. The corresponding computed values from the present method and Curse's BIE method are 1.3002 and 1.5220 respectively. Similarly for the case of surface flaw $a/b = 4.0$, it may be expected that the K_I value in the neighborhood of the deepest penetration (near $\varphi = 90^o$) approaches that of a through the thickness edge crack with the specimen dimension $H \times 2H$ and a crack length of b. For such an edge crack, the value of K_I for an infinite domain (since $b/H = .1$) can be computed as $1.1212\ \sigma_o\sqrt{\pi b} = 1.4056$. The computed results for the corresponding K_I values from the present and Cruse's BIE method are 1.2561 and 1.1928. It can be seen from the above comparison of results with the expected values of K_I, the present method yields closer values than the BIE method. Another interesting fact to note in these two results is that when the ratio of crack depth to the specimen thickness decreases then the ratio of the actual stress intensity factor to the exact stress intensity factor of buried crack should also decrease. When the aspect ratio a/b is decreased from 4.0 to 0.25, the ratio of crack depth to the sepcimen thickness decreases from 0.4 to 0.1 at $\varphi = 0^o$ and increases from 0.1 to

0.4 at $\varphi = 90^{\circ}$. Thus, for decreasing values of aspect ratio a/b, one can expect decreasing values of stress intensity magnification factor (denoted by $K_{ELL.SUR}/K_{ELL.BUR.EXACT}$) at $\varphi = 0^{\circ}$ and increasing values of stress intensity magnification factor at $\varphi = 90^{\circ}$. The present result seems to substantiate this fact at both the ends whereas the result by BIE fails to do so at the deepest penetration, i.e., at $\varphi = 90^{\circ}$.

(c) Quarter-Elliptical Corner Cracks in a Finite Specimen. The K_I variations for quarter-elliptical corner cracks in a finite specimen, normalized again with respect to the exact solutions of buried elliptical cracks in an infinite domain, are shown in Figure 26 for aspect ratios a/b = 4.0, 2.0, 1.5, and 1.0. Once again, it is seen that the maximum stress intensity magnification factor occurs near the point of intersection of the major axis of the ellipse, the crack front and the free surface as may be expected. This maximum stress intensity magnification factor drops as a/b ratio decreases, until when a/b = 1, this quantity is the same at both points of intersection of the crack front with the free surfaces. The result by the BIE method for identical problems is given in Figure 27. Once again, the present results differ significantly from those by Cruse [60]. But the trends in the present solution seems to follow the expected tendencies as in the case of semi-elliptical surface flaws in a finite specimen. The solutions for the aspect ratios 0.667, 0.5 and 0.25 are identical as the solutions for the aspect ratios 1.5, 2.0 and 4.0 respectively with the elliptical angle φ being replaced by $\bar{\Lambda}/2 - \varphi$. However, one reason for the discrepancy may be the particular normalization procedure, mentioned earlier, that is used by Cruse [60].

(d) Surface Flaw Problems. Numerical solutions using the present formulation were also obtained for four other surface problems. The dimensions of the structure and crack geometries are given in Figure 28. The finite element breakdown for these problems are exactly similar to that given in Figure 21. The Poisson's ratio was assumed to be 0.3 and the total degrees of freedoms and total number of elements were 2670 and 156 respectively:

The geometries of the four problems are given below.

1. Semi-circular crack

$$\frac{a}{c} = 1.0; \quad \frac{a}{t} = 0.2; \quad \frac{H}{W} = 2.0; \quad \frac{W}{c} = 5.0$$

2. Part-circular crack

$$\frac{a}{c} = 0.5; \quad \frac{a}{t} = 0.7; \quad \frac{H}{W} = 2.0; \quad \frac{W}{c} = 5.0$$

3. Semi-elliptical crack

$$\frac{a}{c} = 0.5; \quad \frac{a}{t} = 0.25; \quad \frac{H}{W} = 2.0; \quad \frac{W}{c} = 5.0$$

4. Deep semi-elliptical crack

$$\frac{a}{c} = 0.5; \quad \frac{a}{t} = 0.75; \quad \frac{H}{W} = 2.0; \quad \frac{W}{c} = 5.0$$

The solution for the semi-circular surface crack problem is given in Figure 29. This problem is identical to the problem of semi-circular crack (a/b = 1) in Figure 24, expect that the length of the specimen in the present case is twice that of the problem in Figure 24.

The comparison of the present problem with that of Figure 24 shows that the stress intensity magnification factor dropped throughout, by about five percent at the free surface and about two percent at the deepest penetration. The result in Figure 29 was normalized with respect to the exact solution of a buried circular crack in an infinite solid. Figure 30 shows the solution of a part-through circular crack, the dimensions of which were given already. The radius of the part-through circular crack can be computed as 1.25 c. The result was normalized with the solution of an embedded circular crack of radius 1.25 c in an infinite space. It can be seen from Figure 30 the stress intensity magnification is higher at the deepest penetration than at the free surface. The stress intensity factor for the part through circular crack behaves somewhat similar to an elliptical crack of similar dimensions. Figure 31 depicts the variation of K_I solution of the semi-elliptical and deep semi-elliptical surface cracks normalized with corresponding exact solutions of embedded elliptical cracks in an infinite solid. With all the other geometric parameters kept constant, only the ratio of crack depth to specimen thickness was changed between these two problems and one could easily see the effect of higher stress intensity magnitification throughout for deeper semi-elliptical crack. The stress intensity magnification increases by about 20 percent at the free surface and by about three percent at the deepest penetration.

Inner Surface Cracks in an Internally Pressurized Cylinder

Introduction. A surface crack geometry which is commonly encountered in a pressurized cylinder is a semi-elliptical crack which would be either pressurized by the fluid inside the cylinder or remain

unpressurized due to blockage of the fluid by a bladder, scale or dust. Due to difficulties in three-dimensional analysis, semi-elliptical surface cracks in a cylinder have not been studied thoroughly but the two-dimensional counterpart of these two fracture problems has been studied by several investigators. For example, Bowie and Freese [73] and more recently Clifton et al. [74] studied pressurized inner cracks in a pressurized cylinder. Also approximate three-dimensional solutions for a pressurized inner semi-elliptical crack in a pressurized cylinder was considered by Underwood [75]. Another approximate solution for unpressurized inner and outer semi-elliptical crack in a pressurized cylinder was obtained by Kobayashi [76].

In a recent series of papers [63,77,78] Kobayashi, et al. estimated the stress intensity factors of unpressurized and pressurized semi-elliptical cracks in pressurized as well as thermally shocked cylinders where shallow as well as deep surface flaws were considered. In these analyses, stress intensity factors of semi-elliptical cracks in flat plates with appropriately prescribed hoop stresses were modified with curvature correction factors obtained from their two-dimensional analogs. Although these estimates were found to be relatively accurate for many crack and cylinder *geometries*, the estimate is questionable for deeper cracks because they do not take account of the effects of outer cylindrical surface in the analysis.

A natural solution procedure for three-dimensional fracture mechanics is the use of three-dimensional finite element method. Unfortunately, application of three-dimensional finite element method to problems involving surface cracks in cylinders is still limited at

this time, despite increasing access of conventional three-dimensional finite element codes, due to limitations in computer capacity and computing costs. The only three-dimensional finite element solution to either of the two problems under consideration is that of Blackburn and Hellen [79] who used the procedure of virtual crack extension and conventional three-dimensional finite element code to compute stress intensity factors of a pressurized inner semi-elliptical crack and unpressurized outer semi-elliptical crack in a pressurized cylinder with an outer-to-inner radius ratio of $R_o/R_i = 1.461$. In a similar analysis, Ayres [80] used the condensed quarter-point element in a finite element program to compute the transient stress intensity factor of two semi-elliptical cracks in thermally shocked cylinder with $R_o/R_i = 1.90$.

The above brief review of available two-and three-dimensional solutions of the two practical problems mentioned abouve indicates the need for more accurate three-dimensional analysis of surface cracks in a pressurized cylinder, particularly for deep surface flaws in thick walled cylinders because in the above-mentioned region a mere curvature correction factor to the corresponding flat plate solution may be inadequate in modeling a complex three-dimensional problem.

The Problem. The problems considered are that of pressurized and unpressurized inner surface cracks in a pressurized thick walled cylinder, the dimensions of which are shown in Figure 32. In the finite element simulation of this three-dimensional problem, the length of the cylinder was taken to be $L/2a$ (and L/R_o) ≥ 3. To account for end condition of the cylinder, stress σ_{zz}, corresponding to plane strain

condition, viz., $\sigma_{zz} = -\nu(\sigma_{RR} + \sigma_{\varphi\varphi})$ (where R and φ are polar coordinates in the cross-section of the cylinder) were imposed on the faces. Because of symmetry, only a quarter of the cylinder was modelled by finite elements. The finite element mesh that is used is shown in Figure 33, and consists of 156 elements and 2670 total degrees of freedom. Several problems were solved with different dimensions and the dimensions of each problem are given in the corresponding figures (Figures 34 to 39).

Results and Discussions.

(a) Deep Inner Semi-Circular Flaw in Pressurized Thick-Walled Cylinders. The variation of the stress-intensity magnification factor for an unpressurized, deep, inner semi-circular crack with geometric parameters, ($b/a = 1.0$; $R_o/R_i = 2$; $b/(R_o-R_i) = 0.8$) is shown in Figure 34. The computed stress-intensity factor variation is normalized with respect to the exact solution of an embedded circular flaw, in an infinite medium, the faces of which are acted on by a uniform pressure, σ_o, equal to the hoop stress at the inner face of the cylinder due to internal pressure, $p = P_i$. Thus

$$\sigma_o = P_i \left\{ \frac{(R_o/R_i)^2 + 1}{(R_o/R_i)^2 - 1} \right\} \qquad (5.2)$$

It is seen that the maximum stress-intensity magnification (and thus stress intensity itself) for the present deep semi-circular crack occurs at the front surface ($\theta = 0$) and the stress intensity decreases continuously with increasing θ, except for a slight dip near $\theta \approx 75^\circ$.

For comparison purposes, the estimated results of Kobayashi, et al. [78] for a nearly semi-circular flaw (b/a = 0.98) but with same values ($b/(R_o-R_i) = 0.8$ and $R_o/R_i = 2$) are also shown in Figure 34. As noted earlier, References [63, 77, 78] estimate the stress intensity factors for cracks in pressurized cylinders from the solution for SIF for cracks in flat plates (where the crack faces are subjected to normal stress of variation identical to the hoop stress in cylinder) by multiplying them with "curvature correction factors" obtained from two-dimensional analogs of the same problem.

For the present deep semi-circular flaws in a thick walled cylinder, the above "curvature correction factors" can be seen to be the most severe. As seen from Figure 34, the estimates of Kobayashi [78] agree reasonably well (with an error within five percent) with the present direct computation using a fully three-dimensional analysis for this particular problem.

SIF variation for pressurized deep semi-circular flaw in pressurized cylinder ($b/a = 1.0$, $R_o R_i = 2$; $b/(R_o - R_i) = 0.8$) is shown in Figure 35. The value of σ_o used in the normalization procedure is

$$\sigma_o = P_i \frac{2R_o^2}{R_o^2 - R_i^2} \tag{5.3}$$

which corresponds to the sum of hoop stress at R_i corresponding to P_i acting on the inside of cylinder, and the pressure P_i acting on the crack surface. It is seen that in this case also, the maximum SIF occurs at the front surface ($\theta = 0^o$) and the SIF decreases continuously with θ, has a dip at $\theta \approx 60^o$, and again rises slightly at $\theta = 90^o$

(deepest penetration). For this particular case of pressurized crack also it is seen that the estimates of Kobayshi [78] agree within six percent, with the present three-dimensional finite element analysis. It is also seen from Figure 34 and Figure 35, pressurization of the crack surface causes the stress-intensity magnification factor at the front surface ($\theta = 0^{\circ}$) to rise by about six percent.

(b) Inner Semi-Elliptical Flaw ($b/a = 0.5$) in Pressurized Thick-Walled Cylinder. Results for stress intensity magnification factor variation for an unpressurized semi-elliptical flaw ($b/a = 0.5$; $R_o/R_i = 2$; $b/(R_o-R_i) = 0.5$) at the inner surface of a pressurized cylinder is shown in Figure 36. These magnification factors are normalized with respect to the local SIF of a completely embedded elliptical crack in an infinite medium, pressurized by a stress σ_o as in Equation 5.2. As a result, despite an almost monotonic decrease with θ in the stress intensity magnification factor, the actual stress intensity factor at $\theta = 0^{\circ}$ is only slightly higher (by 15 percent) than that at the point of deepest penetration, $\theta = 90^{\circ}$. Results for stress-intensity magnification for a semi-elliptical crack of identical geometry, but with additional crack surface pressurization is shown in Figure 37 wherein σ_o that is used in normalization corresponds to Equation 5.3. Comparing Figure 36 and Figure 37, it is seen that pressurization of crack surface causes the stress intensity magnification factor to increase at all θ locations, by about four percent at $\theta = 0^{\circ}$; and about 13 percent at $\theta = 90^{\circ}$. However, for the pressurized semi-elliptical crack, the actual SIF at $\theta = 0^{\circ}$ is only eight percent higher than at $\theta = 90^{\circ}$.

(c) Inner Semi-Circular Flaw in Pressurized Cylinders. Another example that is considered is an intermediate depth semi-circular crack, $b/a = 1$, $b/(R_o-R_i) = 0.5$, $R_o/R_i = 2$ and is compared with the previous case of a deep-circular crack, $b/a = 1$, $b/(R_o-R_i) = 0.8$ and $R_o/R_i = 2$. The stress intensity magnification factor for the case of an unpressurized crack, with σ_o used in normalization being taken as in Equation 5.2, is shown in Figure 38, which has the same qualitative features as for the deep crack $b/(R_o-R_i) = 0.8$ as shown in Figure 34, with the stress intensity magnification factor at the front surface ($\theta = 0^o$) increasing with depth ratio $b/(R_o-R_i)$. The stress intensity magnification for the case of a pressurized crack (with σ_o used in normalization being taken as Equation 5.3) is shown in Figure 39, which has the same qualitative features as for the deep crack as shown in Figure 35, with the stress intensity at the front surface increasing with depth ratio.

(d) Oblong Inner Semi-Elliptical Flaw in Pressurized Cylinder. An oblong inner semi-elliptical flaw in a pressurized cylinder with geometric parameters $b/a = 0.2$, $b/(R_o-R_i) = 0.8$, $R_o/R_i = 1.5$, with and without crack surface pressure are also solved and the result are presented in Figure 40. The values of σ_o used in normalization procedure are again given by Equations (5.2) and (5.3). The results of this problem are significantly different from that of the solutions estimated by Kobayashi et al. [63]. For an unpressurized semi-elliptical inner crack in a pressurized cylinder, the estimated value of stress intensity magnification factor at the free surface ($\theta = 0^o$) is 1.26 and at the deepest penetration ($\theta = 90^o$) is 1.19. Though the present result is

almost close at the deepest penetration point, the value at the free surface ($\theta = 0^{\circ}$) is about 1.7 times higher than that of Kobayashi's estimation. It can also be seen from Figure 40, the stress intensity magnification increases at all θ values for pressurized crack surface problems. In order to check the present results, since it is significantly different from Kobayashi's result, the problem of pressurized inner semi-elliptical crack in a pressurized cylinder was solved again by removing the stress $\sigma_{zz}(= -\nu\ (\sigma_{RR} + \sigma_{\varphi\varphi}))$ which was applied to simulate the plane strain condition and enforcing the plane strain condition through suppressing the displacements at corresponding faces. The results obtained for this case is also shown in Figure 40 in dotted line. As it can be seen from the figure, the result is very close to the result obtained by enforcing the plane strain condition through the stress $\sigma_{zz} = -\nu(\sigma_{RR} + \sigma_{\varphi\varphi})$. The reason for such large discrepancy of result may be attributed to the estimation of curvature correction factor for oblong semi-elliptical cracks. Another reason might be, though it gave good comparison in the case of deep semi-circular surface flaw, that in the case of "deep", "oblong" semi-elliptical cracks, the estimation may be questionable, because the procedure used by Kobayashi does not study and consider the effect of outer cylindrical surface. (Kobayshi obtains the solution for the semi-elliptical surface flaw in a flat plate, one of the solutions needed in his estimation procedure, using the alternating method. The short-comings of this solution are discussed later). Though the SIF are computed directly in the present procedure, at the end points ($\theta = 0^{\circ}$ and $\theta = 90^{\circ}$) they are computed by COD method as described in previous chapters. The

actual SIF at $\theta = 0^{o}$ is 13 percent smaller than at $\theta = 90^{o}$.

Outer Surface Cracks in an Internally Pressurized Cylinder

Introduction. Another important problem in pressure vessel and pipeline industries is the presence of a semi-elliptical surface flaw on the outer surface of an internally pressurized cylinder. As in the case of inner surface cracks in an internally pressurized cylinder, only limited amounts of work is available with three-dimensional analysis for outer surface cracks in an internally pressurized cylinder. Kobayashi et al. [78] solved this problem also by "correcting" the flat plate solution, obtained through the alternating method, by "curvature-correction factors" estimated from two-dimensional analogs. Again the only three-dimensional solution for the above problem using the virtual crack extension and the conventional finite element method is that of Blackburn and Hellen [79]. In their analysis of an unpressurized outer semi-elliptical crack, the outer-to-inner radius ratio was taken to be 1.461. Thus a more accurate three-dimensional analysis is needed for outer surface cracks in a pressurized cylinder also.

The Problem. Figure 41 shows the dimensions of the unpressurized outer surface cracks in a pressurized thick walled cylinder. Similar to the case of inner surface cracks in a pressurized cylinder, the length of the cylinder for this case also was taken to be $L/2a$ (and L/R_o) ≥ 3 and a stress $\sigma_{zz} = -\nu(\sigma_{RR} + \sigma_{\varphi\varphi})$ was imposed on the ends of cylinder to account for the plane strain condition. The finite element breakdown for one fourth of the cylinder is given in Figure 42. There are 156 elements in the breakdown and the total number of degrees of freedom is 2670.

Results and Discussions

(a) Outer Semi-Elliptical Flaw in Pressurized Thick-Walled Cylinder. The results of the variation of K_I for an unpressurized outer semi-elliptical crack with geometric parameters, ($b/a = 0.6$; $R_o/R_i = 1.5$ and $b/(R_o-R_i) = 0.4$) is shown in Figure 43. The stress intensity factor variation is normalized with respect to the closed form solution of an embedded elliptical flaw in an infinite space, the faces of which are acted on by a uniform pressure, σ_o, equal to the hoop stress at the outer face of the cylinder due to internal pressure $p = P_i$. Thus

$$\sigma_o = P_i \frac{2 R_i^2}{R_o^2 - R_i^2} \tag{5.4}$$

The results estimated by Kobayashi [78] for an identical problem and by Blackburn [79] for slightly different geometry ($R_o/R_i = 1.461$ whereas in the present case $R_o/R_i = 1.5$) are also given in Figure 43. Again, as in the case of inner surface cracks, the computed stress intensity magnification factor is maximum at the front surface ($\theta = 0^o$) and the magnification factor decreases continuously with increasing elliptical angle θ. The actual stress intensity factor at $\theta = 0^o$ is only about 1.5 percent lower than the SIF at $\theta = 90^o$. As it can be seen from Figure 43, the comparison of the present direct computation method with that of Kobayashi's [78] and Blackburn's [79] solution, the present result agrees reasonably well with Blackburn's Solution throughout except for the first 10^o degrees of the elliptical angle. However, Kobayashi's solution seems to differ significantly from the other two solutions. The 13 percent difference in SIF magnification factor

between present and Blackburn's solution at the free surface ($\theta = 0^{\circ}$) could be attributed to the indirect solution procedure in [79], viz., through the virtual crack extension method, and the slight difference in the geometry of the problem. Thus, it appears that the method of estimation of K_I in [78], viz., through the solution for surface flaws in the flat plates modified by curvature correction factor, is questionable.

(b) Outer Semi-Circular Flaws in Pressurized Thick-Walled Cylinder. Results for stress-intensity magnification factor variation for two unpressurized outer semi-circular flaws in a pressurized cylinder is given in Figure 44. The qualitative feature of these two problems are also similar to the previous inner as well as outer semi-elliptical and semi-circular crack problems discussed before. With all the geometric parameters, except the ratio of crack depth to the thickness of the thick-walled cylinder, kept constant, one can easily observe the effect of increased stress-intensity magnification factor at all θ locations for a deeper crack. The comparative estimates of Kobayashi [78], however, were found to differ significantly for these problems, as they were in the case of outer semi-elliptical crack. Keeping these discrepancies in mind, though it gave good agreement in the case of deep inner semi-circular flaw in a pressurized thick-walled cylinder (Figure 34 and 35), the method of obtaining the curvature correction factor might need some refinement for better accuracies of the result. The author [78] himself states that his study does not consider the study of crack depths in which the effect of back surface had to be considered. In view of the results obtained through a rigorous

three-dimensional finite element model, it may be stated that the approximate solution procedure developed by Kobayashi et al. [63,77,78] and a mere curvature correction factor to the equivalent flat plate solution may not be an adequate modeling of a complex three-dimensional problem such as cracks in pressurized vessels.

Cracks Emanating from Holes in Finite-Plates

Introduction. A recent study by the U.S. Air Force on failures of aircraft structural elements shows that about one third of the failures were caused by the presence of corner cracks emanating from fastener holes. Such cracks may occur due to the manufacturing processes, and they grow under the influence of fatigue loading until catastrophic failure occurs. Thus, the problem of cracks originating from fastener holes is very important and a rigorous three-dimensional analysis is very essential to estimate the stress-intensity factors accurately.

The problem of a corner crack emanating from a hole in a plate has been considered by several investigators. A quarter-circular crack emanating from a hole in a finite thickness plate was considered by Liu [82]. But in his analysis he does not consider the variation of stress-intensity factor along the crack front and therefore the single value of stress-intensity factor obtained by him might be considered as an estimation of an average value for this problem. Liu's [82] work was then improved by Hsu and Liu [83] by considering the variation of stress-intensity factor along the crack front. Shah [84] studied the stress intensity factors for through and part through cracks originating at fastener holes. He found the plane strain pressure distribution near a hole in a plate under tension and applied the negative of these

tractions to a circular crack in an infinite solid. He employed shape correction factors to relate the circular crack results to elliptical crack problems. After obtaining the front surface correction factor and back surface "correction factor", he assumed that the results pertain to the double cracks originating from a hole and again he introduced another correction factor to estimate the stress-intensity factors for a single corner crack originating from a hole. A parametric type of study on the quarter-elliptical cracks emanating from holes in plates was done recently by Ganong [85]. He has employed the alternating technique procedure for the solution of stress-intensity factors. Except for the work of Ganong [85], all the other investigators obtain the solution for stress intensity factors by extending the two-dimensional results.

Some experimental investigations were also carried out recently. Experiments on quarter-elliptical cracks originating from holes in plates were conducted by Hall and Finger [86] for aluminum and titanium alloy specimens. Experimental investigation of fracture and fatigue crack growth behavior of surface flaws and flaws originating from fastener holes for steel specimens was done by Hall et al. [87]. A stress freezing photoelasticity technique was used by McGowan and Smith [88] to study the stress intensity factors for deep corner cracks emanating from a hole in a plate. Contrary to the theoretical expectation, their value of stress intensity factor at the front surface was higher than at the hole surface. Thus a more thorough and rigorous three-dimensional analysis of quarter-elliptical corner cracks emanating from a hole in a plate under unaxial tension is needed and such a task is carried out here.

The Problem. For simplicity of modelling, and the knowledge that the stress intensity values for single and double (symmetric) corner cracks originating from holes differ only by about ten percent (Reference [84]), the problem of double (symmetric) quarter-elliptical corner cracks originating from a fastener hole was considered for the analysis by the present three-dimensional displacement-hybrid finite element model. Figure 45 illustrates the nomenclature of the double corner cracked hole problem. The loadings for this problem would be uniaxial tension at $|z| = H$. Six different geometries have been considered and they are given in the following table along with corresponding Poisson's ratios.

a/c	c/R	a/t	Poisson's Ratio
1.0	1.0	0.5	0.25
1.1	0.99142	0.48	0.25
0.5	0.2	0.1	0.3
1.0	0.5	0.5	0.3
1.5	1.0	0.75	0.3
2.0	0.2	0.2	0.3

The dimensions W and H are given by the following two equations

$$2W = 6(2R + c)$$

$$H = 2W$$

Due to the symmetry of the problem, only a quarter of the problem needs to be considered for the finite element breakdown.

The finite element breakdown of quarter of the problem is given

by Figure 46; the total number of finite elements and the total number of degrees of freedom for this breakdown are 156 and 2670 respectively. The quarter ellipse was divided into six segments for this problem to obtain the variation of the stress-intensity factor along the crack front. In the solution procedure, in order to eliminate the translational and rotational movements of the plate, at least one displacement in each direction was suppressed. The symmetry conditions of the problem were obtained by properly suppressing the displacements along the directions perpendicular to the plane of symmetry. The results are presented below.

Results and Discussions. The solutions of the stress-intensity factors for the symmetric corner cracks enamating from holes in finite plates under tension for the six different geometrices are given in Figure 47 through 52. These stress-intensity factors are normalized with respect to the theoretical value of the stress-intensity factor of the point where the crack front and the minor axis intersect when the complete elliptical crack is embedded in an infinite medium and is subjected to remote uniform tension σ_o. The normalizing factor is given by $\sigma_o \sqrt{\bar{\Lambda}\ b/E\ (k)}$, where b is the semi-minor axis (minimum of a and c) and E(k), the complete elliptic integral of the second kind. As a result, Figures 47 through 52 depict the actual variation of the stress-intensity factors, but for a constant. Figure 47 shows the solutions for the variation of stress-intensity factor for the problem of symmetric corner cracks enamating from a hole with $a/c = 1.0$, $c/R = 1.0$ and $a/t = 0.5$. The solutions of the stress-intensity factors for an identical problem by Shah [84] and the solutions of the

stress-intensity factors with only one corner crack, by Ganong [85], are presented in Figure 47. Solutions of the stress-intensity factors for the problem of corner cracks enamating from holes with geometric parameters a/c = 1.1, c/R = 0.99142 and a/t = 0.48 by the present method and by the stress-freezing photoelasticity method by McGowan and Smith [88] are presented in Figure 48. Though the present solution cannot be compared directly with the solution of Ganong [85] (Figure 47) because of the difference in the problem, the present solution seems to differ significantly from the other investigators. Similarly, the solution of the second problem (Figure 48) differs from that of the results obtained from the experiments by McGowan and Smith [88]; where only the end values of the stress-intensity factors were available for comparison. The reasons for the differences and discrepancies of these results are given in the next section.

Comparison of the Results with other Solution Procedures. In the problem of corner cracks emanating from holes in plates under tension, there are six different factors which affect the stress-intensity magnification factor and they can be enumerated as follows.

(1) The first and probably the most important one is the effect of the hole stress concentration. As the stress concentration decays rapidly away from the hole, the effect of stress concentration will be such that it will tend to increase the stress-intensity magnification factor more at the hole surface than at the front surface.

(2) Since the crack intersects with the front surface, the crack can open more and higher stress-intensity magnification factor at the front free surface will result.

(3) The presence of the hole also will increase the magnification factor where the crack intersects the hole surface, because the hole will behave like a free surface. This effect will increase as the crack size becomes smaller.

(4) When the crack is deeper and approaches the back surface of the plate, the stiffness of the material between the crack and back surface decreases resulting in higher magnification factor near back surface.

(5) The effect of the crack shape is another factor. In the case of the elliptical cracks, they tend to grow into circular cracks due to the fact that the stress-intensity factor is more at the point where minor axis and the ellipse intersect for uniform tension.

(6) It is a known fact that the stress concentration along the edge of the hole varies across the thickness of the plate. The stress concentration was found to vary from 3.1 at the center of the plate to 2.7 at the edge of the plate for a plate whose thickness is equal to the hole diameter [85]. This effect will tend to increase the stress-intensity magnification factor near the center of the plate.

In the present procedure all the above mentioned effects are automatically taken into account through the rigorous three-dimensional finite element analysis where all the boundary conditions, such as free surfaces, are satisfied in an integral average sense. In his analysis Shah [84] has incorporated the effect of stress concentration, back surface effect, front surface effect and crack shape effect. His approach does not include the effect of hole surface, and the effect of variation of stress concentration through the thickness. In his

work Ganong [85] states that he has included all the effects in the analysis.

A brief description of the alternating method used by Ganong [85] is given below in order to draw attention to the method and for comparison with the present work.

First the finite body is considered without the crack. The specified tractions are applied on the exterior of the finite body and the stresses are computed where the crack is supposed to have been, by using any procedure including numerical procedures such as the finite element method. Next an infinite body with a completely embedded crack is considered and the stresses computed on the crack surface are applied in opposite direction so that the stresses on the crack surface can be erased. Using the solution for an infinite body with the crack with the above loading on the crack surface, the residual tractions are computed on the boundary of the finite body. Then these tractions are again applied in opposite direction on the exterior of the finite body without the crack to compute residual tractions at the surface where the crack would be present. These tractions are again removed by applying the equal and opposite tractions on the crack surface for an infinite body with a crack. The residual tractions on the exterior of the finite body is computed again and this iteration procedure is continued until the residual traction on the crack becomes negligible.

In the above method, one needs to find the solution for stress in an infinite solid with an embedded crack which is subjected to arbitrary pressure. But the major drawback in the case of the elliptical crack solution is its polynomial representation which is limited to third

order polynomial pressure distribution on the elliptical crack surface due to the mathematical complexity involved in deriving the solution for arbitrary crack surface pressures. Such a third order polynomial stress distribution cannot adequately fit the varying residual surface tractions encountered in the alternating method on the elliptical crack surface. The situation actually becomes worse in the case of corner cracks enamating from holes because the stresses change very rapidly near the hole where the crack is located. Figure 53 shows the actual distribution, least square fitted stress distribution with the polymials $A_{00} + A_{20}X^2$ and $A_{00} + A_{20}X^2 + A_{40}X^4$, prepared by Shah. One can easily see the large deviation of the fitted stress distribution from the actual stress distribution. Moreover, in the case of symmetric corner cracks, the polynomials will be limited to second order due to the fact that X^3 is an odd function. Thus there is a severe restriction on the order of polynomial which is used to represent the actual stress distribution. Shah [84] again approximates the problem of corner cracks emanating from holes by the superposition of the problem of a hole with no crack and the problem of a crack with no hole. Such severe approximations by these investigators might lead to considerable error in their solution of the stress-intensity factors. Ganong [85] also estimates that his results are about 20 percent higher than the previous estimates in [83,84]. Due to the inadequate experimental results, it was not possible to verify the present results with them. The end values of stress-intensity factors obtained by McGowan and Smith [88] through experiments in Figure 48 shows that they agree at the front free surface and not at the hole surface. Theoretically one would expect

the stress-intensity factors be higher at the hole surface due to the stress concentration effect along the hole surface.

Surface Flaws in Plates in Tension and Bending

Introduction. The problem of surface flaws in plates in tension and bending is receiving considerable attention recently due to the fact that in the literature solutions of stress intensity factors vary widely when the plate thickness is smaller when compared with other dimensions of the specimen and crack penetrates deeper in the thickness direction. In the case of bending loads, the maximum stress-intensity factor need not be at the point of deepest penetration, but it could be at the free surface where maximum tensile stress occurs due to bending. Analytical solutions being unavailable, several investigators studied this problem using approximate solution procedures. Kabayashi [64] considered semi-elliptical and semi-circular flaws subjected to tensile and bending loads. Schroedl and Smith [91] used three-dimensional photoelasticity and extensively studied the surface flaw problems. Approximate solutions using alternating technique for surface flaws in bending were obtained by Shah and Kobayashi [92]. The surface flawed tension plate problem was analyzed by Miyamoto and Miyoshi [93] using finite element method. The problems studied by Kobayashi [64] are considered here to be solved by the present finite element model.

The Problem. The problems of semi-circular and semi-elliptical surface flaws in plates with two different depth to thickness ratios are considered and are shown schematically in Figure 54. The finite element breakdown is given in Figure 21 with 156 total number of finite elements and 2670 total number of degrees of freedom. The geometric

parameters of the problems considered are given below.

a/c	a/t	2W/2c	2H/2c
1.0	0.8	4.0	4.0
1.0	0.6	4.0	4.0
0.2	0.8	4.0	4.0
0.2	0.6	4.0	4.0

The Poisson's ratio is assumed to be 1/3 and both the tensile as well as bending loads are considered.

Results and Discussions. The solutions of the stress-intensity factors along the crack front for the semi-circular surface flaws in a plate subjected to tension and bending for crack depth to thickness ratios 0.8 and 0.6 are given in Figures 55 and 56 respectively. The corresponding solutions obtained by Kobayashi [64] are also given in these figures. From Figures 55 and 56, it can be seen that the solutions of stress-intensity factors for bending loads by the present procedure agrees well with the results estimated by Kobayashi except for a 15 percent difference at the intersection of crack front and the front free surface. However, there is a large difference in the solutions of the stress-intensity factors for tensile loads between the present and Kobayashi's procedures. Kobayashi's procedure estimates lower values of stress intensity factors. The values are normalized with respect to the exact solution of stress-intensity factors for a completely embedded circular crack in an infinite solid subjected to a remote tension.

The solution for the stress-intensity factors along the crack front for the semi-elliptical surface flaws in a plate subjected to tension and bending for crack depth to thickness ratios 0.8 and 0.6 are given in Figures 57 through 60. They are normalized with respect to the value of stress intensity factor at the minor axis of the ellipse, when the ellipse is completely embedded in an infinite solid and subjected to remote tension. Thus, Figures 57 through 60 represent the actual variation of stress intensity factors but for a constant.

Comparison of the Result with other Solution Procedures. Even though the present results are higher at free surface points, the results in general compare favorably with the solutions by Kobayashi [64] in the case of semi-circular surface flaws in a plate subjected to tension and bending. However, in the case of semi-elliptical surface flaws subjected to tension the nature of variation of the stress-intensity factors are different from the other investigators. The results obtained for a similar problem with slightly different geometry by Miyamota and Miyashi [93] show the same tendency of variation of stress-intensity factor as the present results. As in the case of others, in the present procedure also, the maximum value of stress intensity factors occur at the point of deepest penetration. For plates subjected to bending with semi-elliptical surface flaws, the results agree reasonably well except at regions near the free surface. The value of the stress-intensity factor at the free surface obtained by Schrodel and Smith [91] through experiments for a problem with geometric parameters $a/c = 0.25$, $a/t = 0.79$, and Poisson's ratio $= 0.5$ is also marked in Figure 58. As it can be seen from the figure, Kobayashi [64] estimates

much lower value of stress-intensity factor at the free surface. The present procedure also differs by about 20 percent from the experimental value. This difference can be accounted by the higher value of Poisson's ratio in the experiments (0.5 compared to 0.33 used presently) and the difference in the geometry considered. It should be noted here that the effect of Poisson's ratio is such that the stress-intensity factor increases as the value of Poisson's ratio increases.

As mentioned in the last section, in the alternating method, the representation of stress distribution by a quadratic polynomial may not be adequate enough to reflect the true nature of variation of residual stress distribution on the crack surface in the alternating procedure. Another approximation was also made by Kobayashi [64] and F. W. Smith [99] in solving the problem of surface cracks in plates in bending and is described in the following. During the iteration procedure, they apply the crack pressure, fitted by quadratic polynomials, and compute the stresses on the external boundary of the specimen. Then equal and opposite stresses are applied on the boundary of the finite body to remove the surface stresses. It is to be noted here that such removal of surface stresses are carried out over an area of two or three crack lengths in extent. The argument used by them is that the stresses due to the application of crack surface decay very rapidly and become negligible within few crack lengths. Such an argument would be acceptable if the bending rigidity of the plate is infinite. But in the case of plate with finite bending rigidity, even small forces away from the crack could cause significant bending stresses at the crack cross-section due to the large lever arm of these neglected residual surface

stresses. This process is continued in all the interations and these neglected moments act in the opposite direction of the bending deformation of the plate. This essentially acts as an elastic edge constraint and the solution would correspond to a finite plate with elastic edge constraint. This in turn would reduce the opening of the crack, thereby yielding lower values of stress-intensity factors. In a study by Parmerter [94], it is concluded that no definite conclusions can be reached regarding the quantitative nature of these edge constraints, but it would be most severe when the crack geometrics are such that $c/a \gg 1$ and $a/h \to 1$. This fact can be observed from Figures 55 and 60. For a change of a/c from 1 to 0.2, keeping other parameters constant, it can be noticed that the alternating technique provides much lower value near the free surface when compared with the present solution or the experimental results.

For all the problems solved in this dissertation the applied loads are the energy equivalent generalized nodal forces corresponding to the specified tractions.

CHAPTER VI

CONCLUSIONS AND RECOMMENDATIONS

Conclusions

This dissertation presents an efficient and general embedded singularity element using an assumed displacement hybrid finite element procedure which can solve three-dimensional linear elastic fracture mechanics problems with arbitrarily curved three-dimensional crack front. The present procedure can be applied to three-dimensional mixed mode fracture problems with complex crack geometries. The accuracy of the above procedure has been demonstrated through the numerical solution of several problems for which solutions exist. These numerical solutions agree well within reasonable limits with the benchmark problems such as through the thickness straight crack problems and buried circular and elliptical cracks in finite specimens. For some problems, the results of the present procedure are found to differ significantly from the solutions of other investigators. The reasons for these discrepancies are explained in the respective places where the solutions are presented. Again, for problems with such discrepancies, it is found that the present results are much closer to available experimental results and other available analytical results obtained through conventional finite element methods which do not have the previously enumerated shortcomings of the alternating method. The utility of the present formulation is also demonstrated through solving several other problems with

complicated geometries of structure as well as crack, for which solutions do not exist.

The prominent features of the hybrid displacement model in comparison to the conventional and other finite element models can be enumerated as follows:

(1) This is a more general formulation and is capable of computing the solutions for mixed mode problems (i.e., computation of k_1, k_2 and k_3 simultaneously) whereas references like [52] solve only mode I problems.

(2) The total number of finite elements and the total number of degrees of freedom in the present formulation is much smaller than the conventional finite element procedure. Even with less number of finite elements and total degrees of freedom, accurate results for stress intensity factors can be obtained. This is not a surprising fact because the whole idea of embedding proper singularity in the finite element procedure is to obtain the convergence of the solution with fewer number of elements along the crack front.

(3) The stiffness matrices of the regular elements need not be generated by the hybrid displacement model. The conventional finite element model can be used to generate the stiffness matrices of regular elements, still maintaining the compatibility conditions across the interelement boundary.

(4) The hybrid displacement model allows one to choose arbitrary mathematical functions as field functions for the interior displacements and surface tractions.

(5) The correct type behavior of displacement and traction

singularities near the crack front can be embedded easily in the finite element procedure.

(6) The Lagrange multiplier, T_{Li}, are physically the boundary surface traction and should be derived from an equilibrated stress field. For better convergence of the finite element solution, the assumed boundary surface traction of singular element should also include the asymptotic solution of stresses with correct singularity.

(7) With the correct type of displacement and traction singularities embedded in the procedure, it is very easy to satisfy the interelement boundary displacement continuity condition and thus ensure compatibility.

(8) Though there was no study made on the effect of optimum shape and size of the singular elements on the stress intensity factors, it may be stated that singular elements with a square cross-section and size of about 1/10 of the characteristic half crack length yield reasonably accurate results for the stress intensity factors.

(9) In order to ensure a better matching condition and thus ensure better convergence of the solution, the boundary displacement assumption was so chosen that $\sqrt{r}$ variation of the displacements was built-in also.

(10) Since the hybrid displacement procedure poses the need for a special solution technique, the concepts of obtaining the condensed stiffness matrices of the singular element were introduced. The stress intensity factors can then be obtained by using the concept of crack opening displacement discussed previously. The present COD method provides better accuracy in the solution of stress intensity factors

than the original COD method. In the original COD method stress intensity factors were computed by considering only the closest node to the crack front whereas in the present COD method, they are obtained as $r \rightarrow 0$.

(11) The present "singular" element stiffness matrix generation program may be incorporated into sophisticated three-dimensional finite element programs thus enabling them to solve three-dimensional linear fracture mechanics problems in a routine fashion.

(12) The stress intensity factors can be solved for directly as unknowns in the finite element solution instead of fitting the approximate displacement or stress solutions obtained from the finite element solution.

Recommendations

The hybrid-displacement finite element model is used to solve several problem as discussed in the previous chapter. The method can easily be applied without any further modification to fracture problems with complicated structural geometries like nozzle-to-cylinder junctions with corner cracks.

In this work, only problems with arbitrarily curved crack boundaries which lie in a plane perpendicular to z-axis were considered. In other words, the crack boundaries considered were plane curves. The present method can be easily extended without any further modification to three-dimensional crack problems, where the crack boundaries are described by curves in space which are not necessarily planar curves. In this category of problems, the loading conditions would be generally

mixed mode (modes I, II and III) type; and the present formulation is capable of handling general mixed mode problems whereas the methods developed by other investigators are capable of solving only pure mode I problems.

As mentioned earlier, there still exists a controversy whether the stress intensity factors tend to zero at the intersection of the free surface and the crack front. This result has been only predicted and not yet proved. Thus, in the present work, the stress intensity factors were forced to assume zero values by two methods and the effect was studied and presented in the previous chapter. Once the question is settled regarding the structure of singularities at the free surfaces, then the formulation of the finite element model can be modified to account for the free surface effects of the crack.

During the preparation of compact tension specimen for the experimental investigation of fracture, the specimen will be cut by sharp edges and then it will be put in the fatigue testing machine to create a microsharp crack front. This in turn might leave some residual stresses in the specimen near the crack front. Thus consideration of the problem of initial stresses and initial strains in fracture problems are also very important. In the problem of pressurized cylinders with inner or outer surface crack, the liquid or the gas, which is stored inside and gives rise to the internal pressure, might be at elevated temperature. This would induce thermal stresses and strain in the cylinder. Similarly, in the case of nuclear fuel elements and reactor pressure vessels, they are exposed to elevated temperature. The present hybrid finite element model may be

modified to account for the initial stress and initial strain problems.

The present method can also be extended, with some modifications, to three-dimensional elastic-plastic fracture problems, which provides a more realistic fracture criterion in real materials where the plastically yielded region near the crack front is no longer small and the elastic fracture analysis is not adequate enough. Though there exists a theoretical solution for stresses and displacements in the vicinity of the crack front for linear elastic fracture analysis, the theoretical solution for elastic-plastic fracture analysis involving modes I, II and III does not exist. For two-dimensional fracture problems, Rice and Rosengren [95] and Hutchinson [96] suggested a 1/r singularity for strains and non-singular stresses at the crack tip for elastic-plastic problems. A similar idea may be used and a hybrid displacement model which contains a 1/r singularity in strains and non-singular stresses may be developed. This would allow us again to assume an independent displacement field which contains 1/r singularity in strains. The stresses and thus the traction can be assumed as regular polynomials so that non-singular stresses can be generated. With such assumed functions, the present finite element procedure would model more realistically the elastic-plastic fracture analysis. Thus the present hybrid displacement finite element model is probably the most natural procedure for analyzing the three-dimensional elastic-plastic crack problems for the purpose of assisting in the development of physically realistic ductile fracture criteria.

The hybrid displacement model can be extended to the solution of bimaterial tension plate problem with a through-the-thickness

straight crack with one crack front in first material and the other crack front in the second material. In this kind of problem, there will be singularities along three lines, two being the two crack fronts and the third being the line of intersection of the crack surface and the two materials. The nature of singularities along the two crack fronts would be $1/\sqrt{r}$ type and along the interface front would be $\frac{1}{r^{\alpha}}$ (where α depends on material properties). The stiffness matrices of singular elements which contain $\frac{1}{r^{\alpha}}$ singularity may be developed similar to the stiffness matrices of the singular elements with $\frac{1}{r^{\frac{1}{2}}}$ singularity using the hybrid displacement model.

Three-dimensional fracture analysis of orthotropic materials can also be made once the theoretical strength of the singularity due to the presence of crack is established.

The present "basic element" is a 20 node isoparametric brick element in which the boundary displacements are interpolated quadratically. The procedure can be easily modified to develop singular elements in which the boundary displacements on the boundaries, which adjoin the regular elements, are interpolated linearly so that eight node isoparametric brick elements, for regular elements, can be used for the analysis.

APPENDICES

APPENDIX A

SOLUTION PROCEDURE FOR LINEAR SIMULTANEOUS EQUATIONS

One of the most important phases in the analysis of structural problems by numerical methods such as the finite element method is the solution of the set of linear simultaneous equations. When there is a large system of equations to be solved, as in the present three-dimensional analysis of fracture problems, the stiffness matrix of the structural system cannot be accommodated in the core storage of the computer. This calls for a special out-of-core equation solver in which the data are manipulated in and out of core through the use of a tape handling procedure. Such a special computer program to solve large system of symmetric linear equations has been developed by Mondkar and Powell [100]. They have employed the Crout reduction procedure in the program and it can solve a set of equations of almost unlimited size. This program is used for the solution of linear equations in the present work.

In a Gauss elimination procedure, the kth ($k = 1$ to N; N = total number of equations) equation is eliminated by combining it with all the subsequent equations such that the entries a_{jk} ($j = k + 1$ to N) are reduced to zero. This procedure results in upper triangular form, and the solution can be obtained by back substitution procedure. Thus, in Gauss elimination, each term of the reduced coefficient matrix is modified every time an equation is eliminated.

But in Crout reduction, the coefficient matrix is modified only once, because each term of the coefficient matrix is changed from its initial value to the final value directly so as to obtain the final triangularized form (which is based on the fact that in Gauss elimination, row i in the triangularized form is obtained as a linear combination of rows 1 to i-1).

If the set of equations is represented by

$$[A]\{x\} = \{b\} ,$$

then the formulae for the reduction of coefficient matrix, the reduction for load vector and the back substitution in Crout reduction procedure are given below respectively,

$$a_{ij}^{(i-1)} = a_{ij} - \sum_{k=1}^{i-1} \frac{a_{ki}^{(k-1)} a_{kj}^{(k-1)}}{a_{kk}^{(k-1)}} \qquad \begin{matrix} j = 2,\ldots,N \\ i = 2,\ldots,j \end{matrix}$$

$$b_j^{(i-1)} = b_i - \sum_{k=1}^{i=1} \frac{a_{ki}^{(k-1)}}{a_{kk}^{(k-1)}} b_k^{(k-1)} \qquad i = 2,\ldots,N$$

$$x_N = b_N^{(N-1)}/a_{NN}^{(N-1)}; \quad x_i = \frac{b_i^{(i-1)} - \sum_{j=i+1}^{N} a_{ij}^{(i-1)} x_j}{a_{ii}^{(i-1)}} , \; i = N-1,\ldots,1$$

where the superscript (i-1) indicates the value after elimination of (i-1)th equation.

APPENDIX B

NUMERICAL EVALUATION OF VOLUME AND AREA INTEGRALS

The product Gaussian quadrature formula for volume integral is given as

$$I = \int_{-1}^{+1} \int_{-1}^{+1} \int_{-1}^{+1} f \; dr \, ds dt \tag{I.1}$$

where f is the function to be integrated and f already contains the determinant of the Jacobian. The above integral can be numerically integrated as follows

$$I = \sum_{i=1}^{5} \sum_{j=1}^{5} \sum_{k=1}^{5} B_i B_j B_k \, f(r_i, s_j, t_k) \tag{I.2}$$

where B_i, B_j, B_k are the weighting factors and r_i, s_j, t_k are the abscissas. The values of the abscissas and weighting factors are given below (Reference [97])

$\pm (r,s,t)_i$	B_i
0.00000 00000 00000	0.56888 88888 88889
0.53846 93101 05683	0.47862 86704 99366
0.90617 98459 38664	0.23692 68850 56189

Thus the total number of Gaussian points for volume integral would be 125.

A non-product quadrature rule due to Rabinowitz and Richter (Reference [98]) with 48 points for area integral is given by

$$I = \int_{-1}^{+1} \int_{-1}^{+1} g \; dr\,ds \tag{I.3}$$

$$= \sum_{i=1}^{48} B_i \, g(r_i, s_i) \tag{I.4}$$

The corresponding abscisses and weight factors are tabulated below:

(r_i, s_i)	B_i
Fully symmetric	
$i = 1,2,\ldots,3$	
$r_1 = 0.99153\ 77816\ 777667$	$B_1 = 0.03012\ 45207\ 981210$
$r_2 = 0.80201\ 63879\ 230440$	$B_2 = 0.08711\ 46840\ 209092$
$r_3 = 0.56486\ 74875\ 232742$	$B_3 = 0.12500\ 80294\ 351494$
$r_4 = 0.93543\ 92392\ 539896$	$B_4 = 0.02676\ 51407\ 861666$
$r_5 = 0.76245\ 63338\ 825799$	$B_5 = 0.09596\ 51863\ 624437$
$r_6 = 0.21561\ 64241\ 427213$	$B_6 = 0.17508\ 32998\ 343375$
$r_7 = 0.97696\ 62659\ 711761$	$s_7 = 0.66844\ 80048\ 977932$
$r_8 = 0.89371\ 28379\ 503403$	$B_7 = 0.02831\ 36372\ 033274$
$s_8 = 0.37352\ 05277\ 617582$	$B_8 = 0.08664\ 14716\ 025093$
$r_9 = 0.61224\ 85619\ 312083$	$B_9 = 0.11501\ 44605\ 755996$
$s_9 = 0.40789\ 83303\ 613935$	

$$s_1 - s_2 = s_3 = 0 \qquad s_4 = r_4 \qquad s_5 = r_5 \qquad s_6 = r_6$$

Thus the function has to be evaluated at 288 total number of quadrature points for the area integral for all the six surfaces of the element.

APPENDIX C

ILLUSTRATIONS

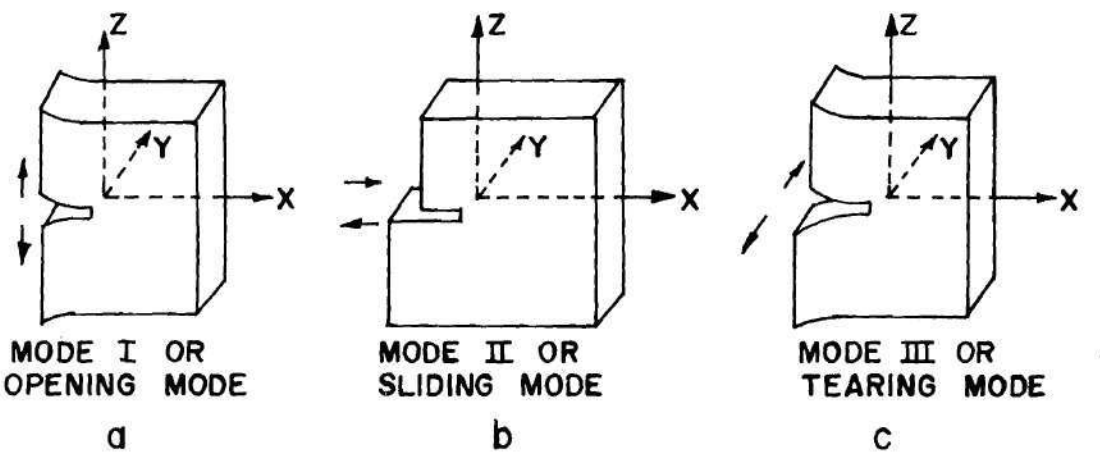

FIG. 1: Three Basic Modes of Crack Tip Deformation

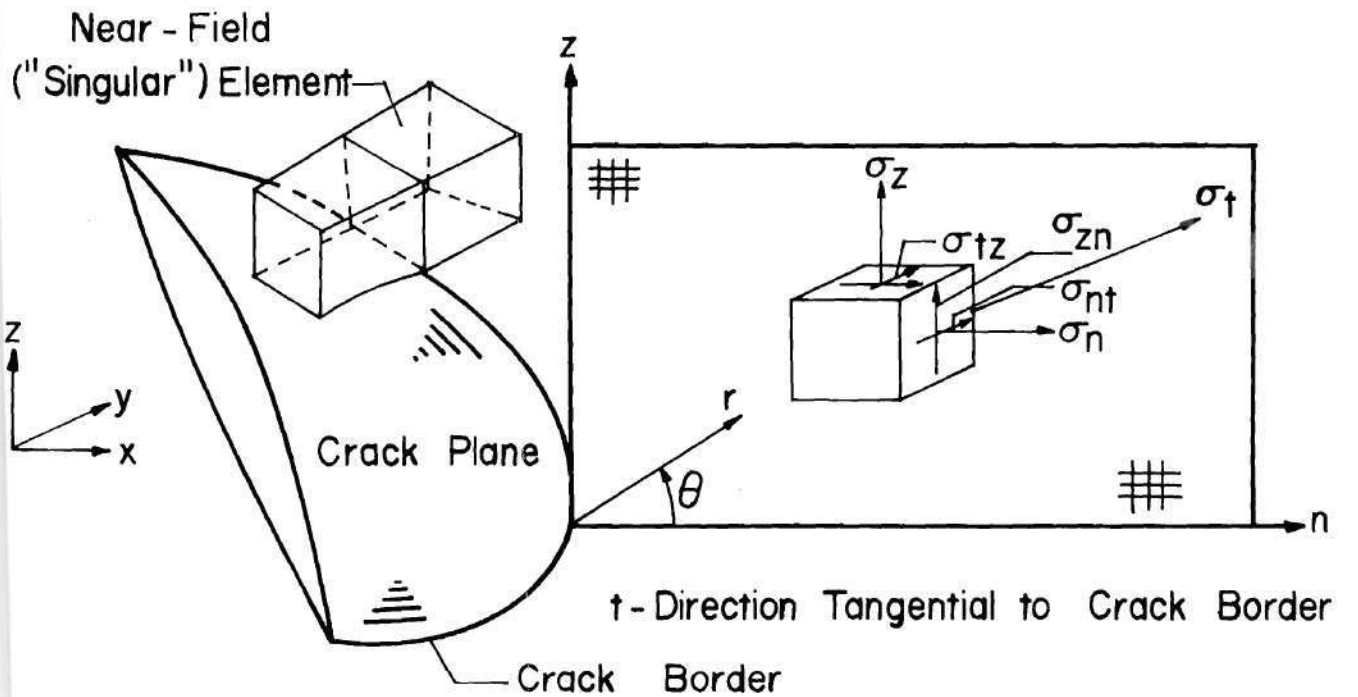

FIG. 2: Nomenclature Near Crack Front

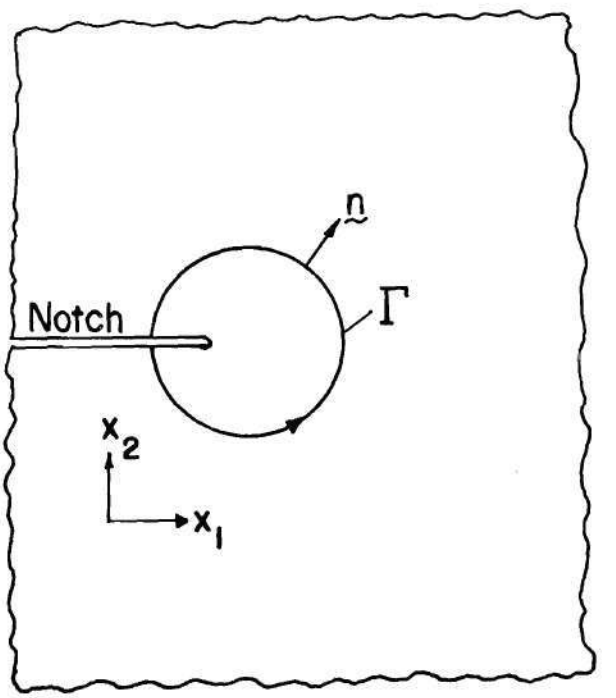

(Γ is any curve surrounding crack tip)

FIG. 3: Crack in Two-Dimensional Field

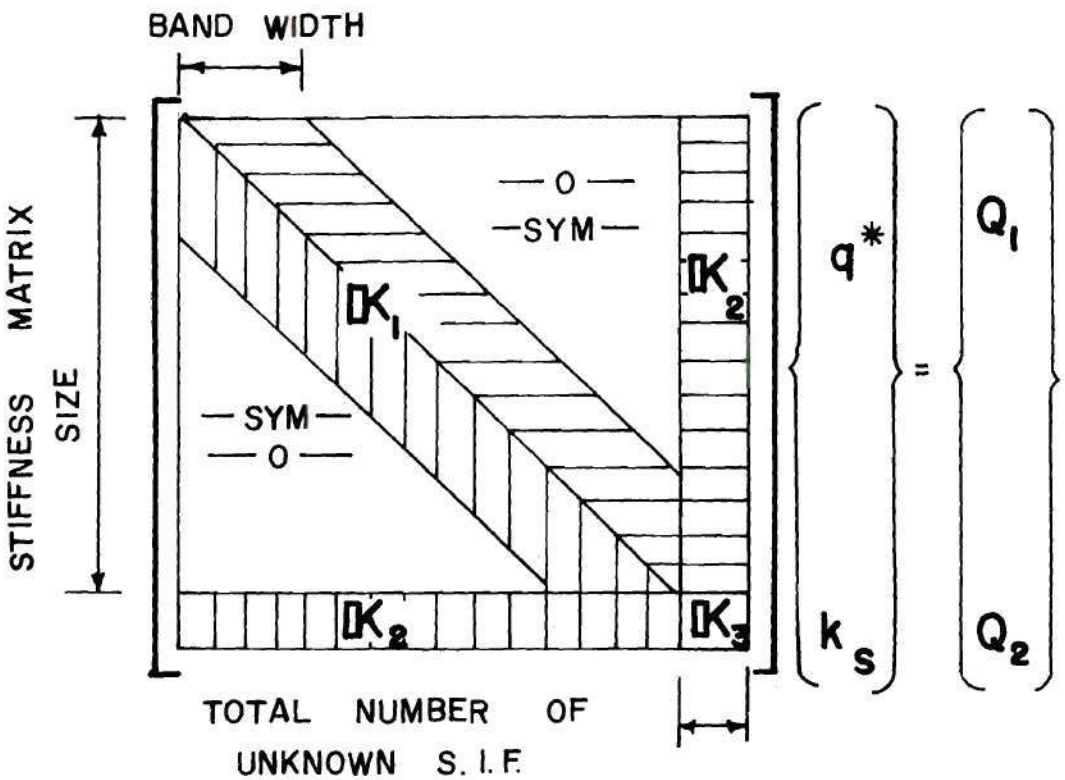

FIG. 4: Global Stiffness Matrix

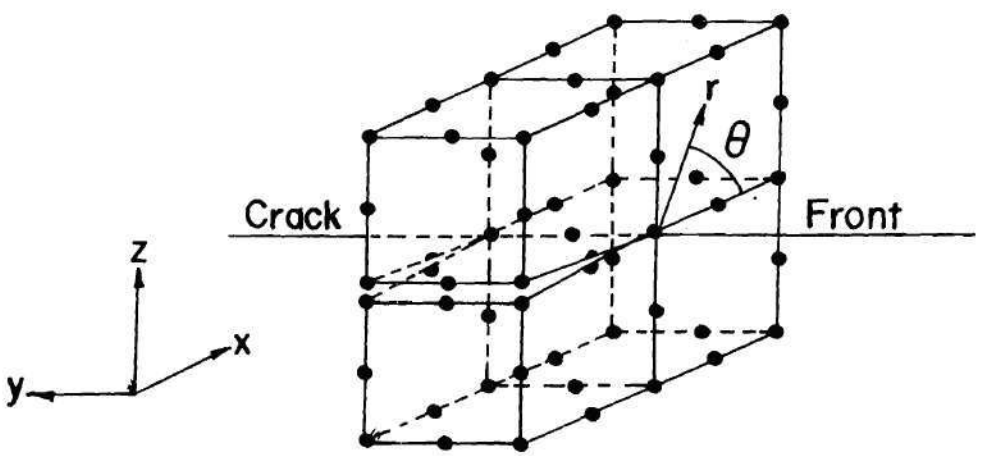

FIG. 5: Assembly of Four Singular Elements

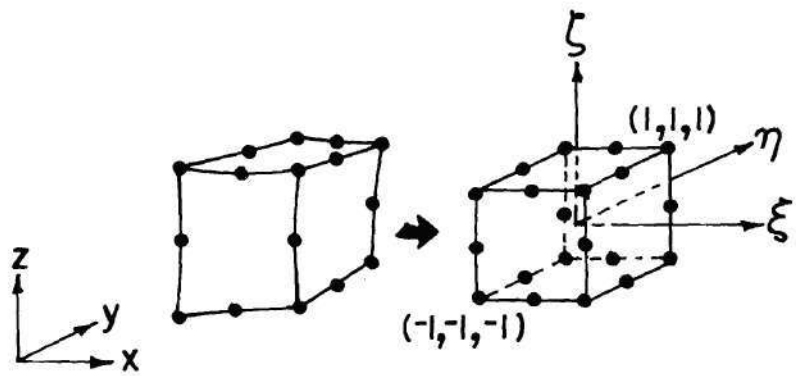

FIG. 6a: Three Dimensional Mapping

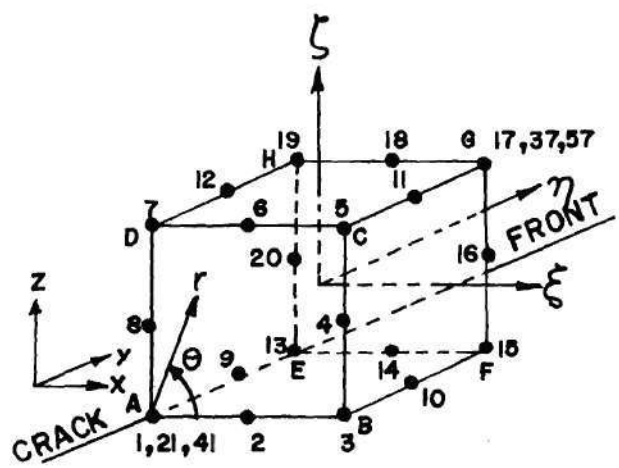

DISPLACEMENTS IN CARTESIAN DIRECTIONS

FIG. 6b: Nodal Displacements (Cartesian)

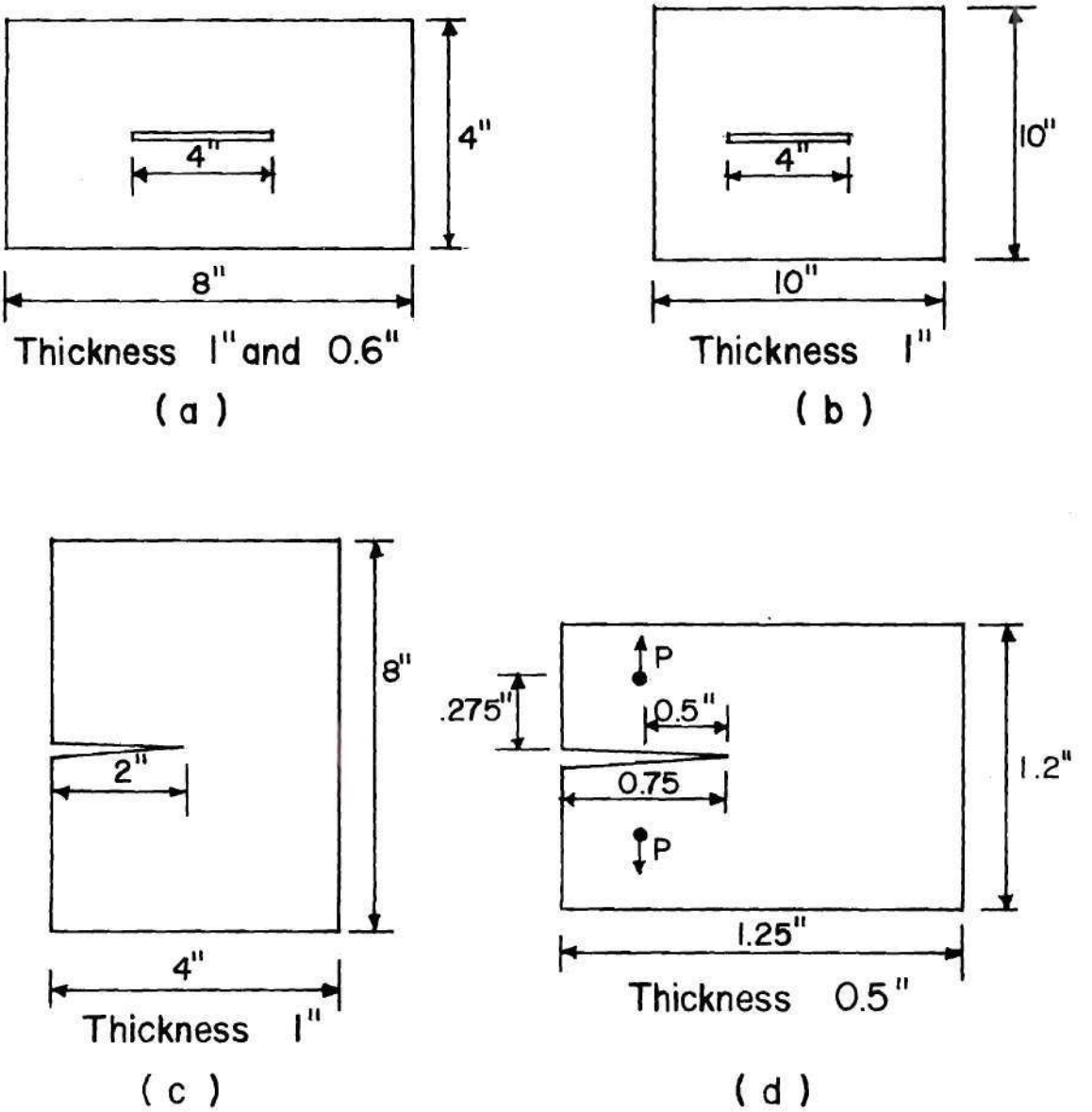

FIG. 7 : Geometries of Through the Thickness Straight Crack Problems

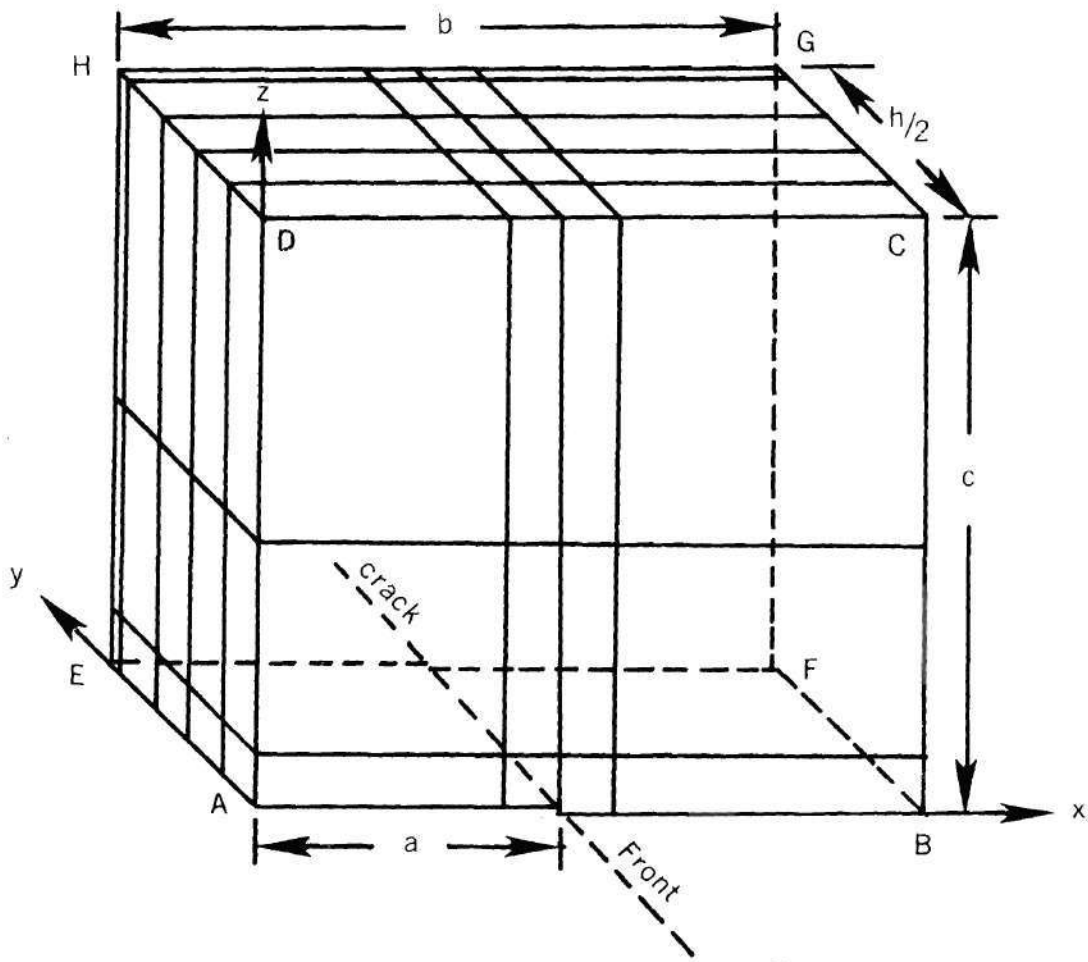

on faces ABCD, ADHE and ABFE boundary conditions can be applied appropriately.

FIG.8. FINITE ELEMENT BREAKDOWN FOR THROUGH THE THICKNESS CRACK PROBLEMS

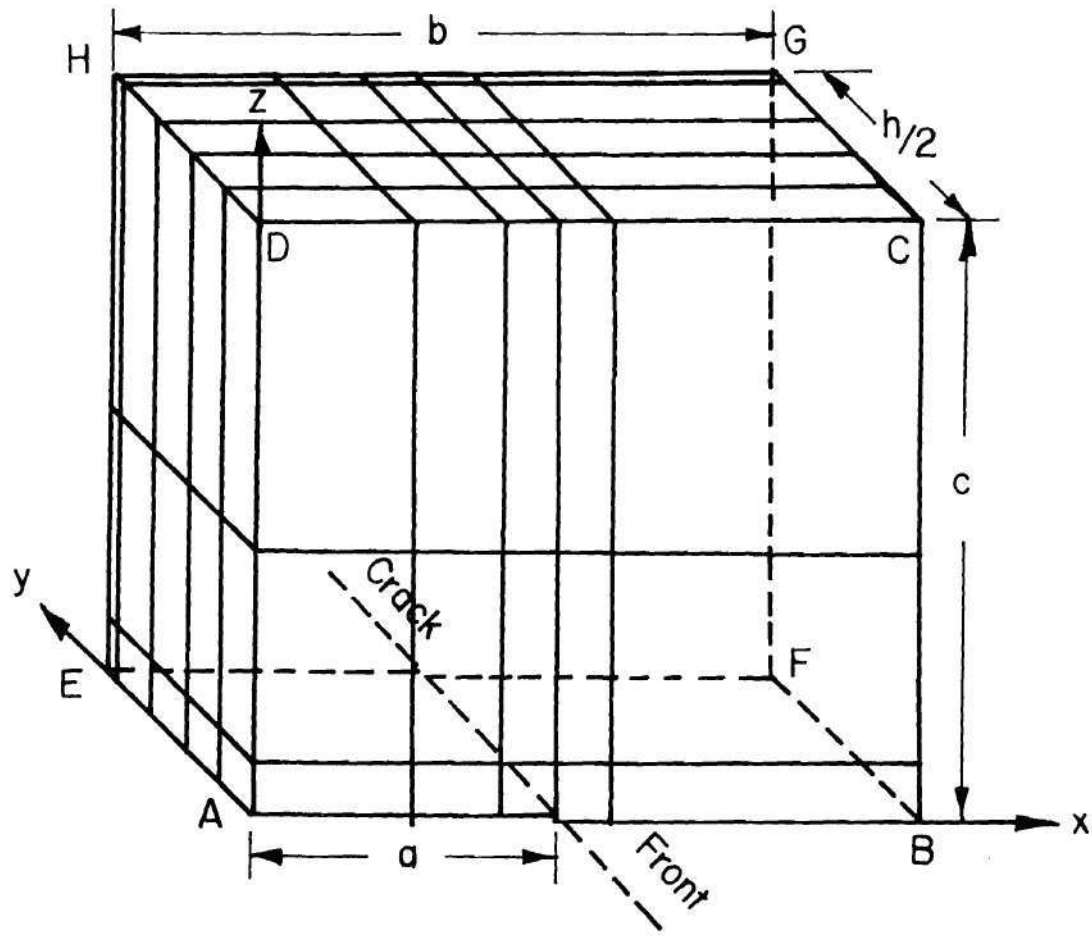

FIG. 9: Finite Element Breakdown for the Compact Tension Specimen Problem

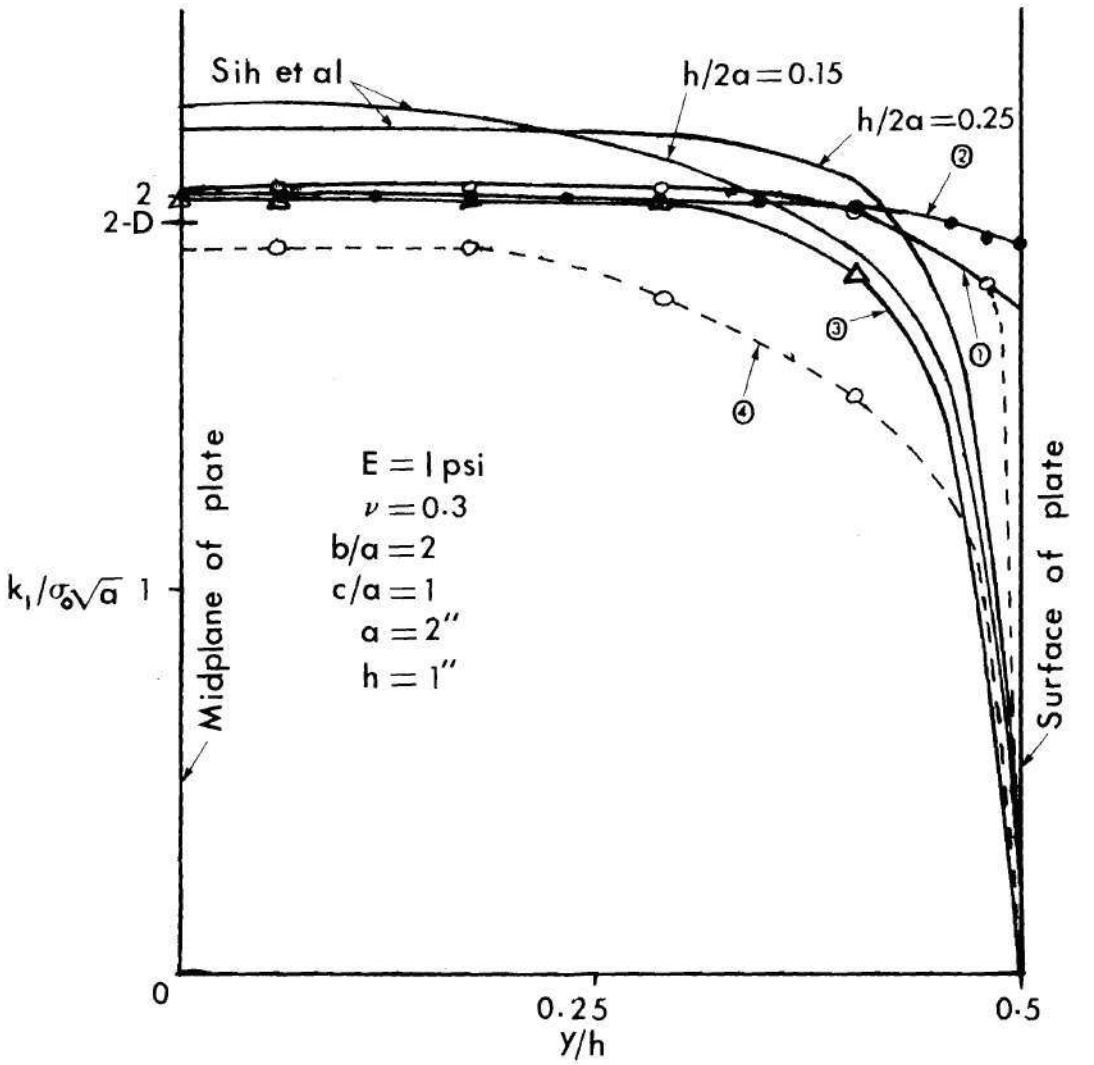

Fig.10. Variation of Stress Intensity Factor Along Crack Front For A Through Thickness Central Crack.

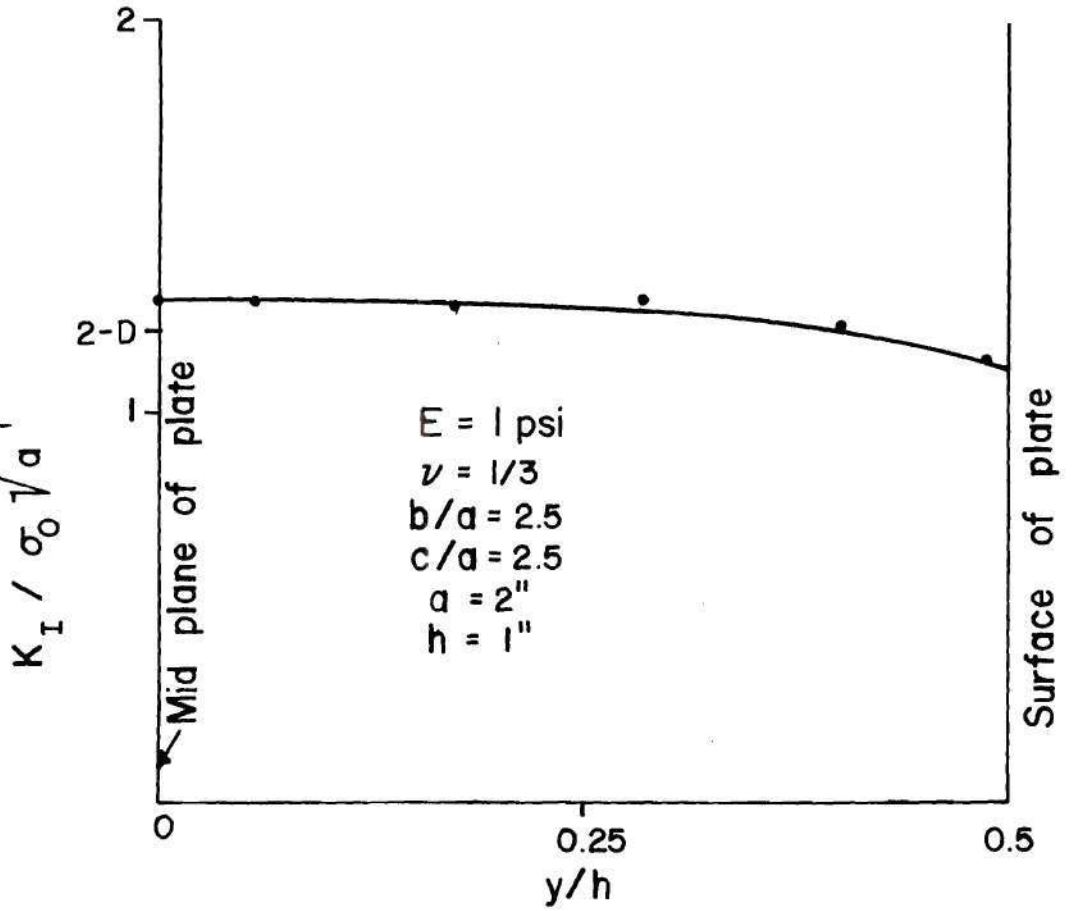

FIG. 11. Variation of Stress Intensity Factor Along Crack Front for a Through Thickness Central Crack

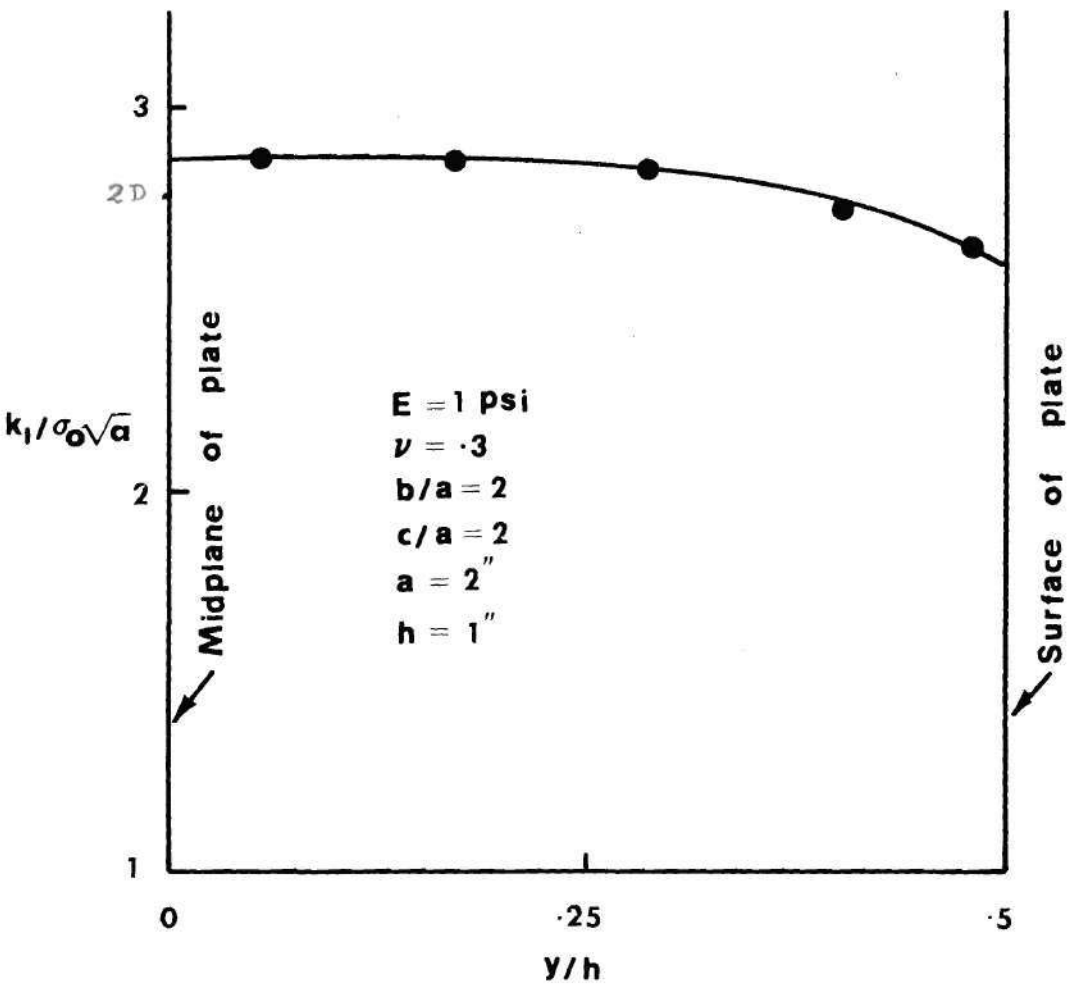

FIG.12.VARIATION OF STRESS INTENSITY FACTOR ALONG CRACK FRONT FOR A THROUGH THE THICKNESS EDGE CRACK

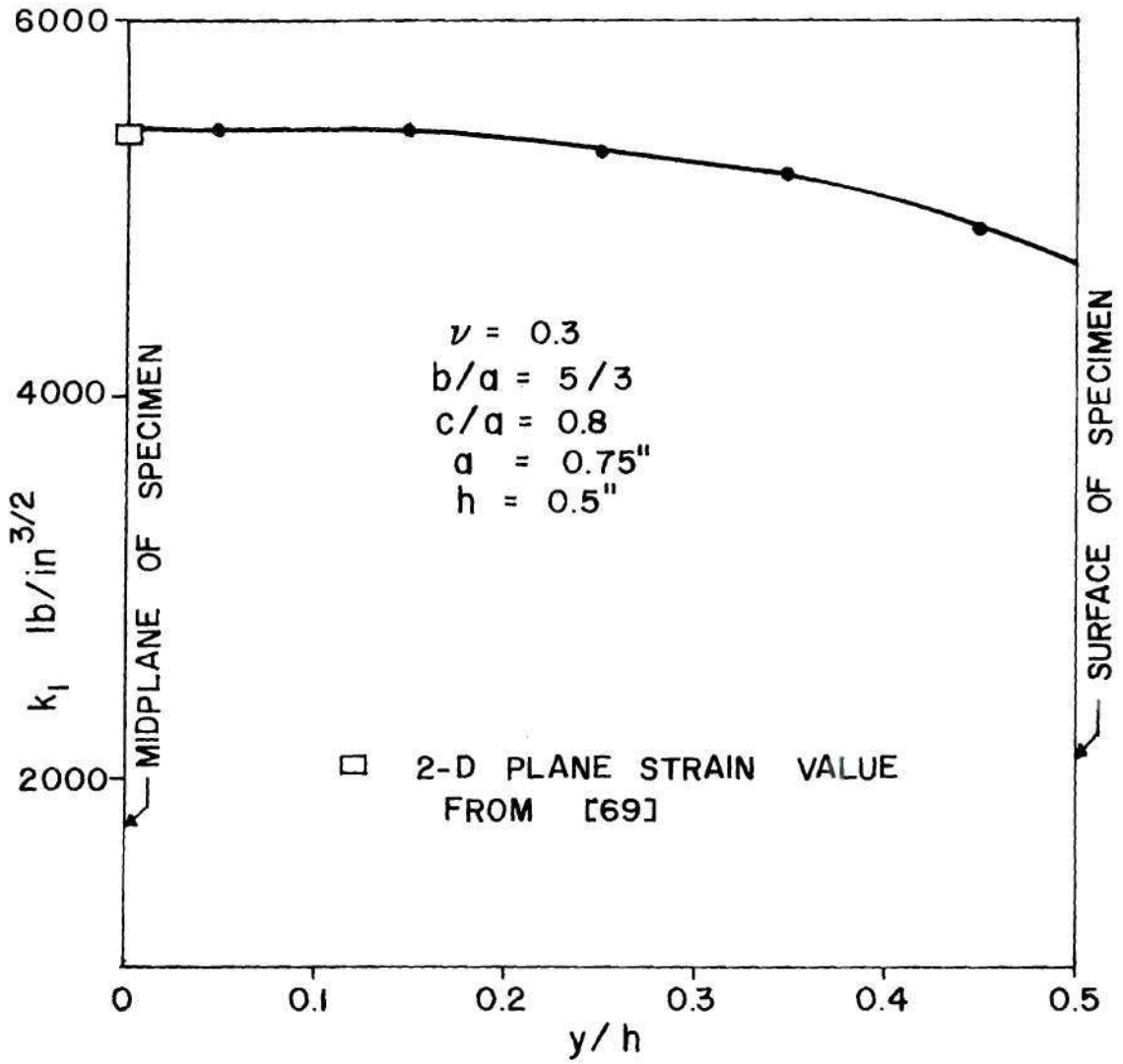

FIG. 13: Variation of Stress Intensity Factor for the Compact Tension Specimen Problem

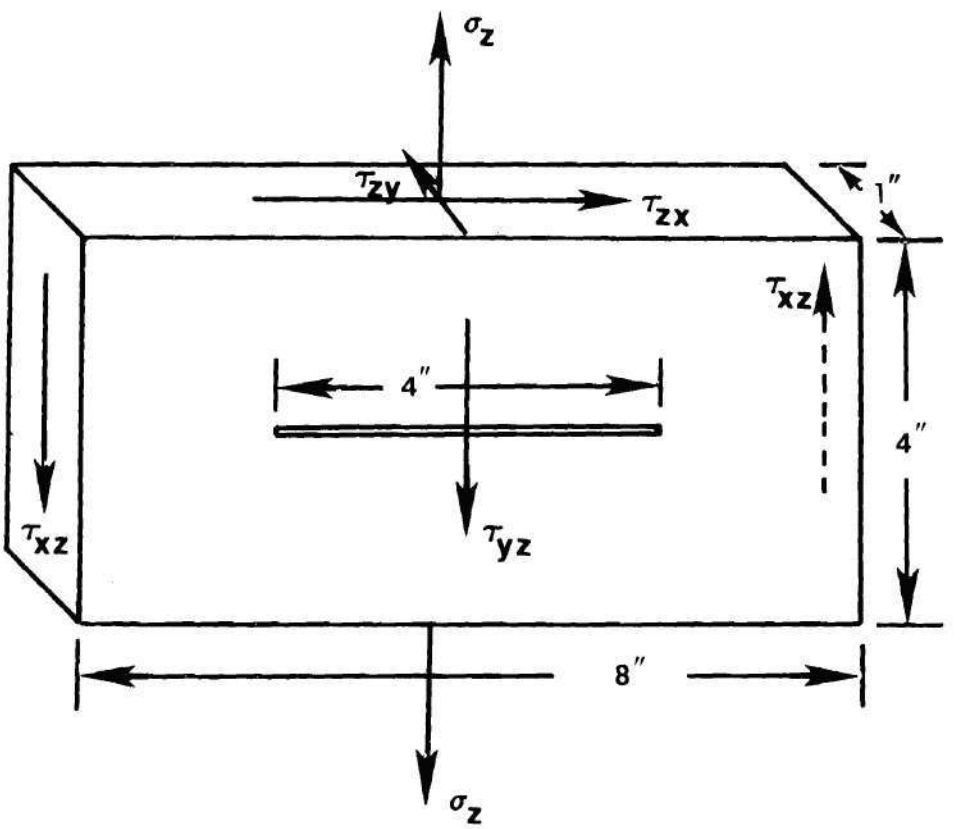

$$\sigma_z = \tau_{zx} = \tau_{yz} = 1 \text{ psi}$$

FIG.14.MIXED MODE PROBLEM OF A THROUGH THE THICKNESS CENTRAL CRACK

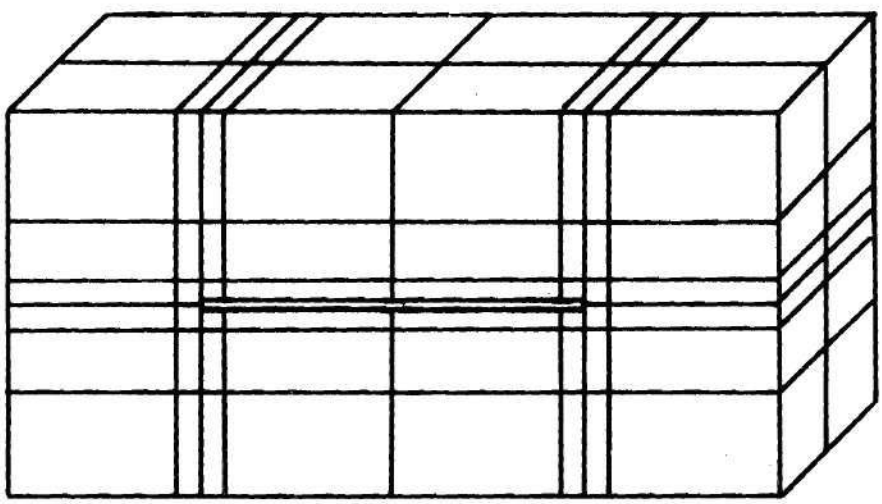

FIG.15.
FINITE ELEMENT BREAKDOWN FOR MIXED MODE PROBLEM

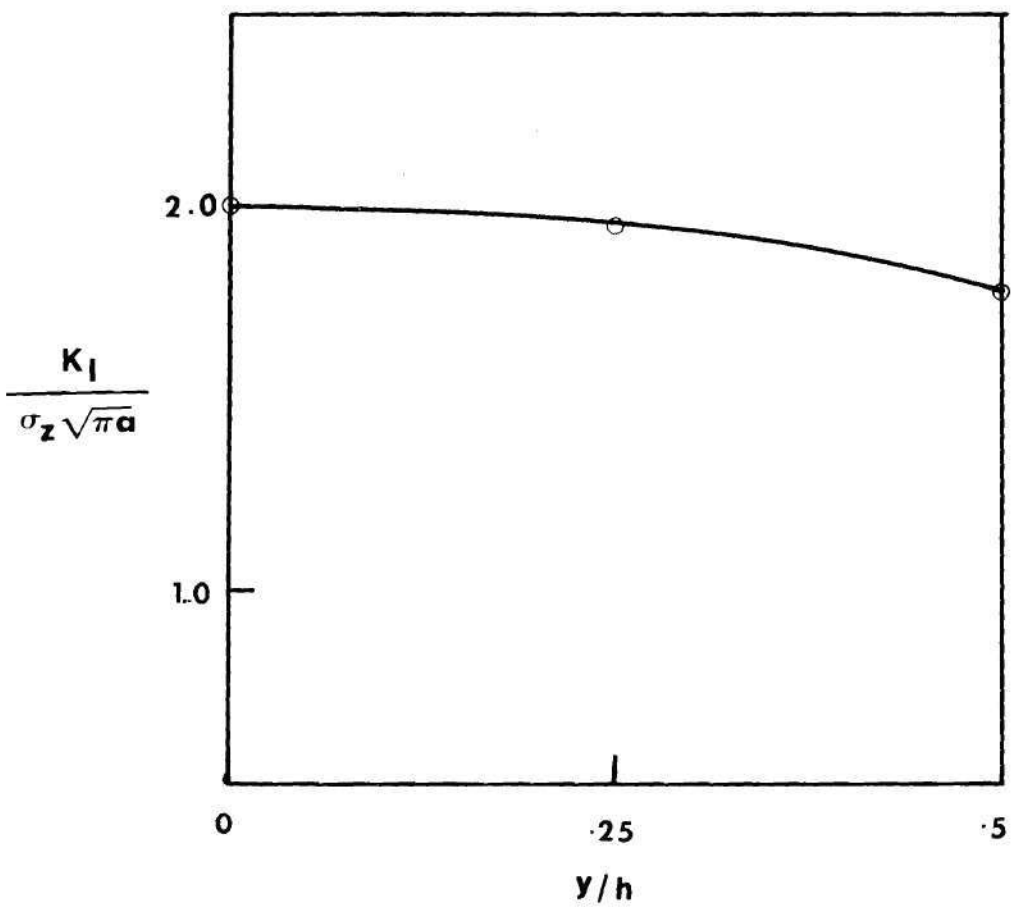

FIG.16.VARIATION OF K_I THROUGH THE THICKNESS FOR THE MIXED MODE PROBLEM

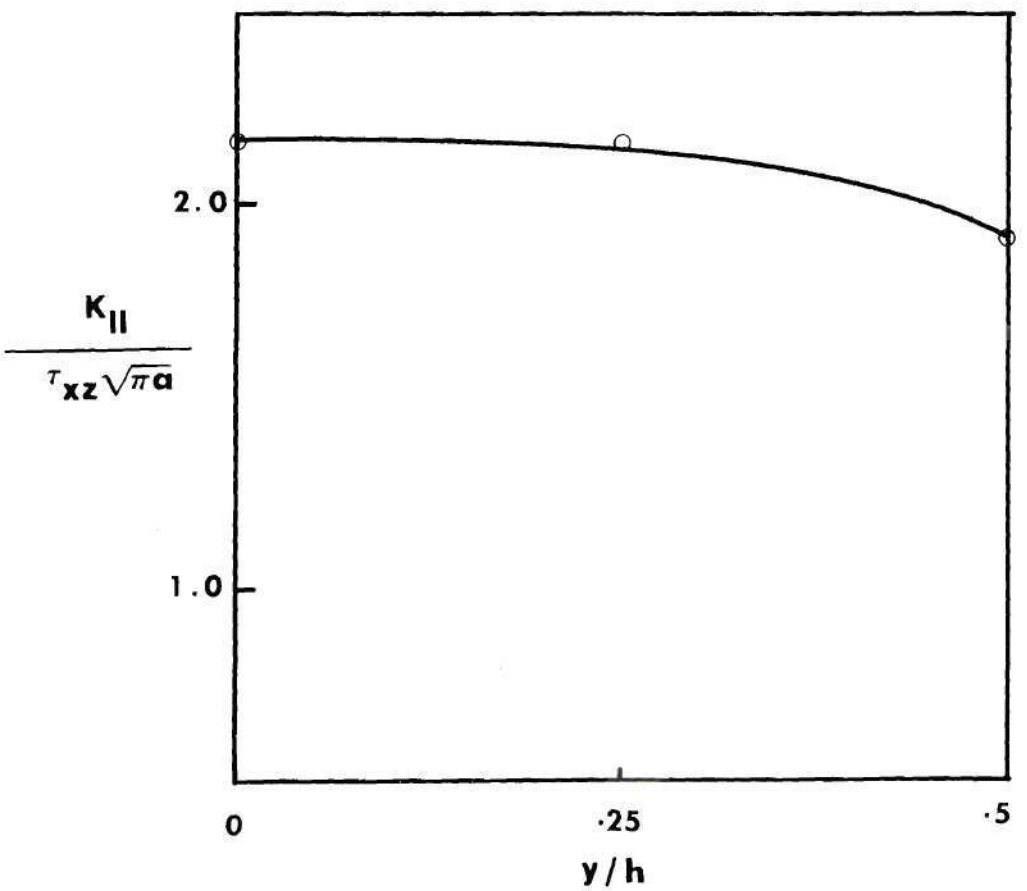

FIG.17.VARIATION OF K_{II} THROUGH THE THICKNESS FOR THE MIXED MODE PROBLEM

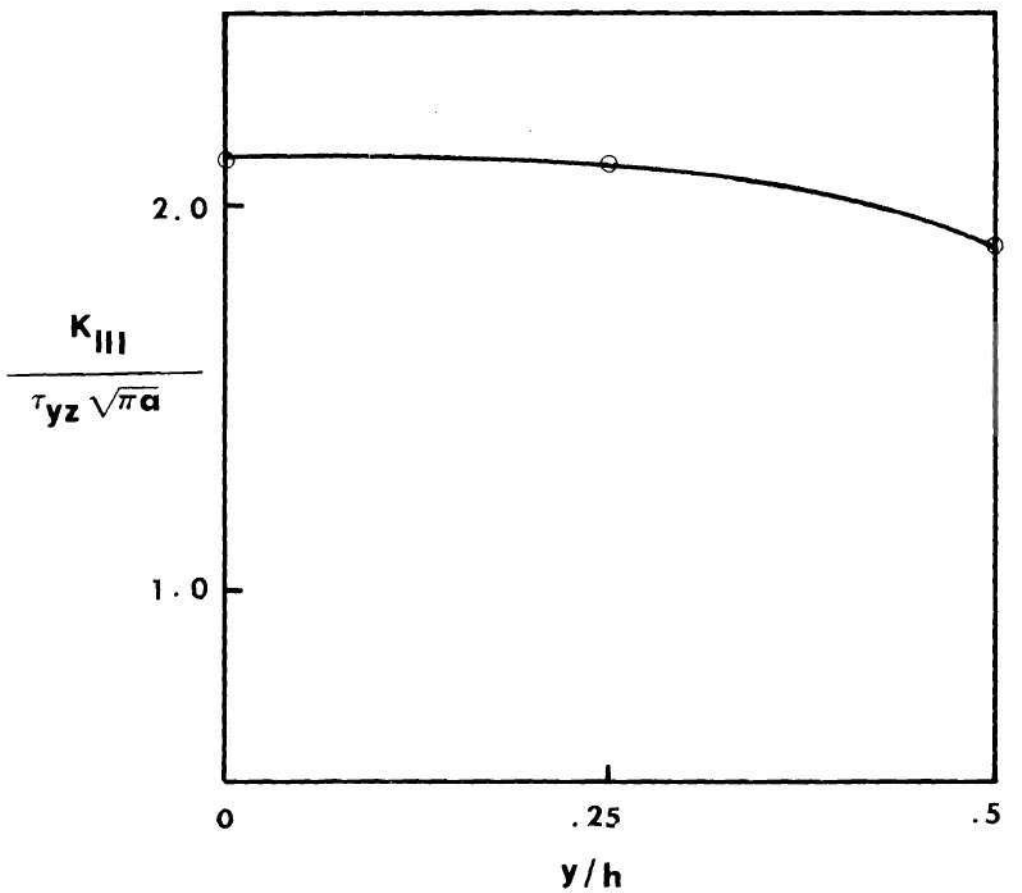

FIG.18.VARIATION OF K_{III} THROUGH THE THICKNESS FOR THE MIXED MODE PROBLEM

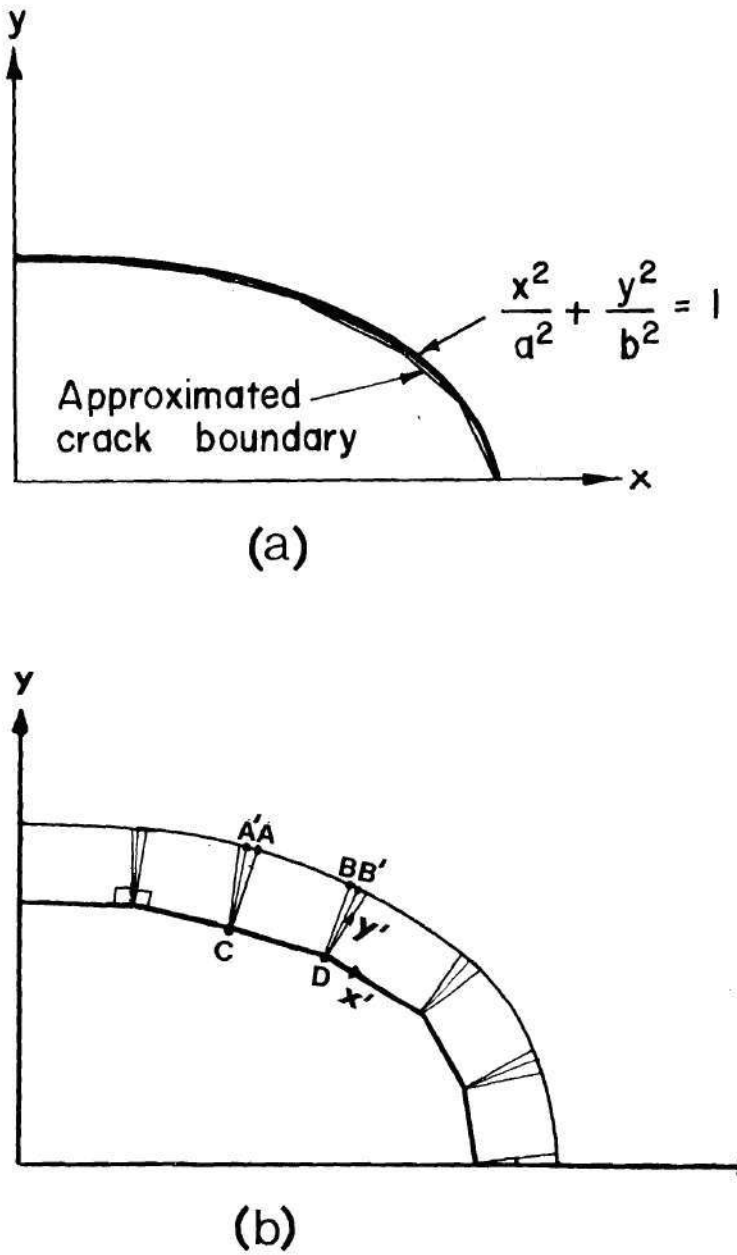

FIG. 19: Approximation of the Elliptical Crack Boundary by Straight Lines

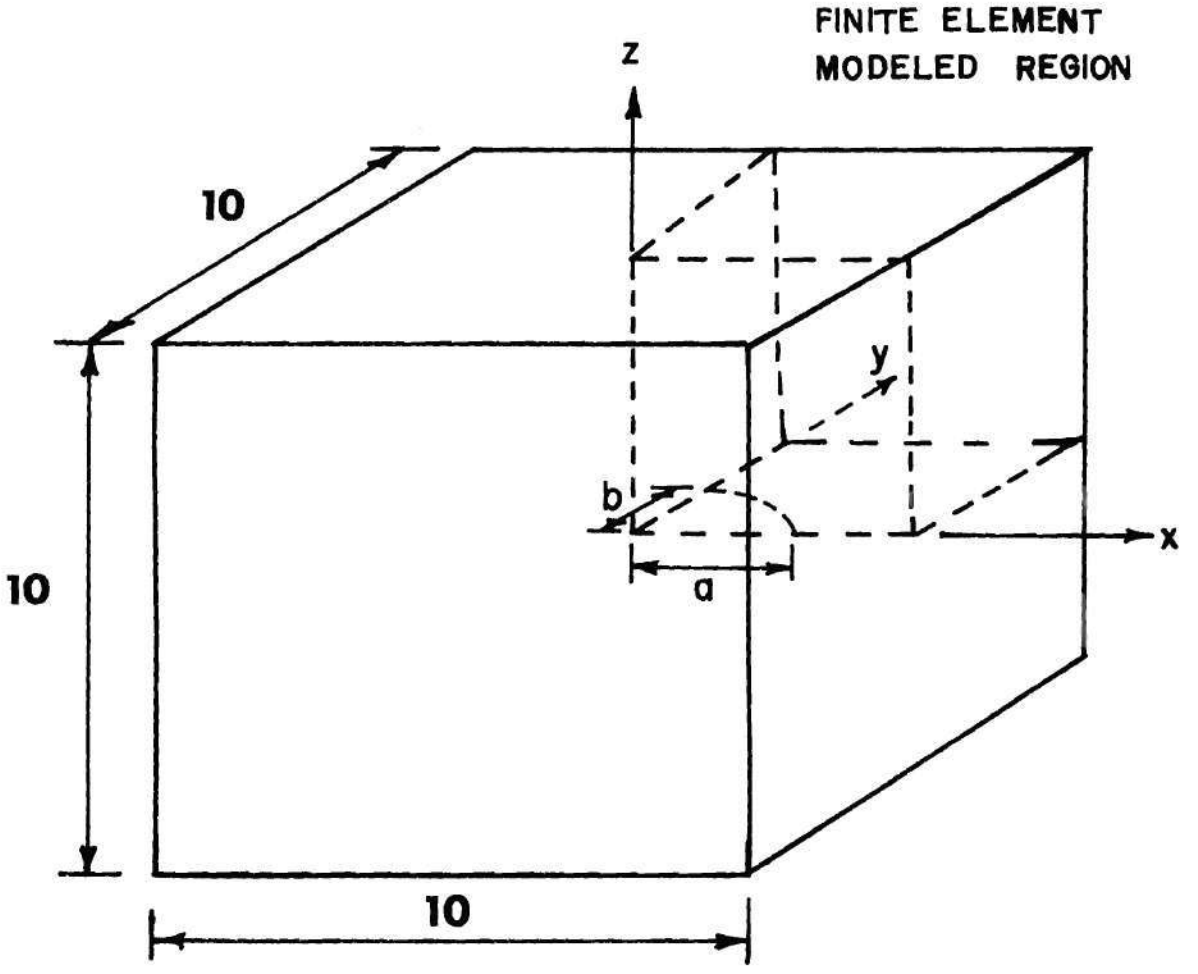

AREA OF QUARTER ELLIPSE = $\frac{\pi}{4}$

ASPECT RATIOS: a/b = 0.25, 0.5, 0.667, 1.0, 1.5, 2.0, 4.0

FIG. 20 Problem Definition (Cube Containing Buried Elliptical Crack)

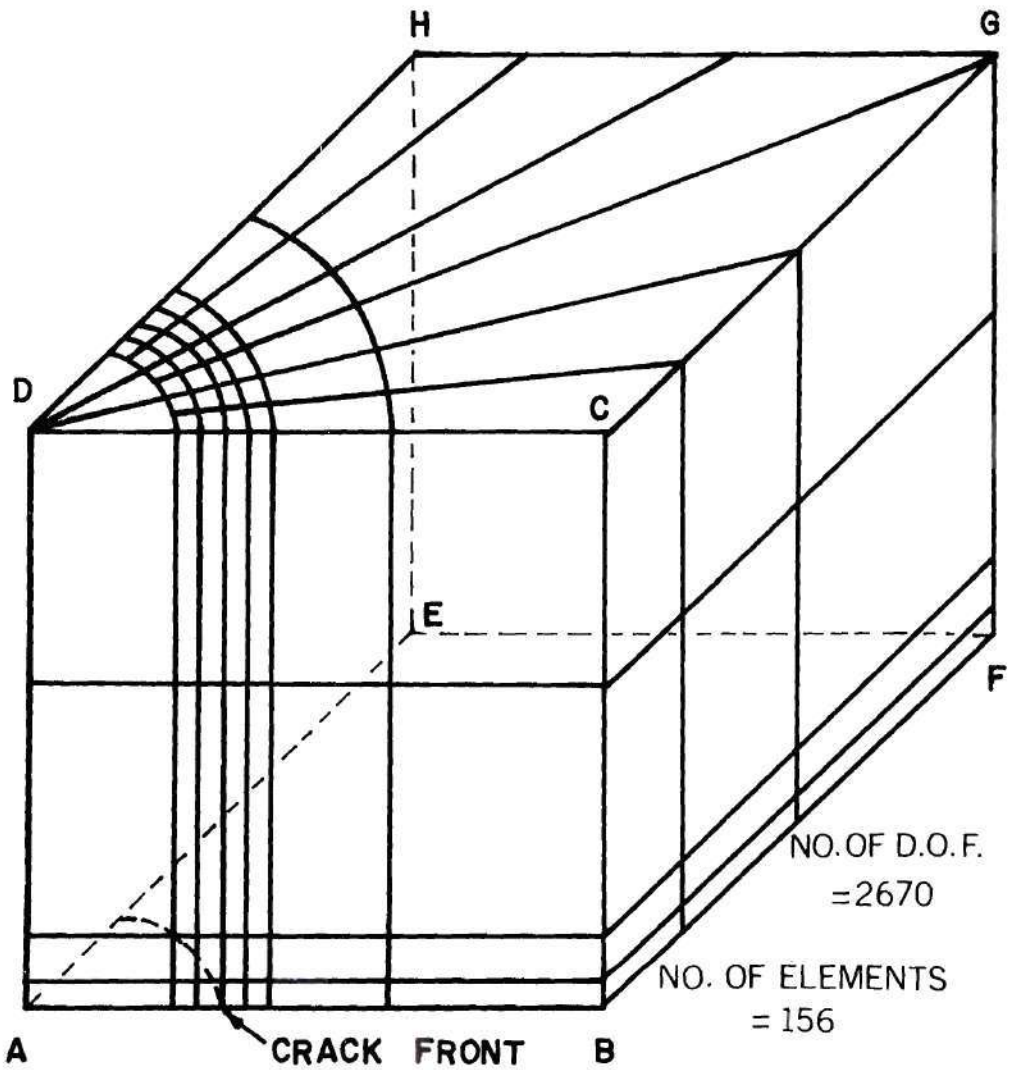

ON FACES ABCD, ADHE AND ABFE BOUNDARY CONDITIONS CAN BE APPLIED APPROPRIATELY TO GENERATE BURIED, SURFACE AND CORNER CRACK PROBLEMS

FIG. 21 Finite Element Breakdown for Circular and Elliptical Crack Problems

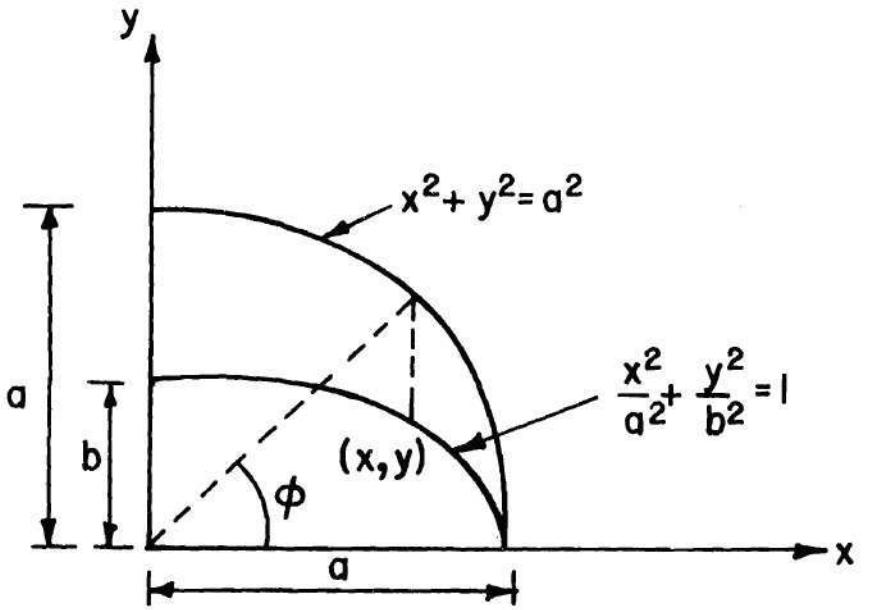

$$K_I = \frac{\sigma\sqrt{\pi b}}{E(k)}\left\{\sin^2\phi + \left(\frac{b}{a}\right)^2\cos^2\phi\right\}^{1/4} \qquad a > b$$

ϕ = ELLIPTICAL ANGLE

σ = STRESS NORMAL TO PLANE OF ELLIPSE

$$E(k) = \int_0^{\pi/2} \sqrt{1-k^2\sin^2\psi}\; d\psi$$

$$= \frac{\pi}{2}\left[1-(1/2)^2 k^2-\left(\frac{1}{2}\cdot\frac{3}{4}\right)^2\frac{k^4}{3}-\left(\frac{1}{2}\cdot\frac{3}{4}\cdot\frac{5}{6}\right)^2\frac{k^6}{5}-\cdots\right]$$

$$k^2 = 1 - b^2/a^2$$

FIG.22 Exact Solution for Buried Elliptical Crack in an Infinite Solid

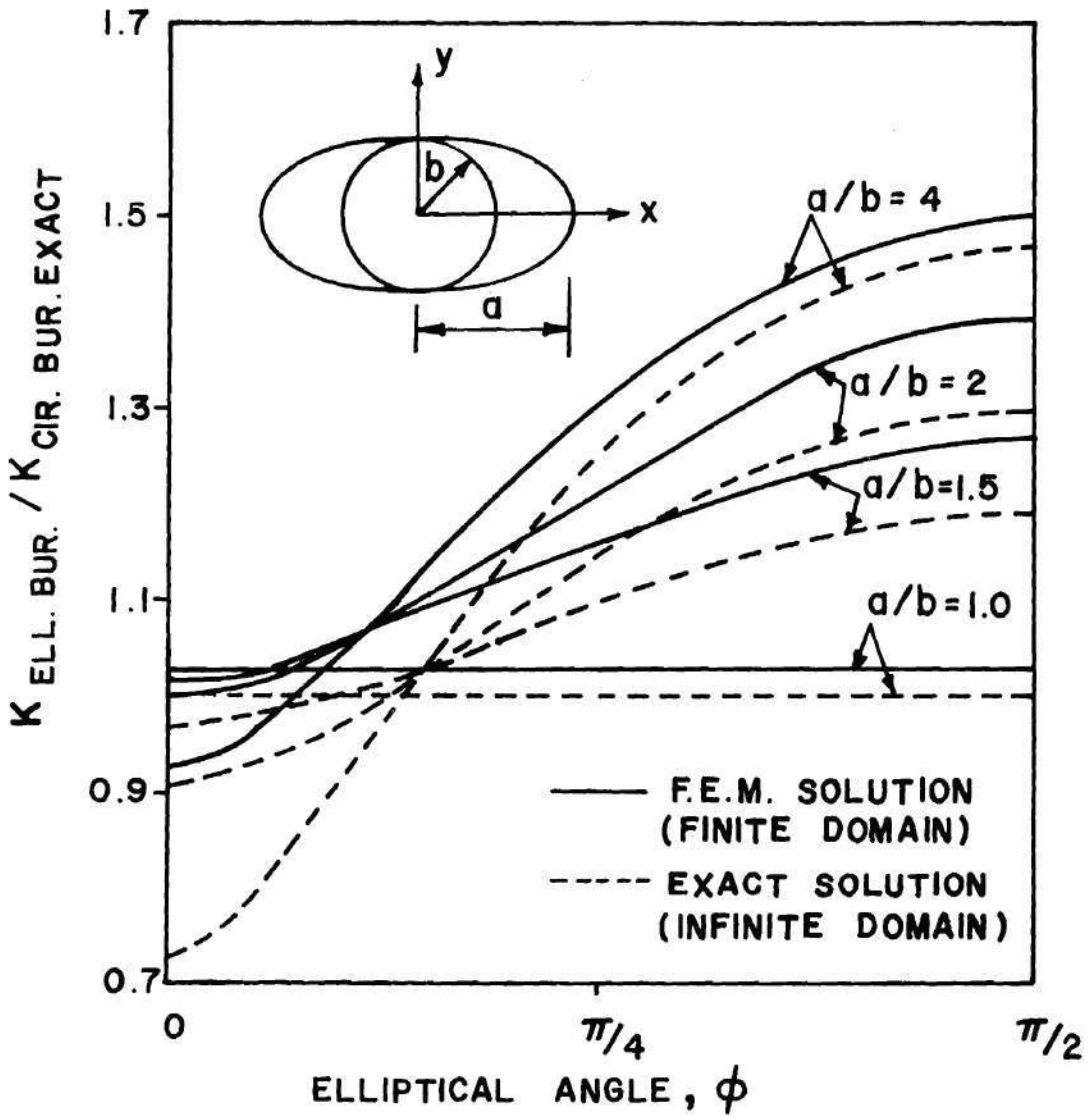

FIG.23 Variation of Stress-Intensity Factors for Buried Elliptical Cracks

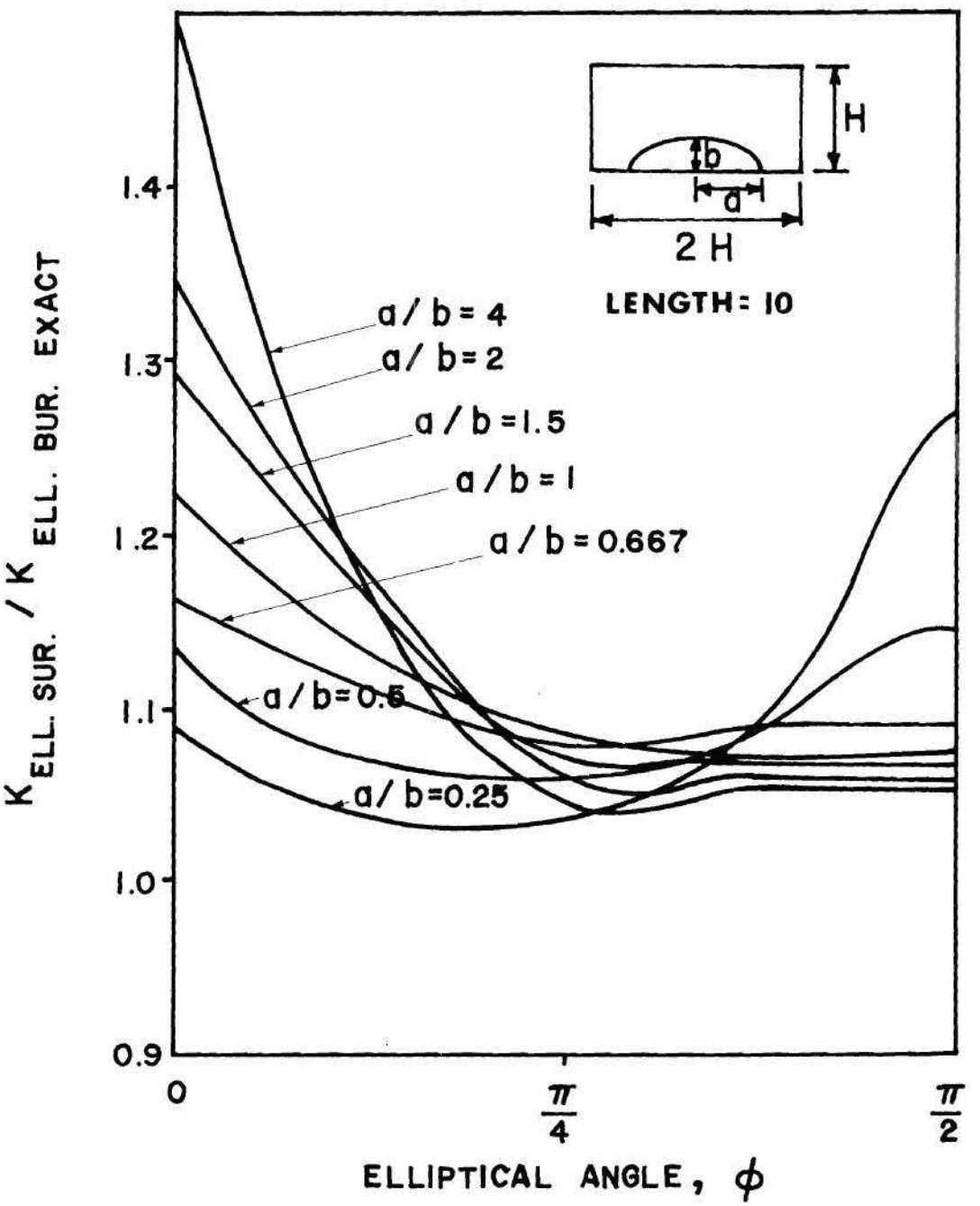

FIG.24 Variation of Stress Intensity Factors for Semielliptical Surface Cracks

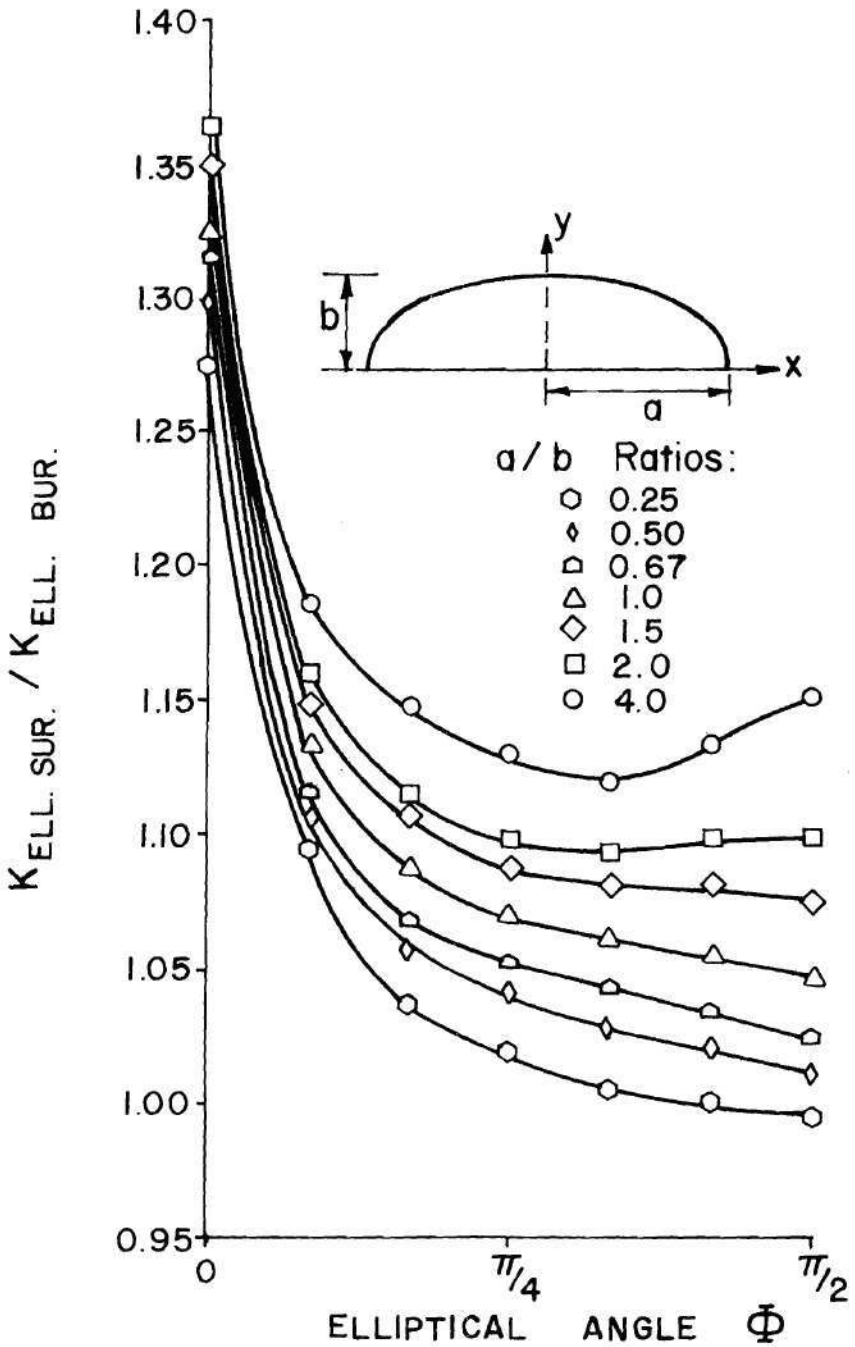

G. 25: Cruse's Solution of Stress Intensity Magnification for Surface Crack

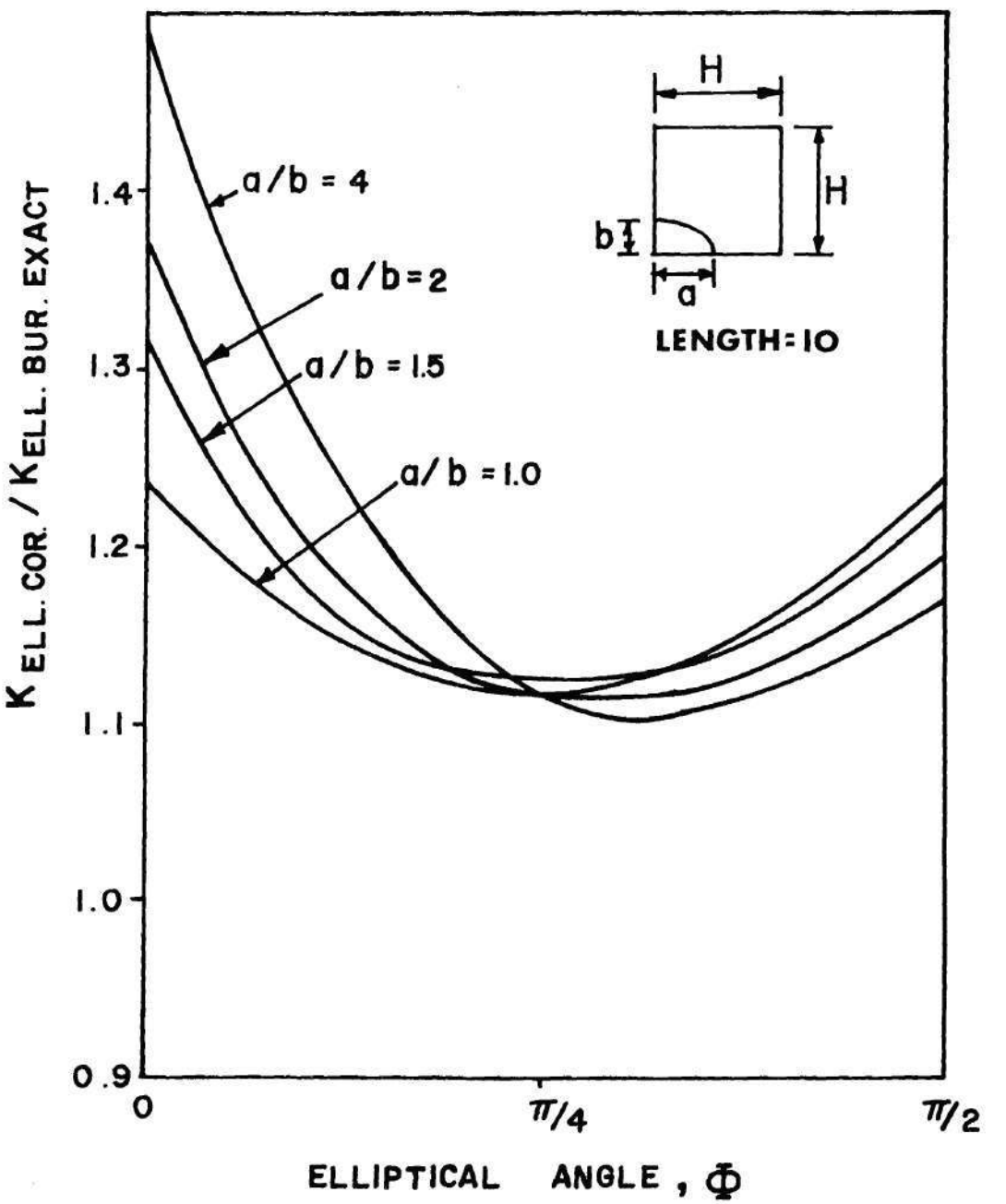

FIG.26 Variation of Stress - Intensity Factors for Quarter Elliptical Corner Cracks

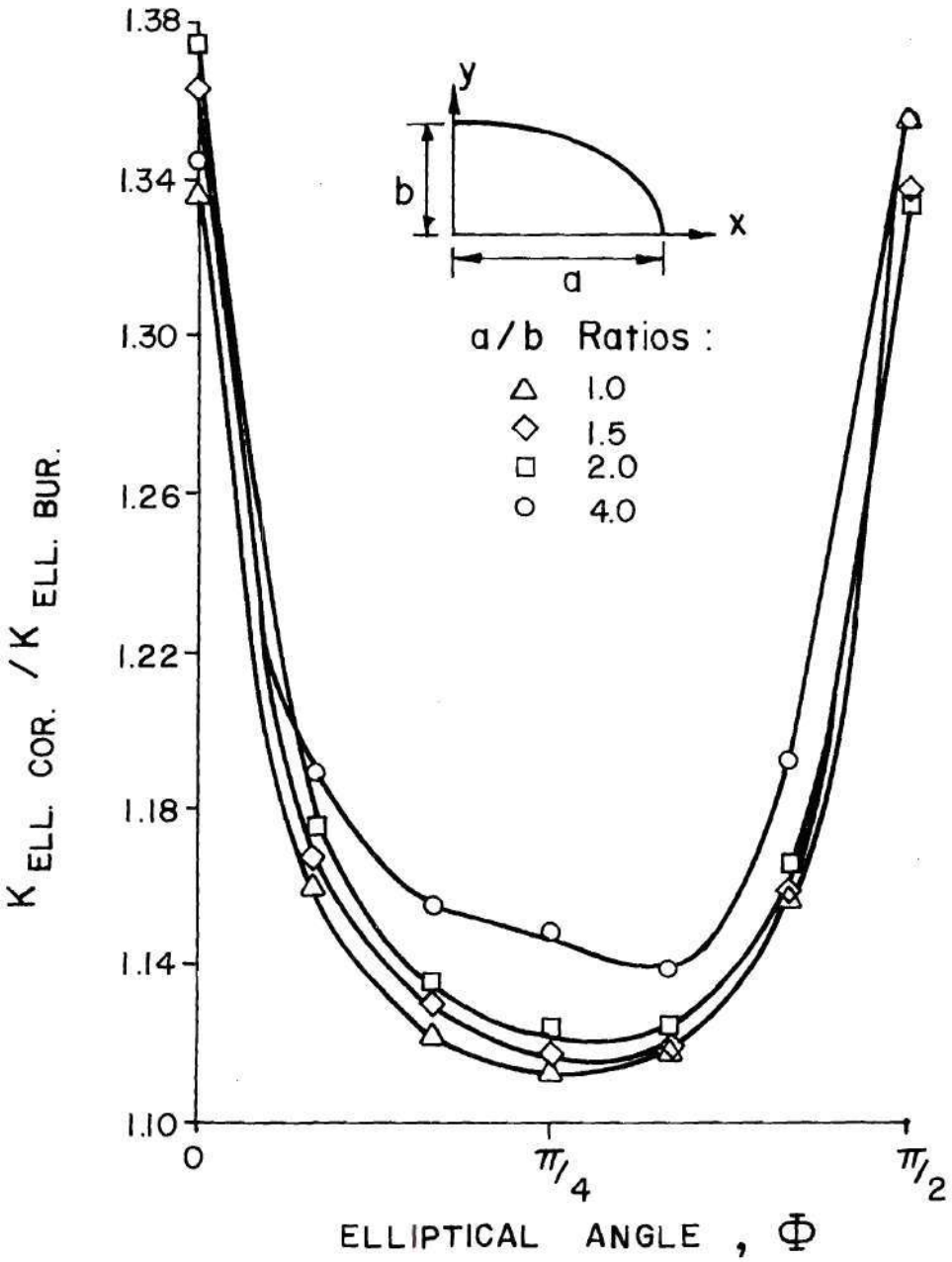

FIG. 27: Cruse's Solution of Stress Intensity Magnification for Corner Crack

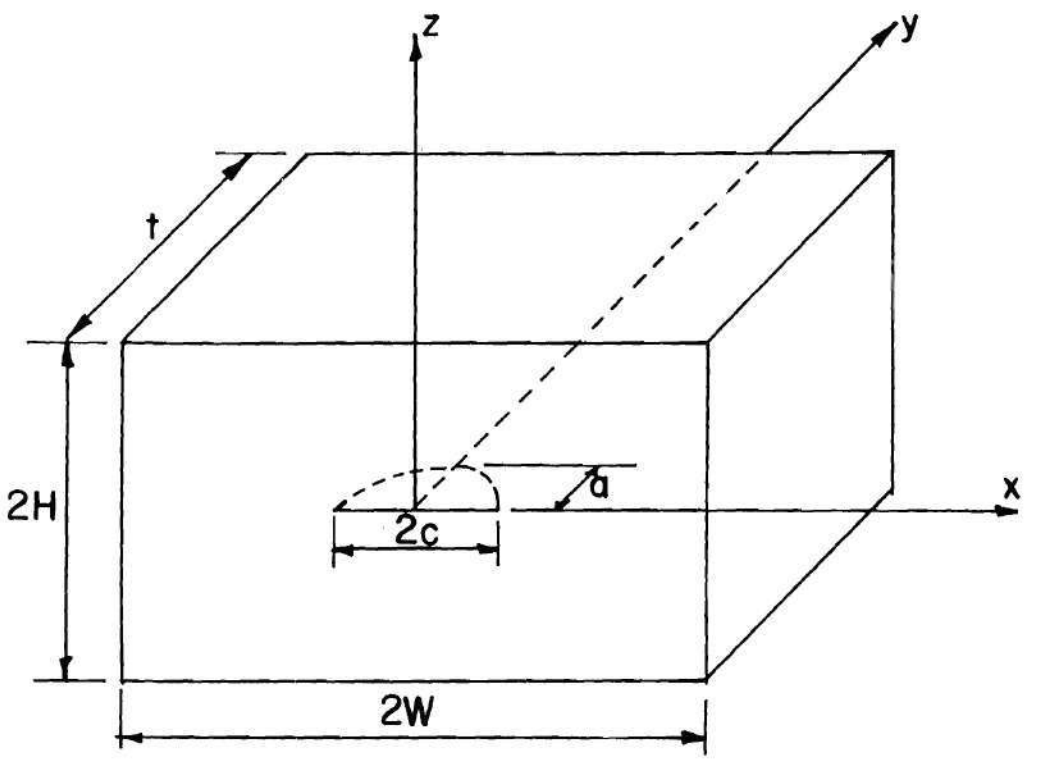

FIG. 28: The Surface Crack Problems

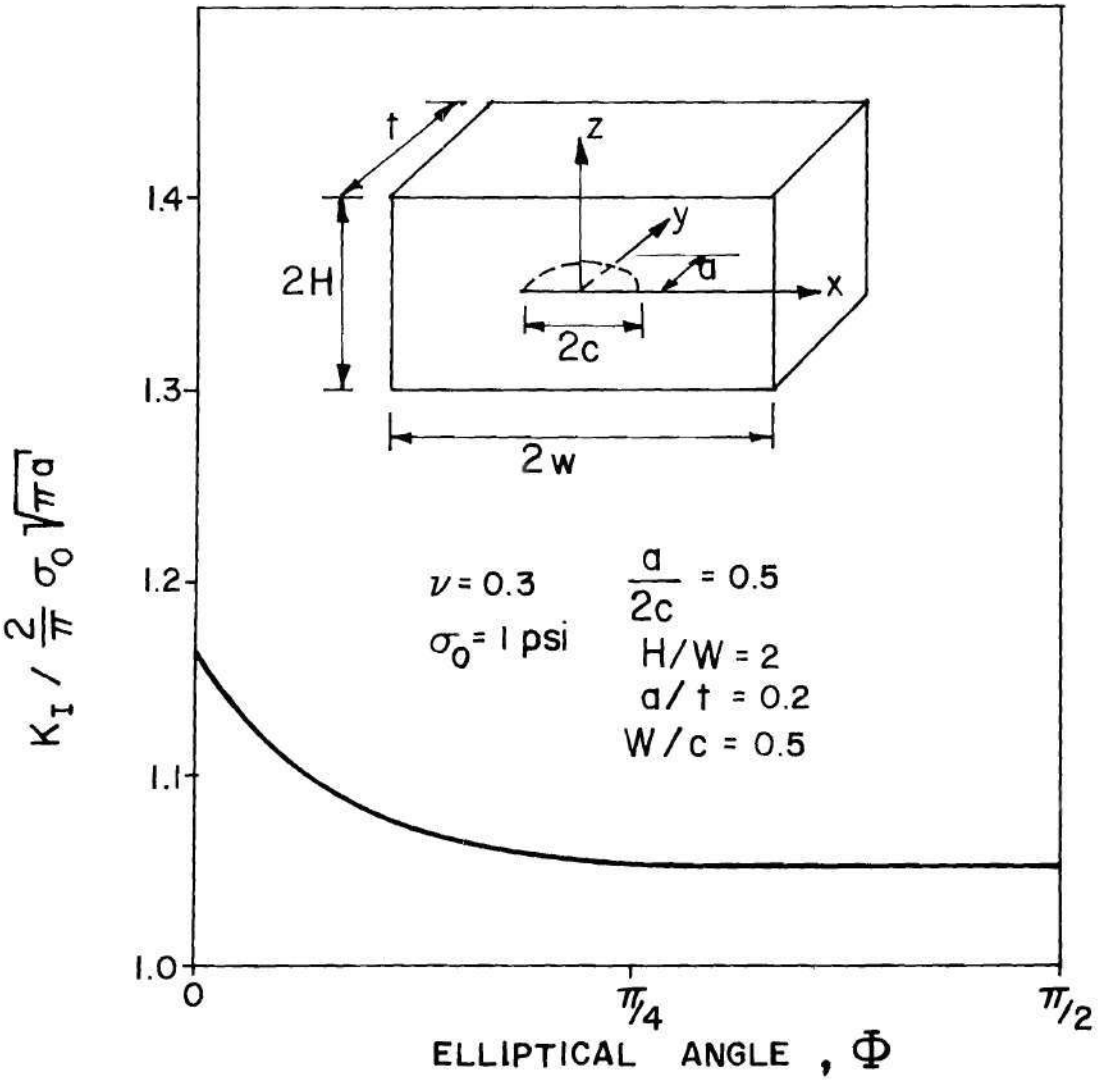

FIG. 29: Variation of Stress Intensity Factor for Semicircular Surface Crack in a Tension Specimen

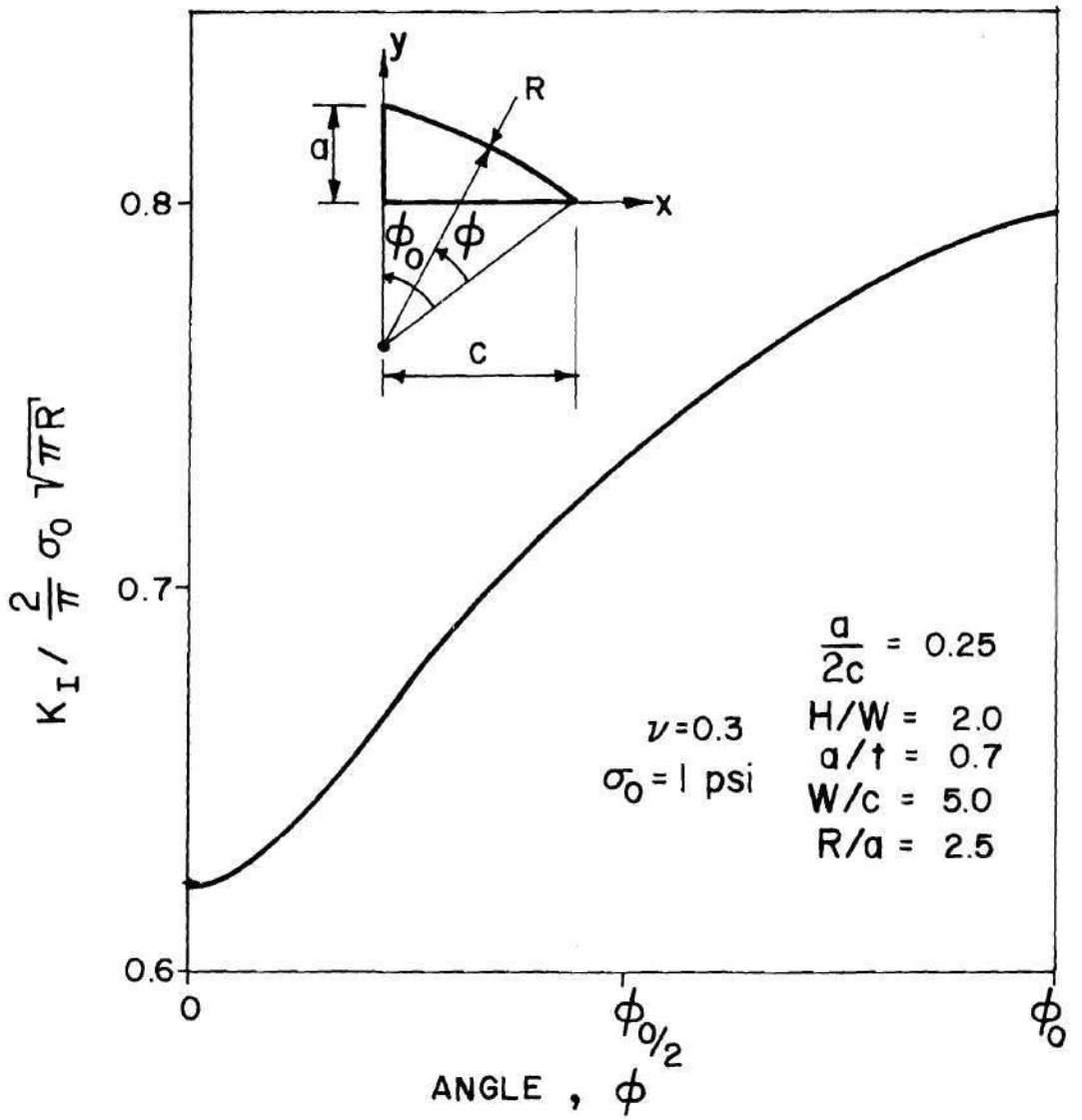

FIG. 30: Variation of Stress Intensity Factor for Part Circular Surface Crack in a Tension Specimen

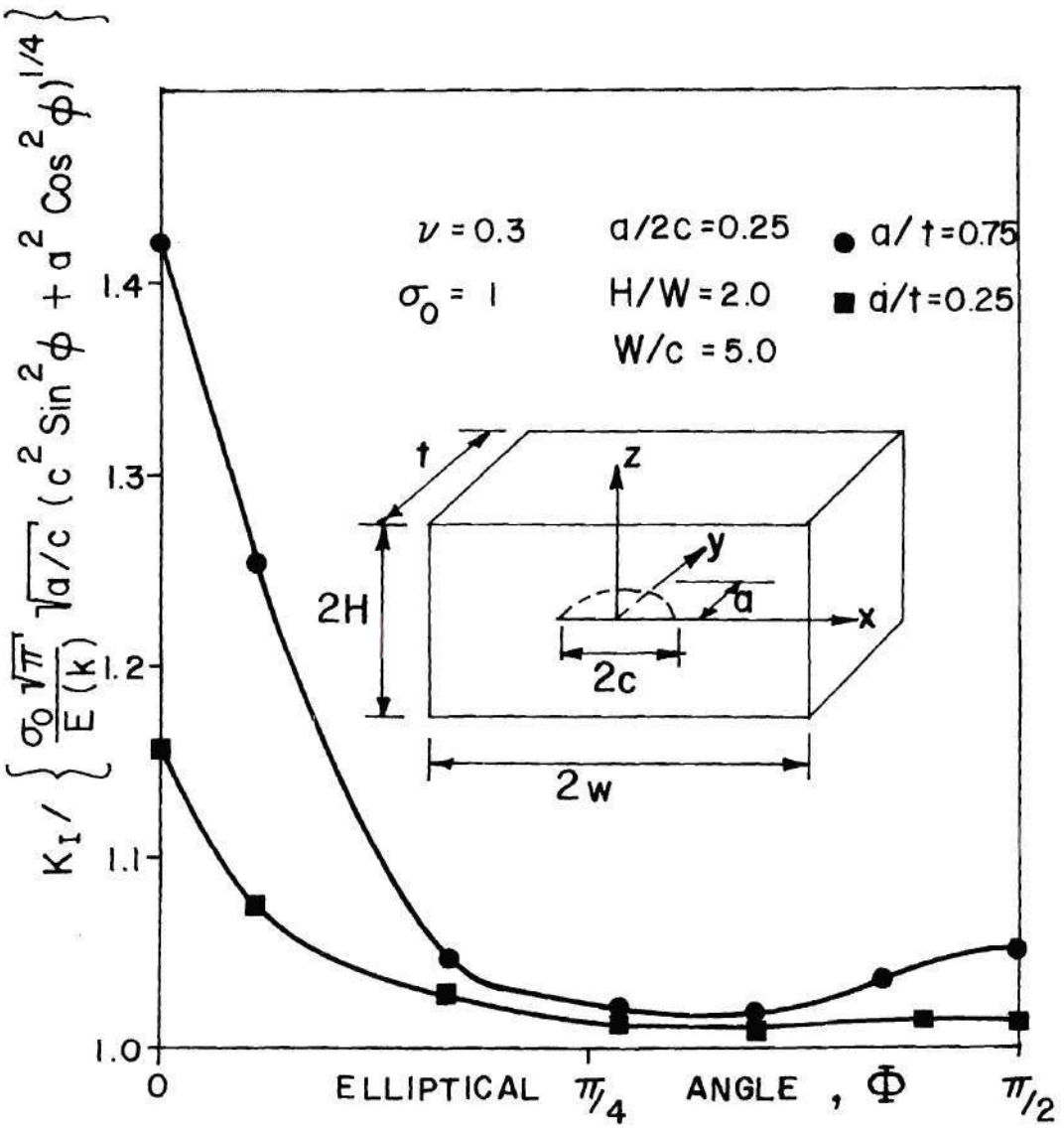

FIG. 31: Variation of Stress Intensity Magnification Factor for Semi-Elliptical Surface Cracks in a Tension Specimen

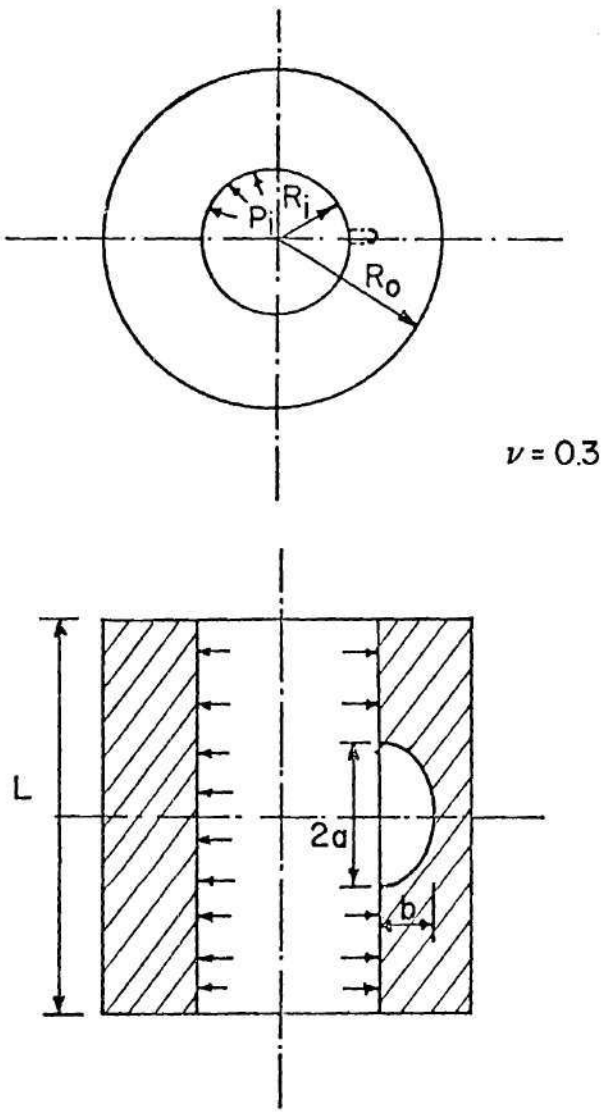

FIG. 32. Inner Semi - Elliptical Crack in a Pressurized Cylinder

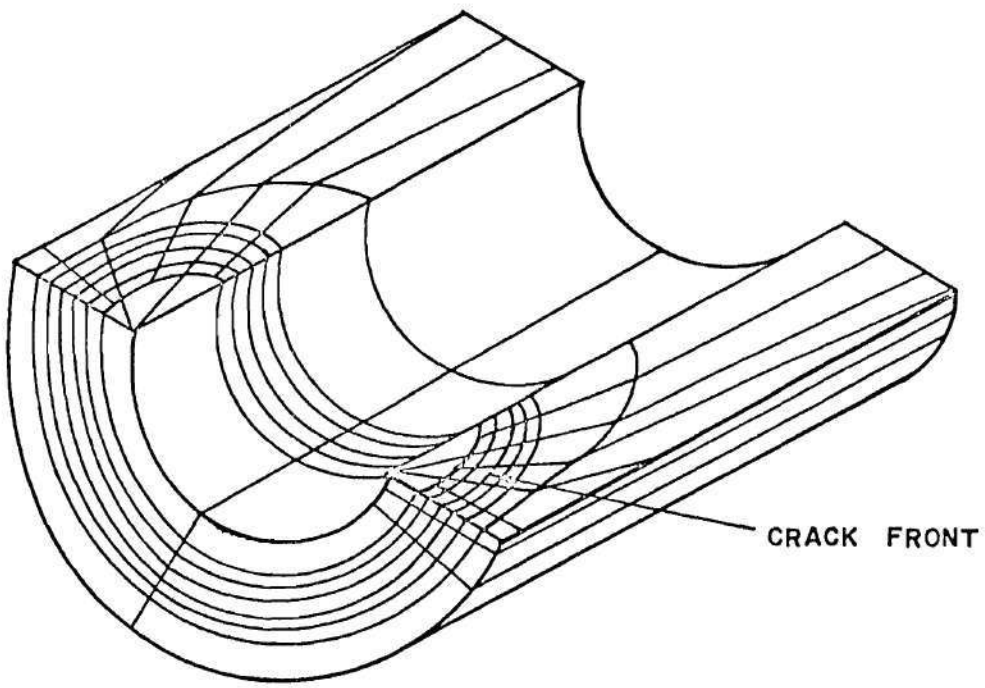

FIG. 33 Finite Element Breakdown of Qudrter of the Pressurized Cylinder with Inner Crack

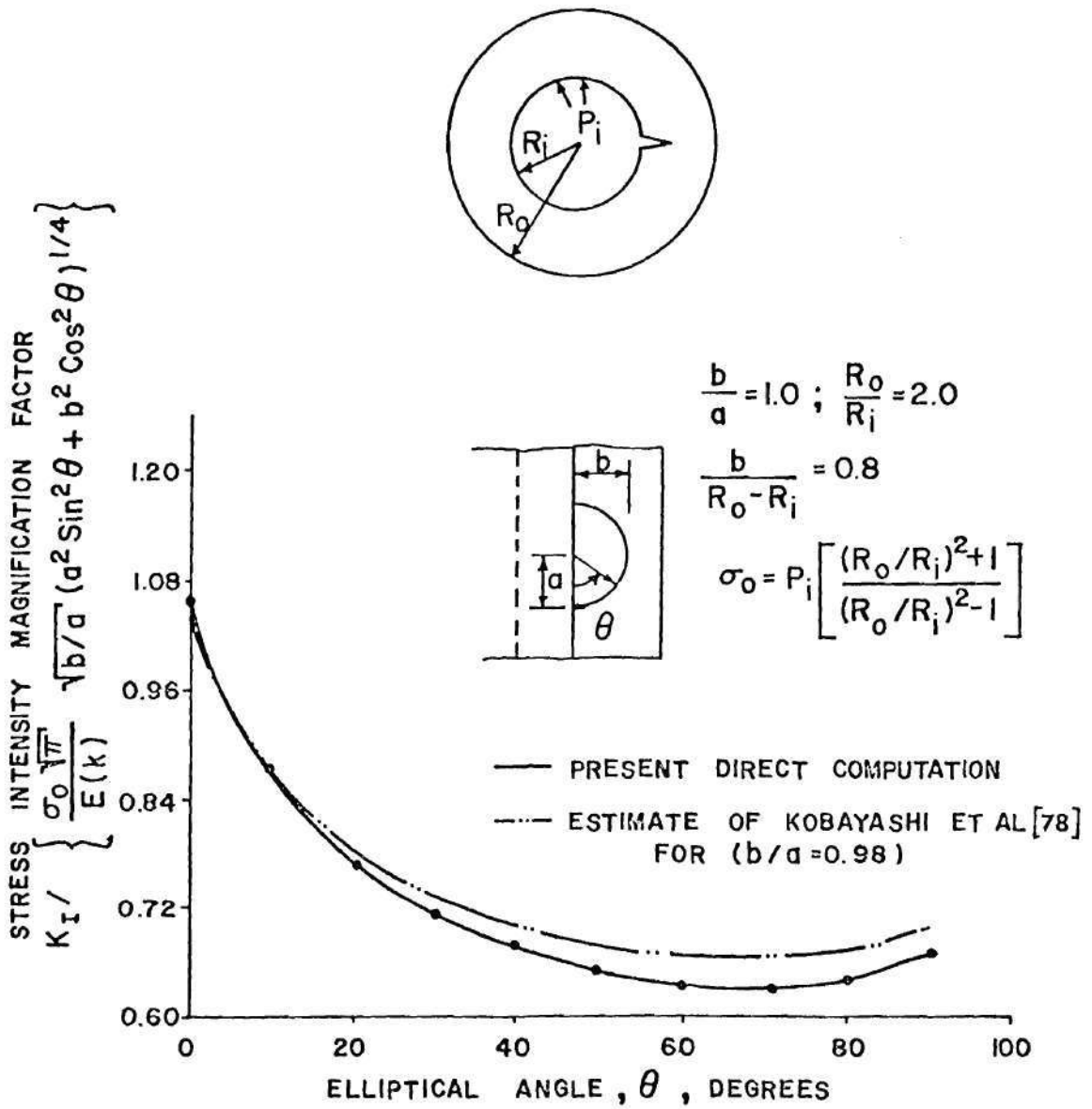

FIG.34 Stress Intensity Magnification Factor for an Unpressurized Inner Semicircular Crack in a Pressurized Cylinder

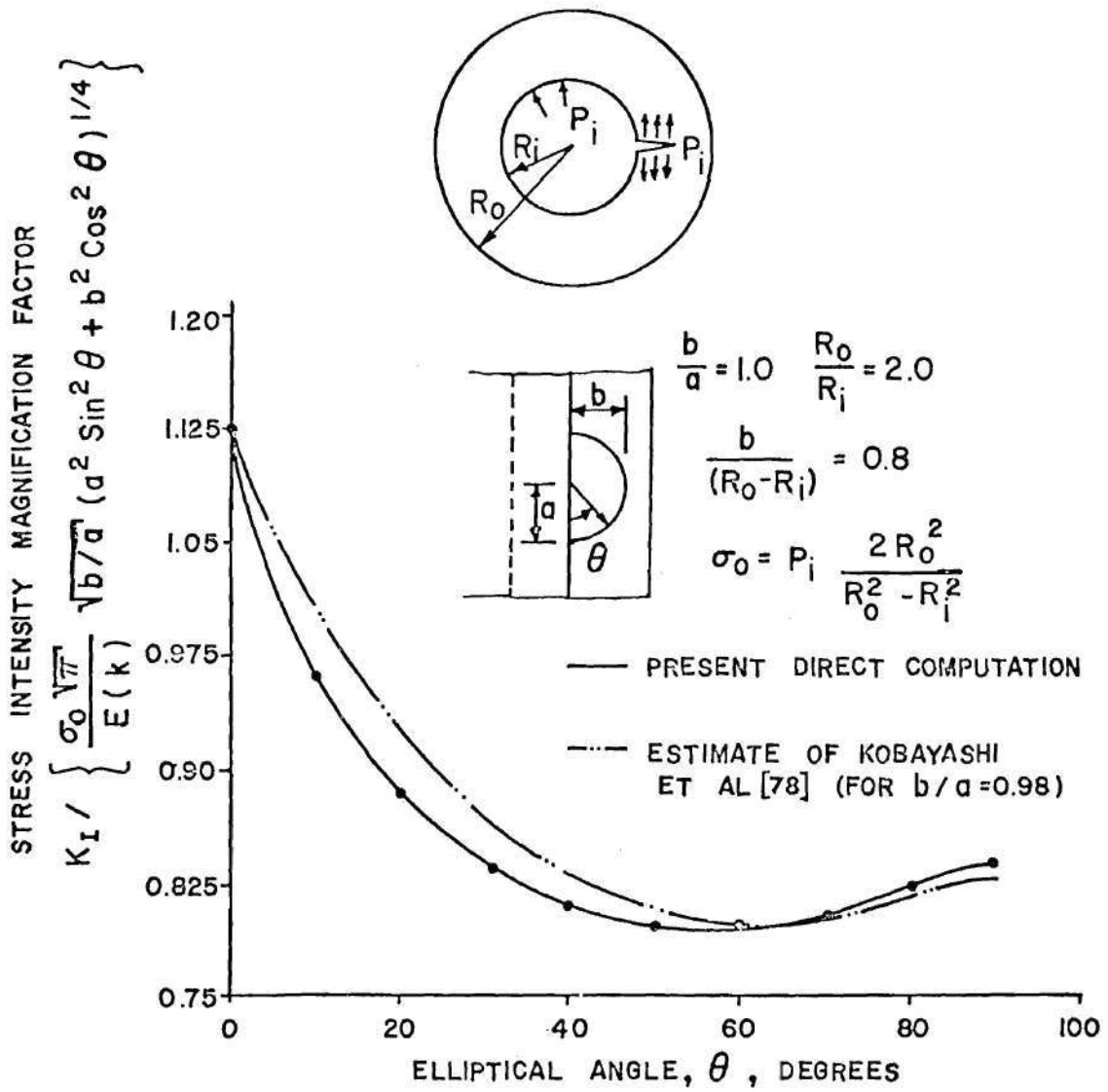

FIG. 35 Stress Intensity Magnification Factor for a Pressurized Inner Semicircular Crack in a Pressurized Cylinder

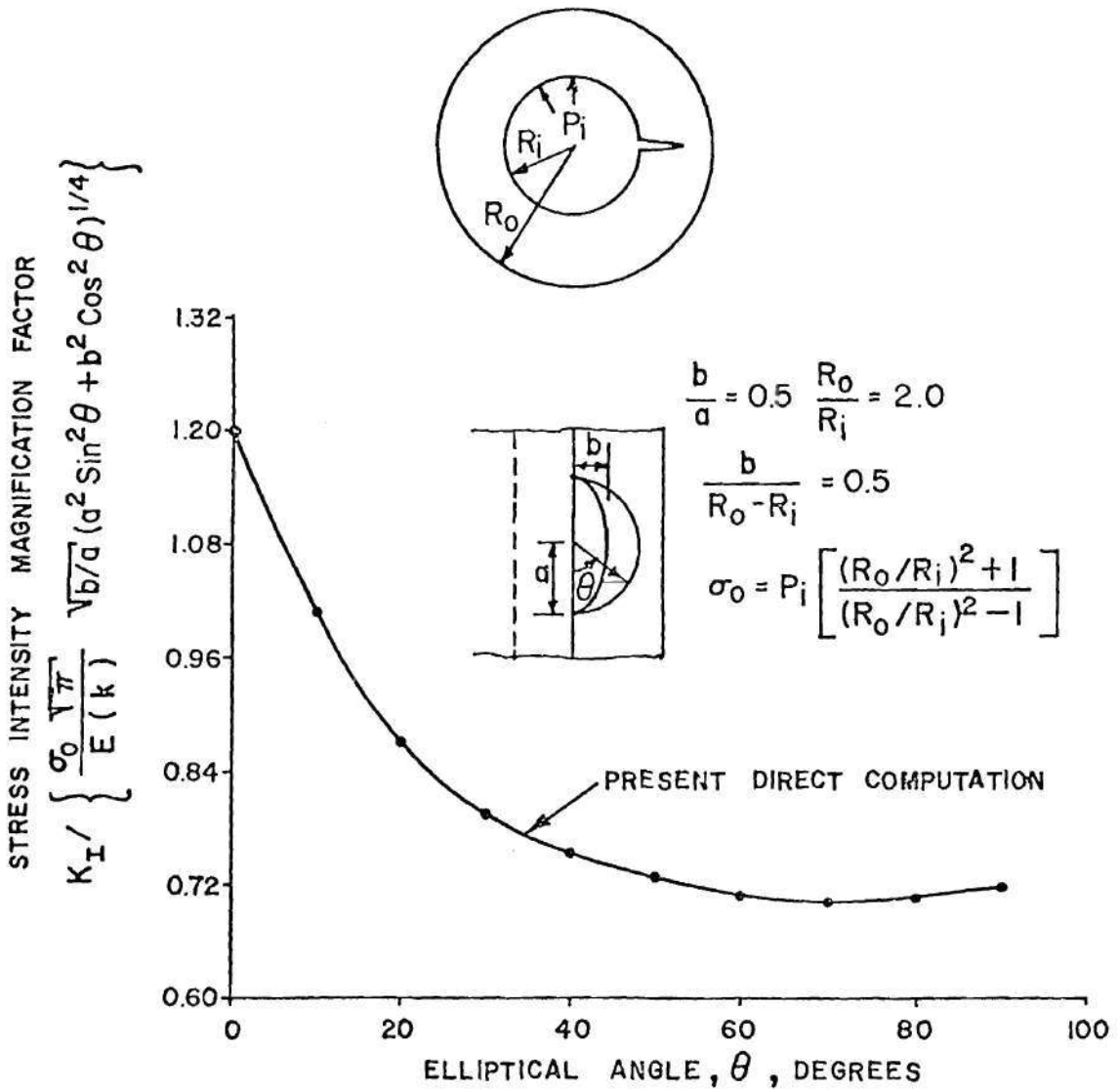

FIG.36 Stress Intensity Magnification Factor for an Unpressurized Inner Semielliptical Crack in a Pressurized Cylinder

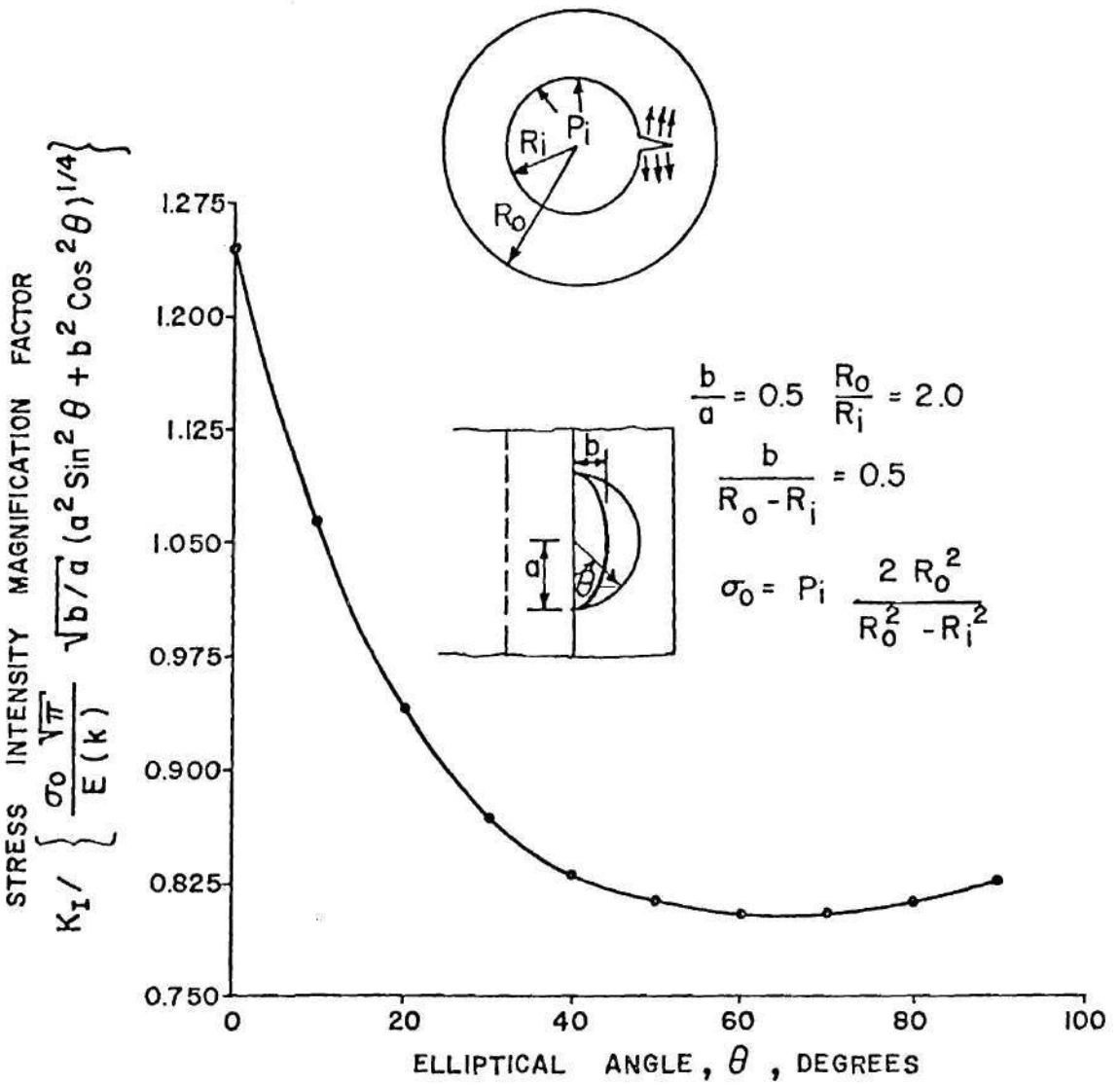

FIG. 37 Stress Intensity Magnification Factor for a Pressurized Inner Semielliptical Crack in a Pressurized Cylinder

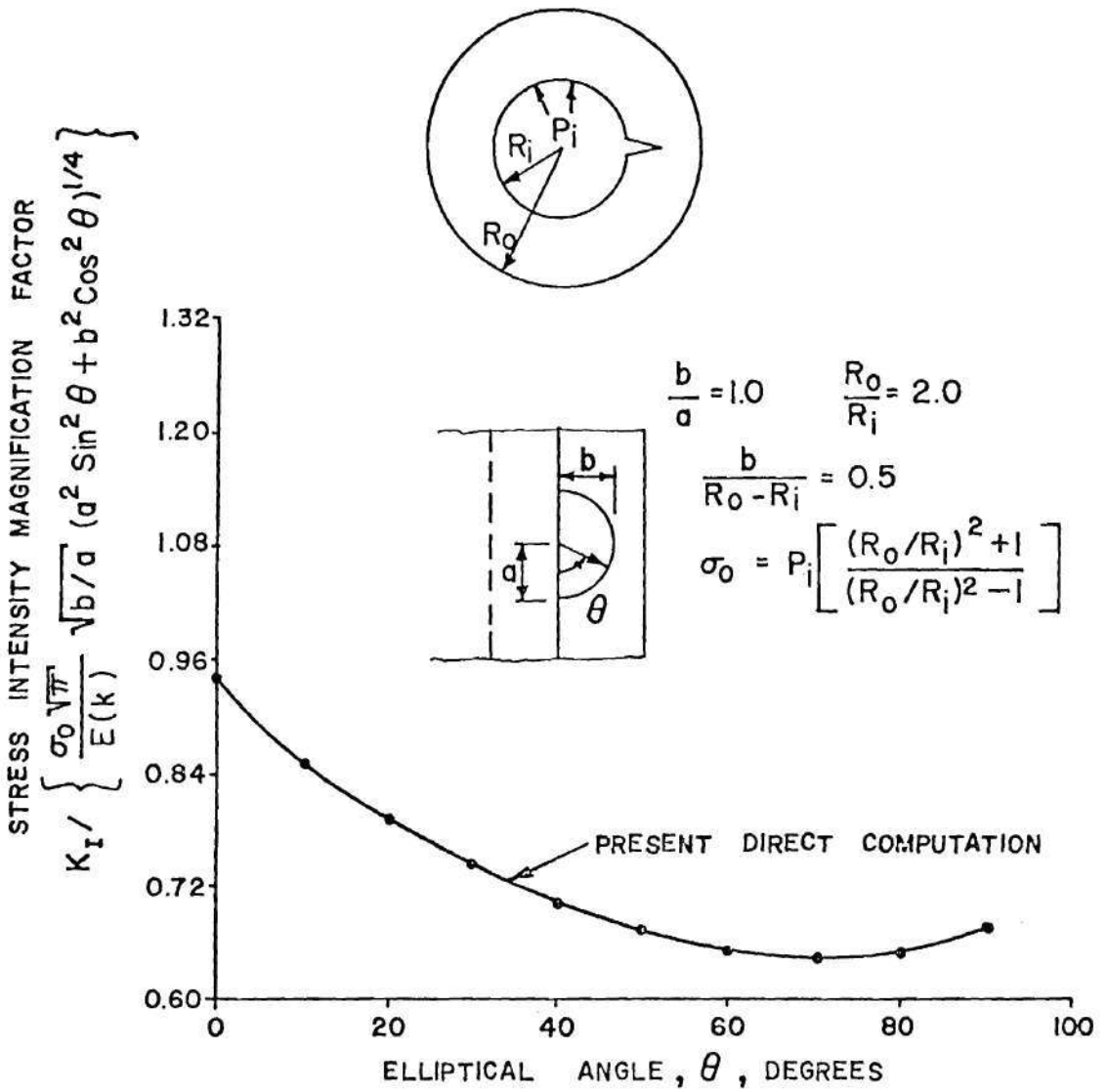

FIG. 38 Stress Intensity Magnification Factor for an Unpressurized Inner Semicircular Crack in a Pressurized Cylinder

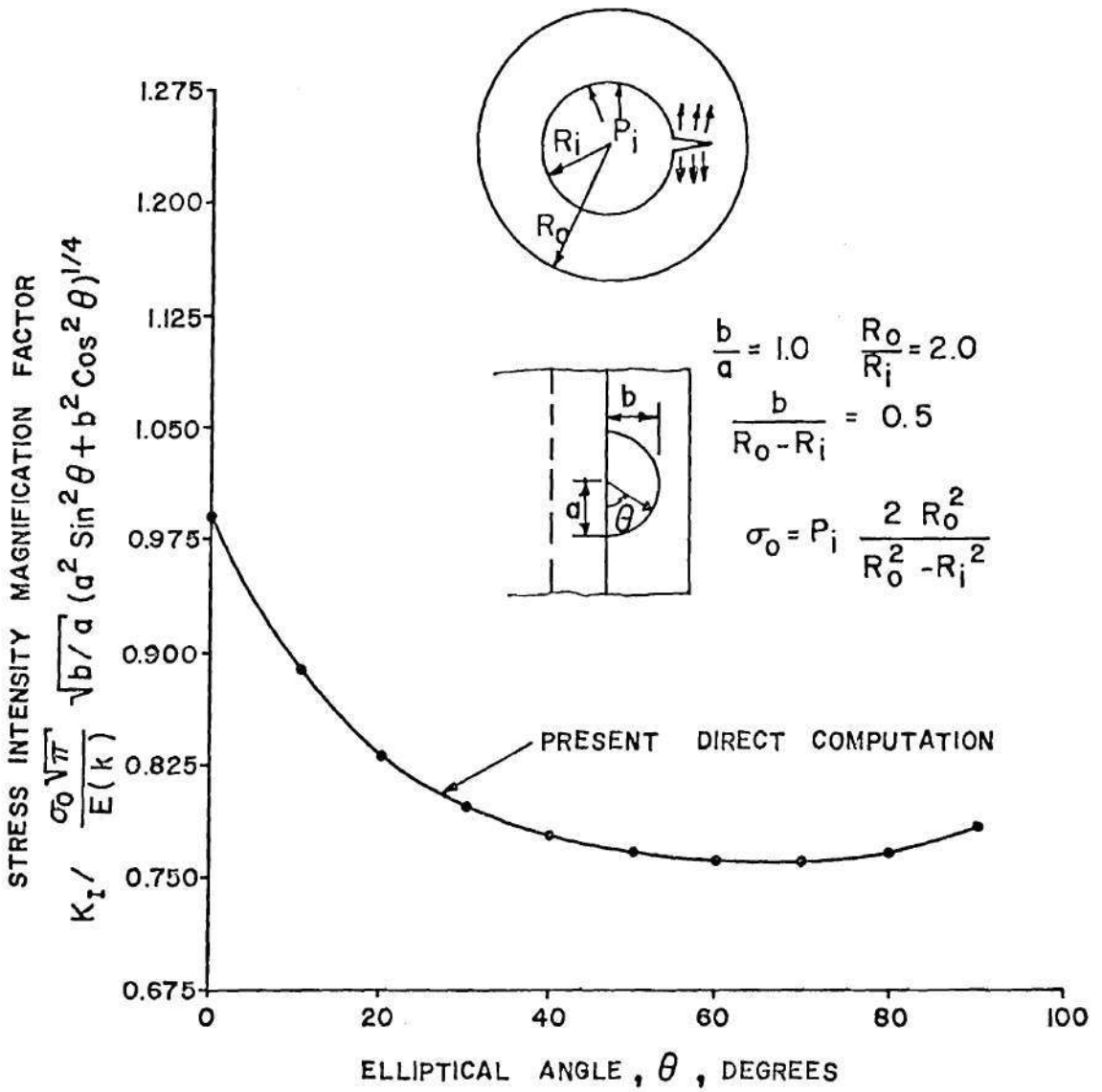

FIG.39 Stress Intensity Magnification Factor for a Pressurized Inner Semicircular Crack in a Pressurized Cylinder

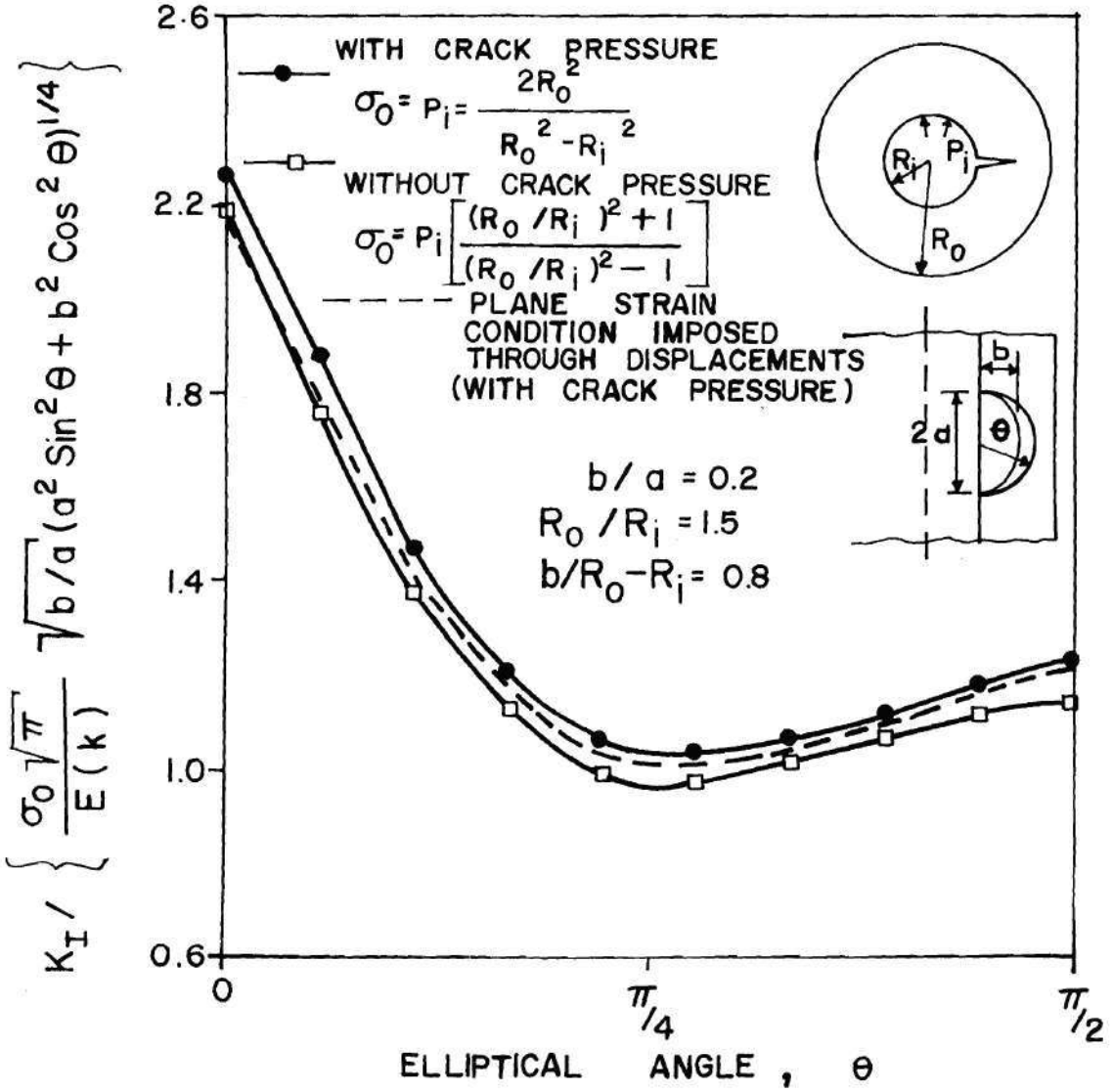

FIG. 40: Stress Intensity Magnification Factor for an Oblong Inner Semi-Elliptical Crack in a Pressurized Cylinder

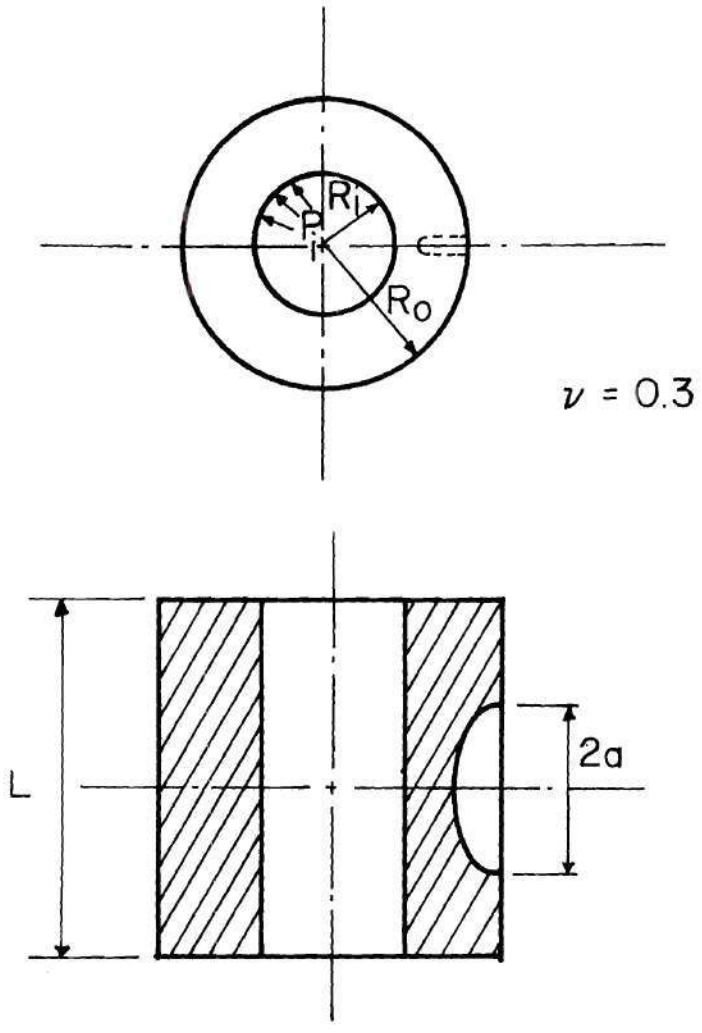

FIG. 41: Outer Semi-Elliptical Crack in a Pressurized Cylinder

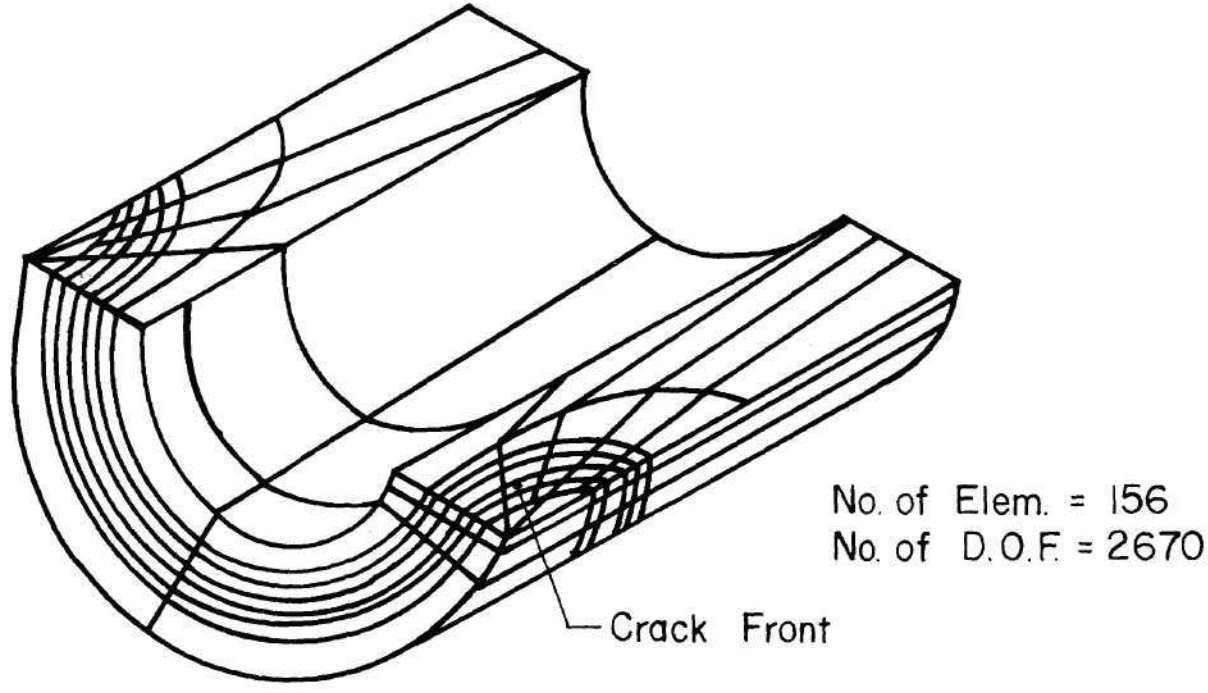

FIG. 42: Finite Element Breakdown of Quarter of the Pressurized Cylinder with Outer Crack

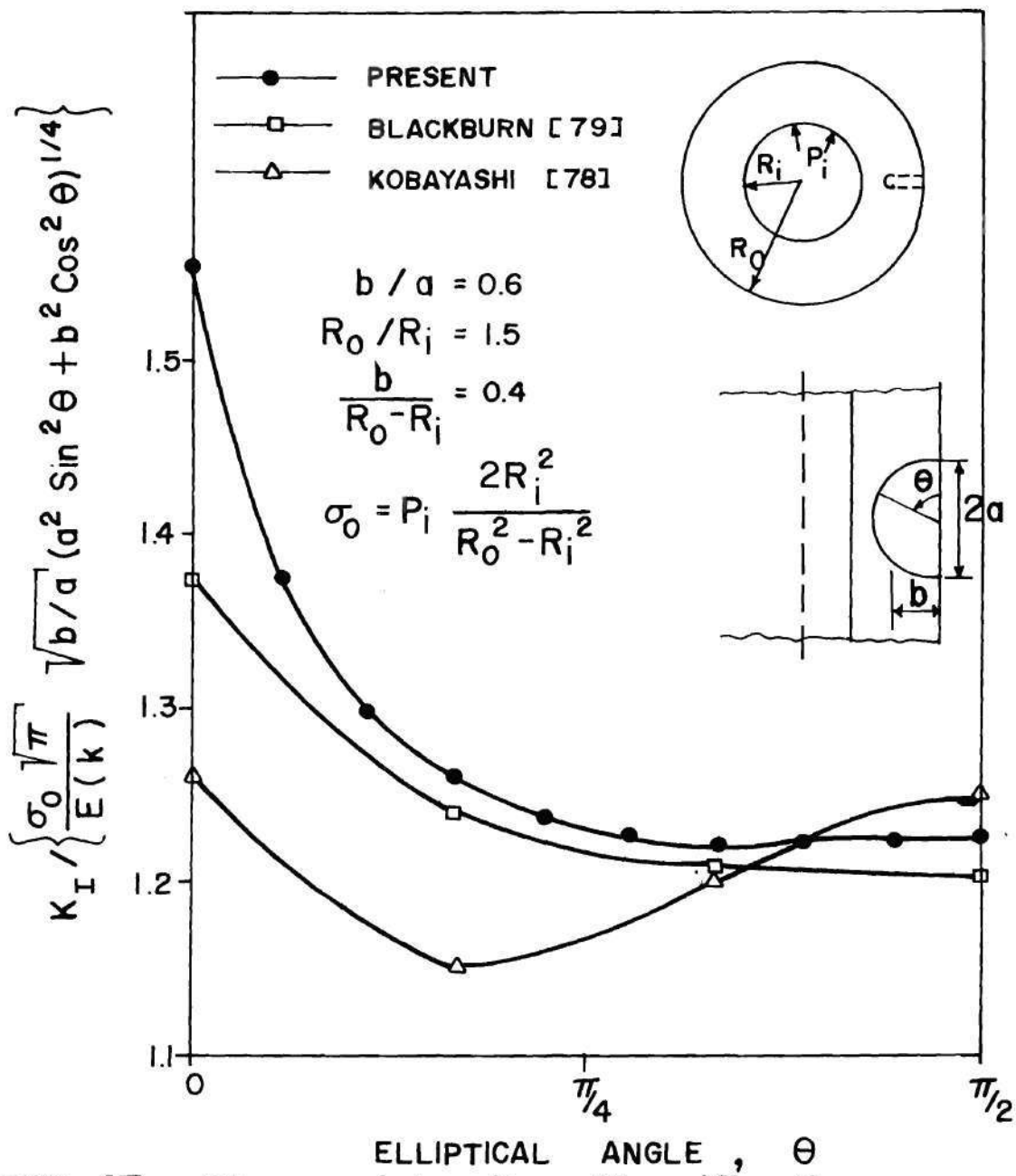

FIG. 43: Stress Intensity Magnification Factor for an Outer Semi-Elliptical Crack in a Pressurized Cylinder

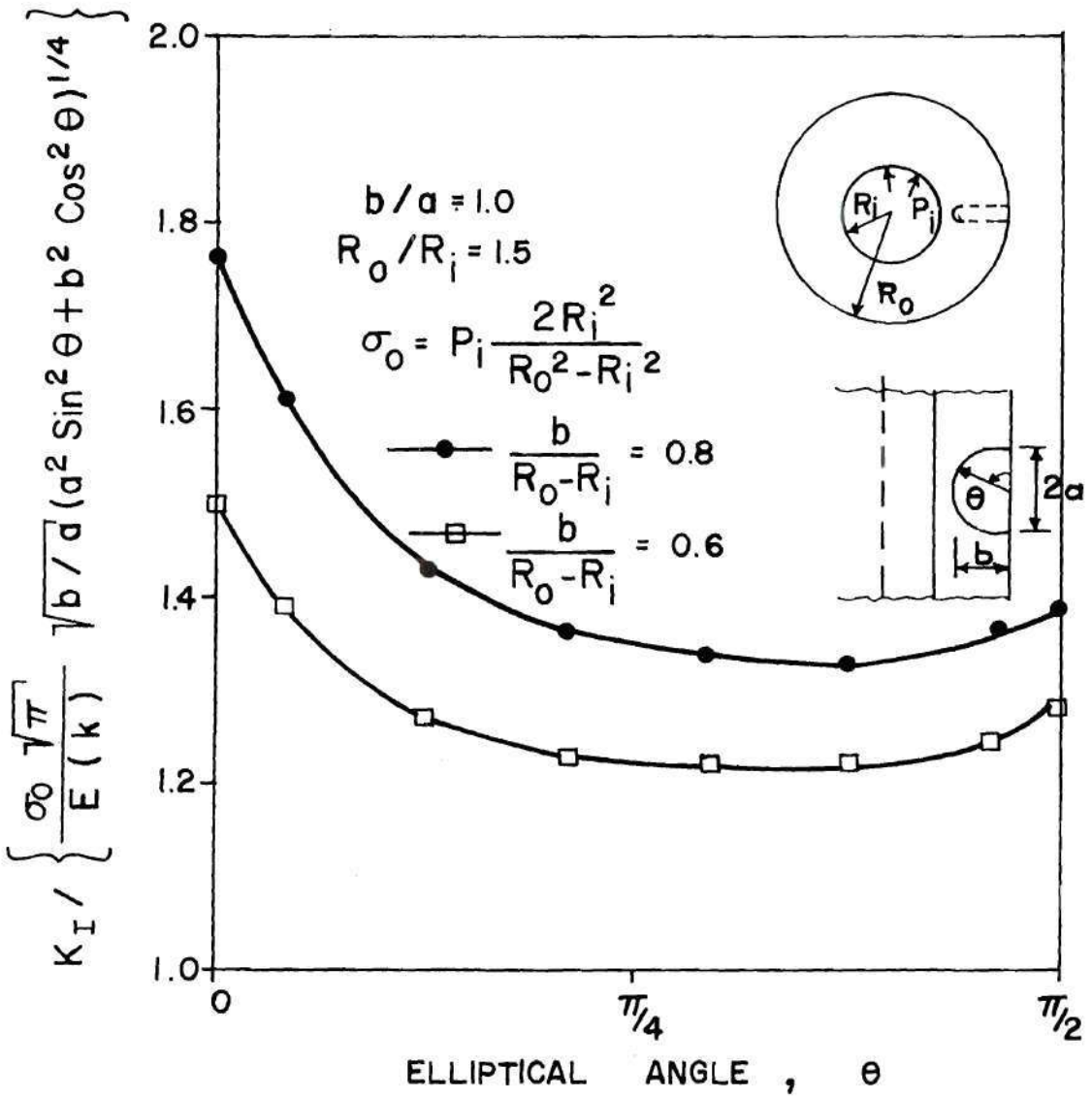

FIG. 44: Stress Intensity Magnification Factor for Outer Semi-Circular Cracks in a Pressurized Cylinder

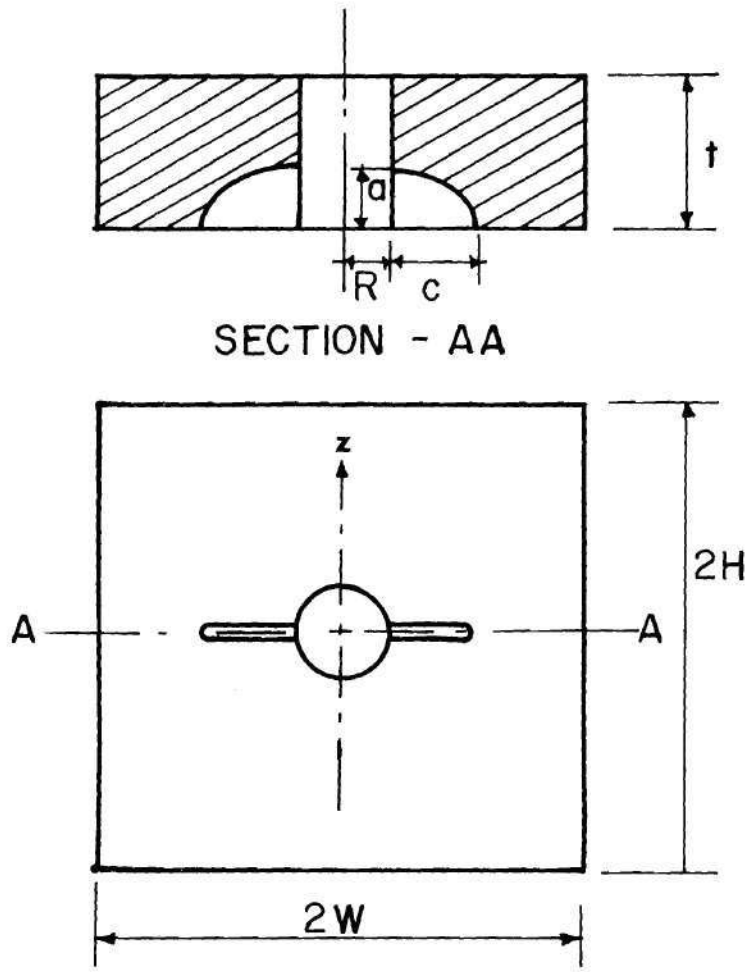

FIG. 45 : Corner Cracks Emanating from Holes in Plates

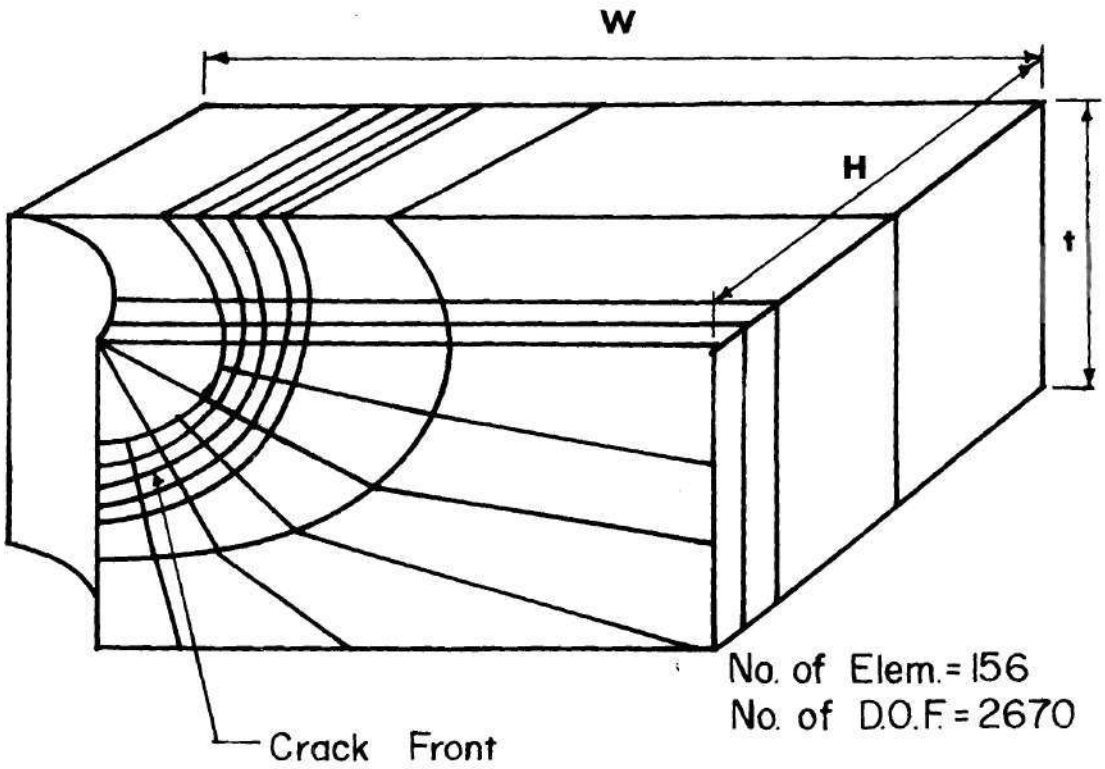

FIG. 46: Finite Element Breakdown of Quarter of the Corner Cracked Hole Problem

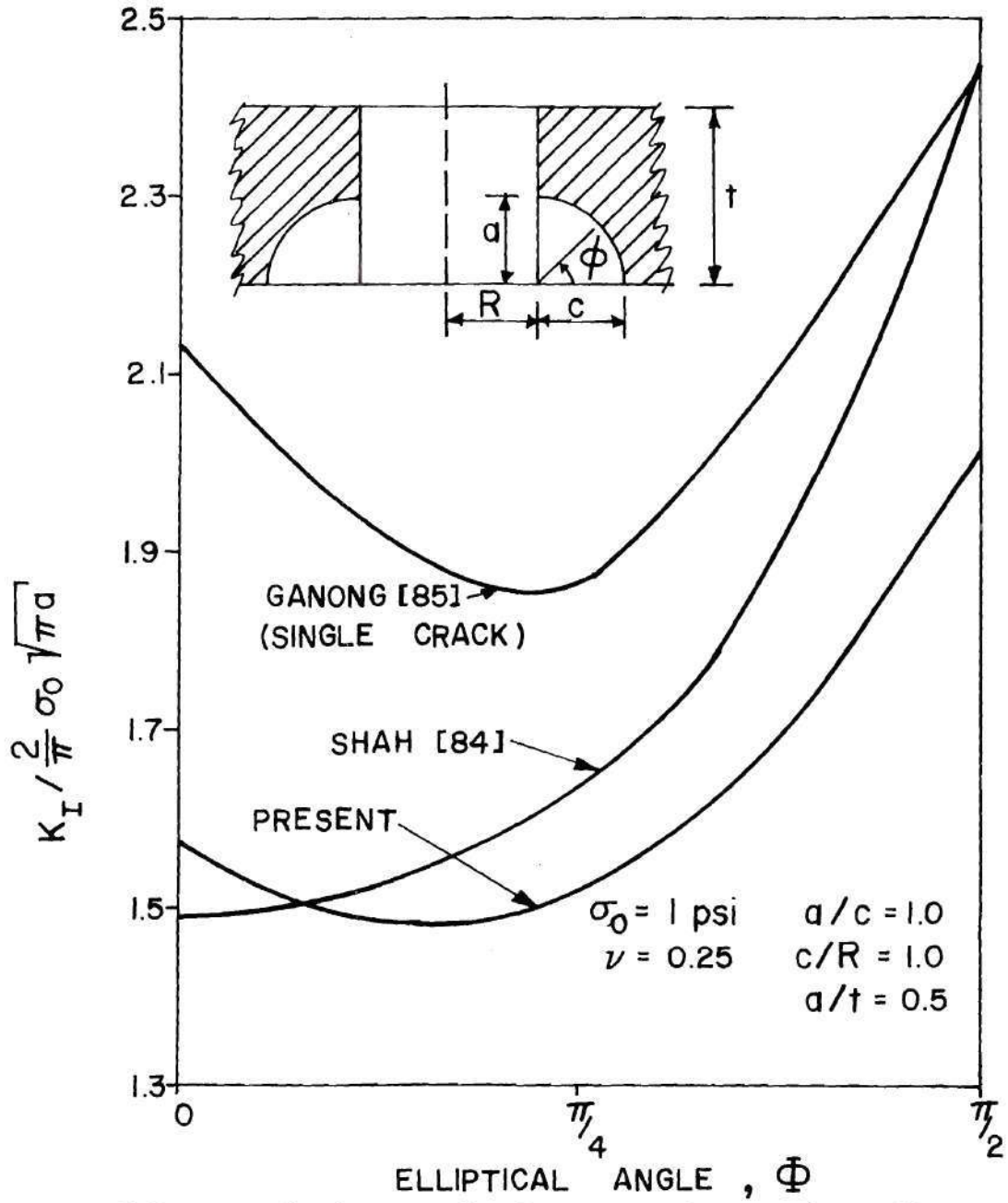

FIG. 47: Variation of Stress Intensity Factor for Corner Cracks Emanating from Hole
(a/c=1.0; c/R=1.0; a/t=0.5)

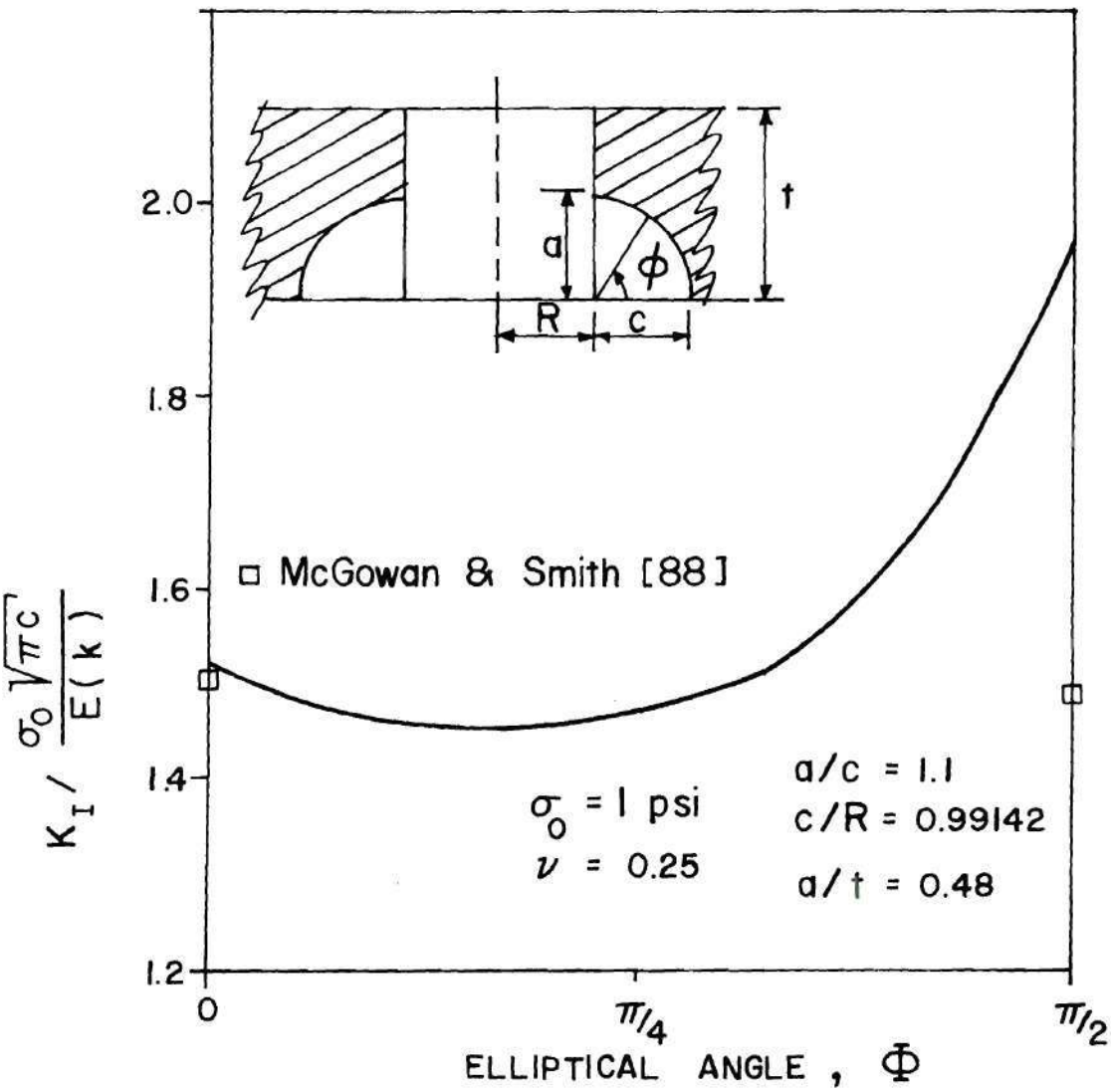

FIG. 48: Variation of Stress Intensity Factor for Corner Cracks Emanating from Hole
(a/c = 1.1 ; c/R=0.99142 ; a/t=0.48)

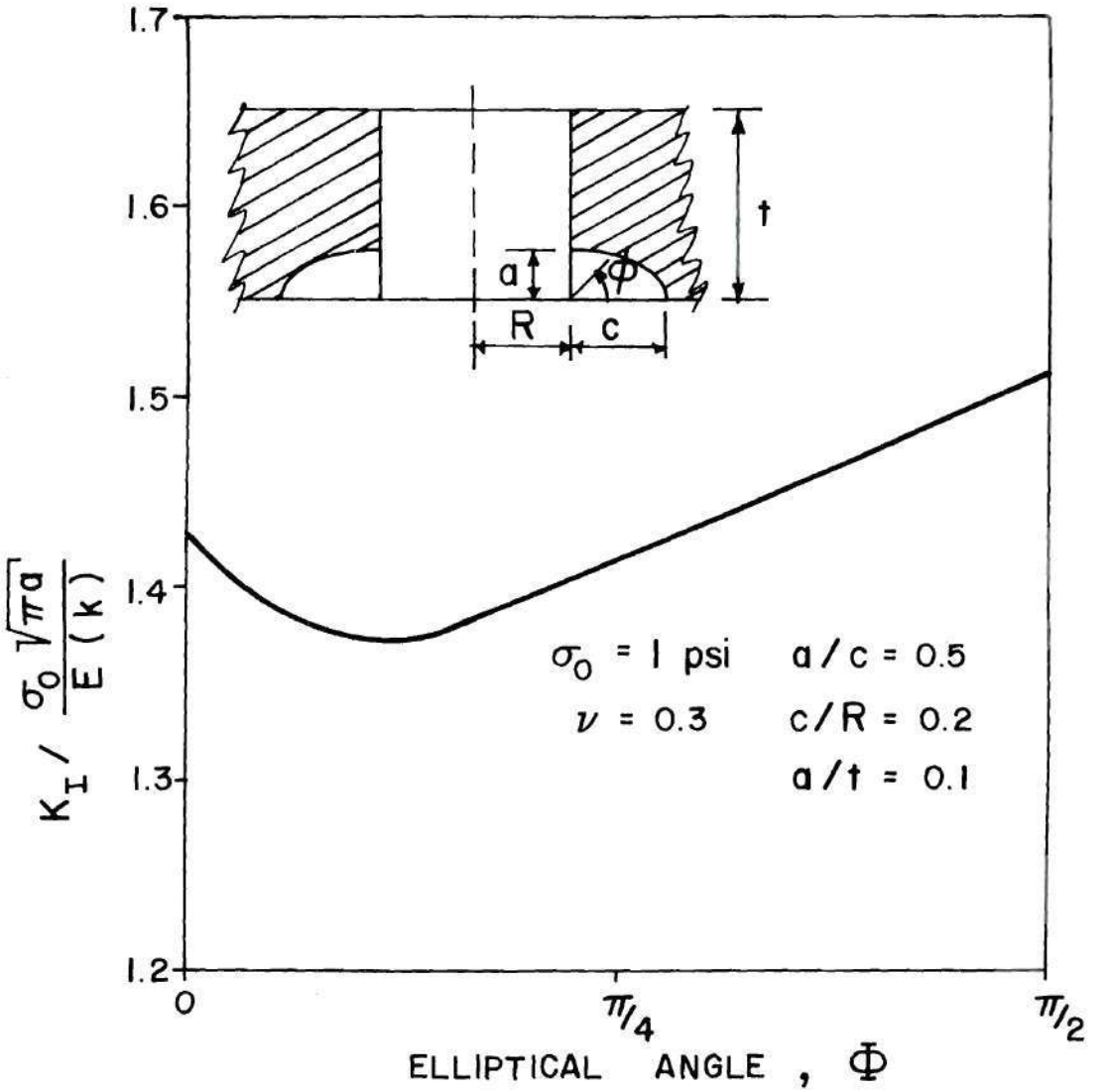

FIG. 49: Variation of Stress Intensity Factor for Corner Cracks Emanating from Hole
(a/c = 0.5; c/R = 0.2; a/t = 0.1)

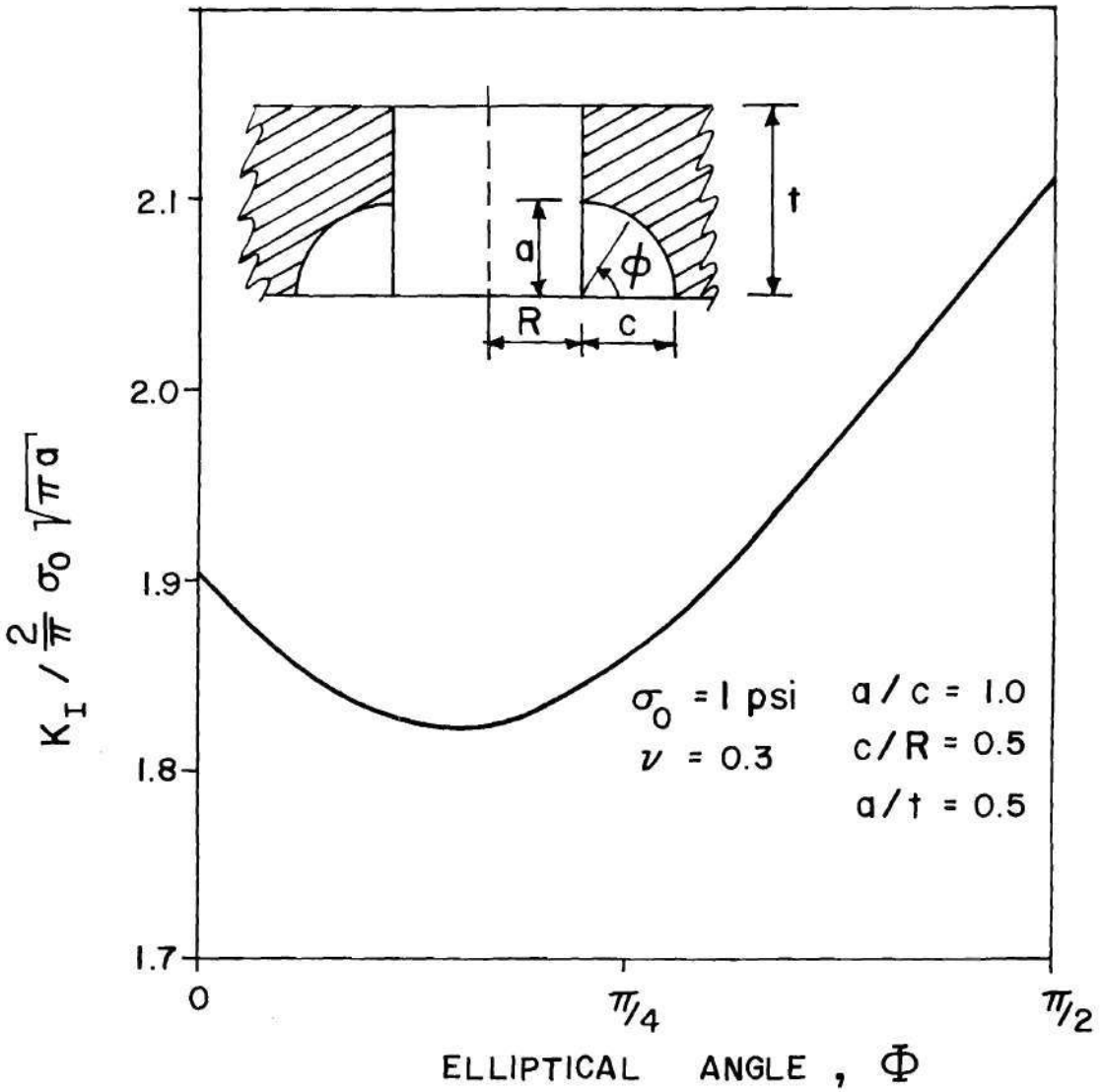

FIG. 50: Variation of Stress Intensity Factor for Corner Cracks Emanating from Hole

(a/c = 1.0; c/R = 0.5; a/t = 0.5)

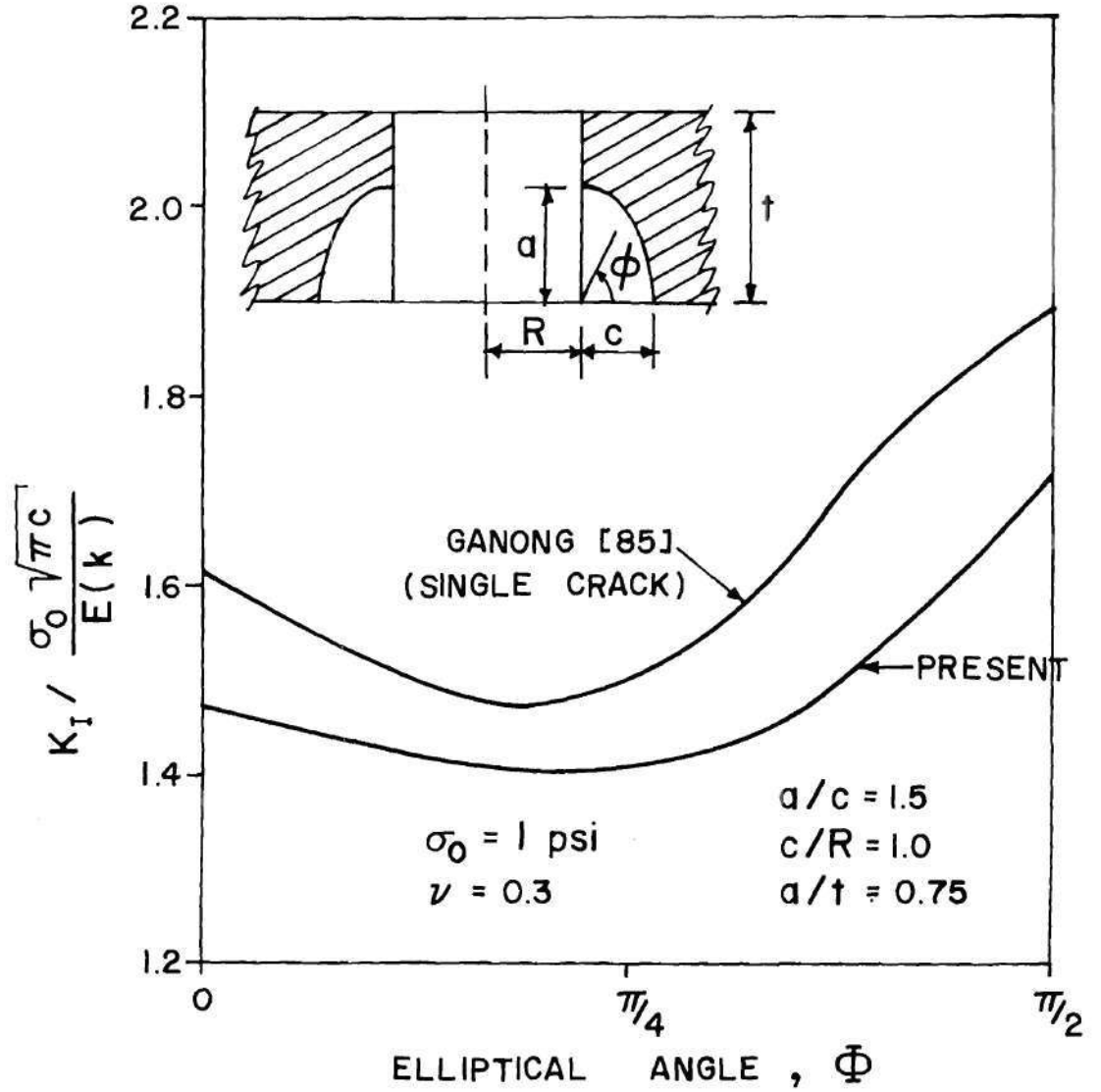

FIG. 51: Variation of Stress Intensity Factor for Corner Cracks Emanating from Hole
(a/c = 1.5 ; c/R = 1.0 ; a/t = 0.75)

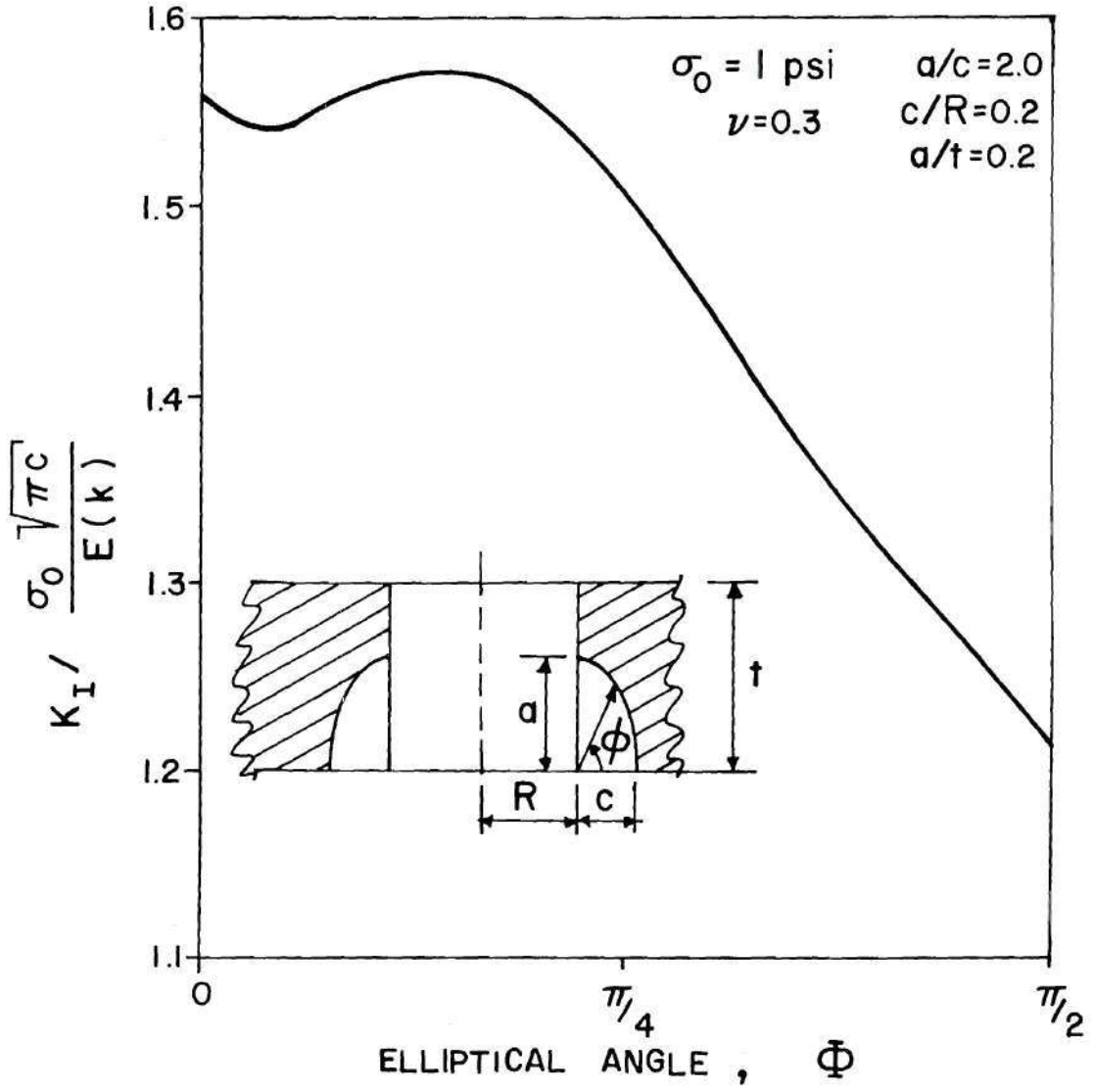

FIG. 52: Variation of Stress Intensity Factor for Corner Cracks Emanating from Hole
(a/c = 2.0 ; c/R = 0.2 ; a/t = 0.2)

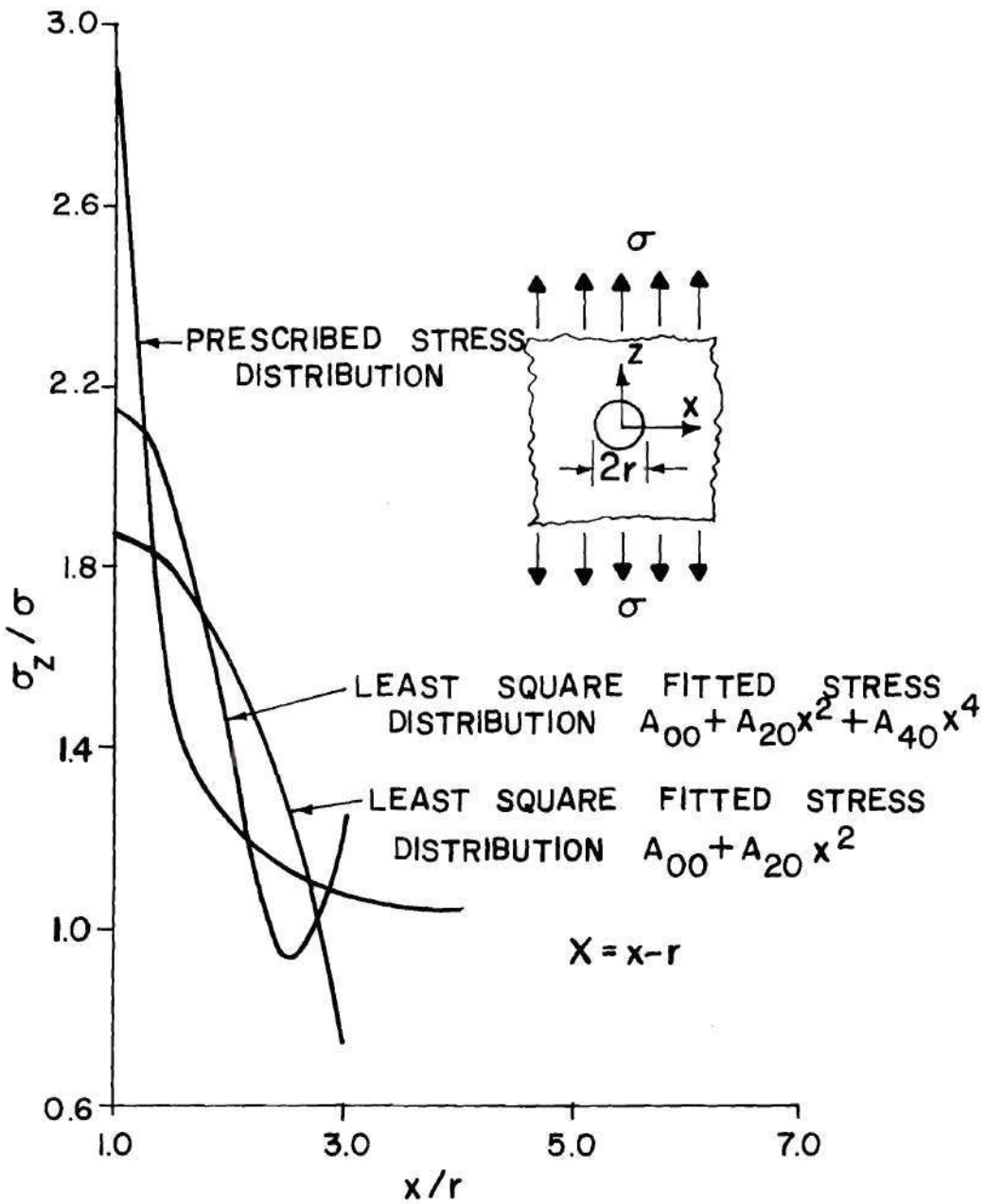

FIG. 53: Actual and Fitted Stress Distribution Near a Hole in a Plate in Tension

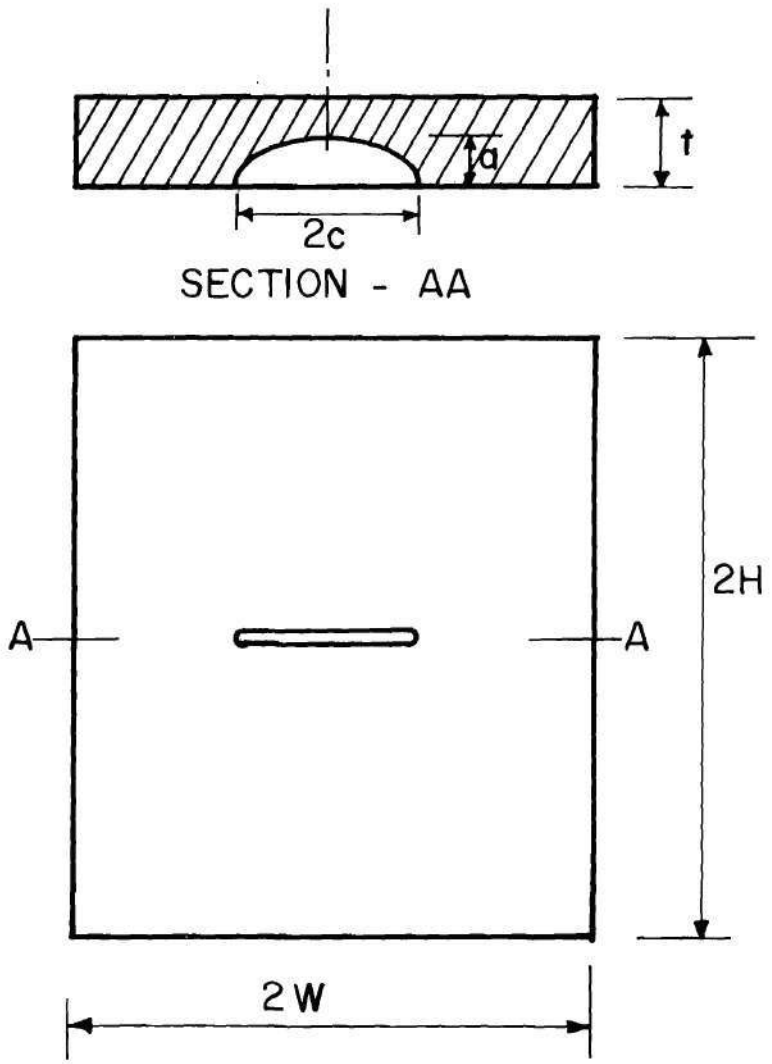

FIG. 54: Semi-Elliptical Surface Flaws in Plates in Tension and Bending

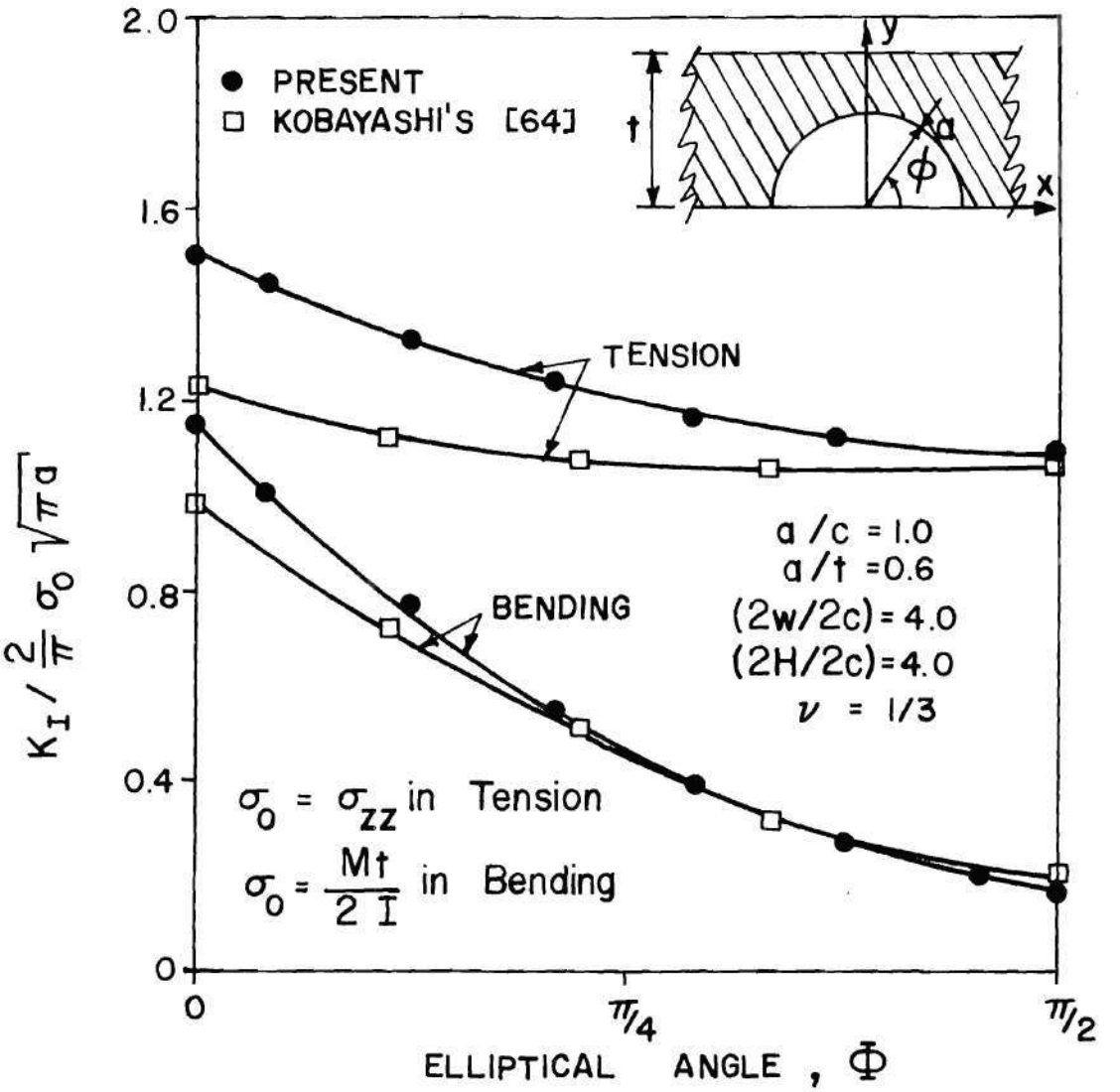

FIG. 55: Variation of Stress Intensity Factor for a Semi-Circular Surface Crack in a Plate Subjected to Tension and Bending

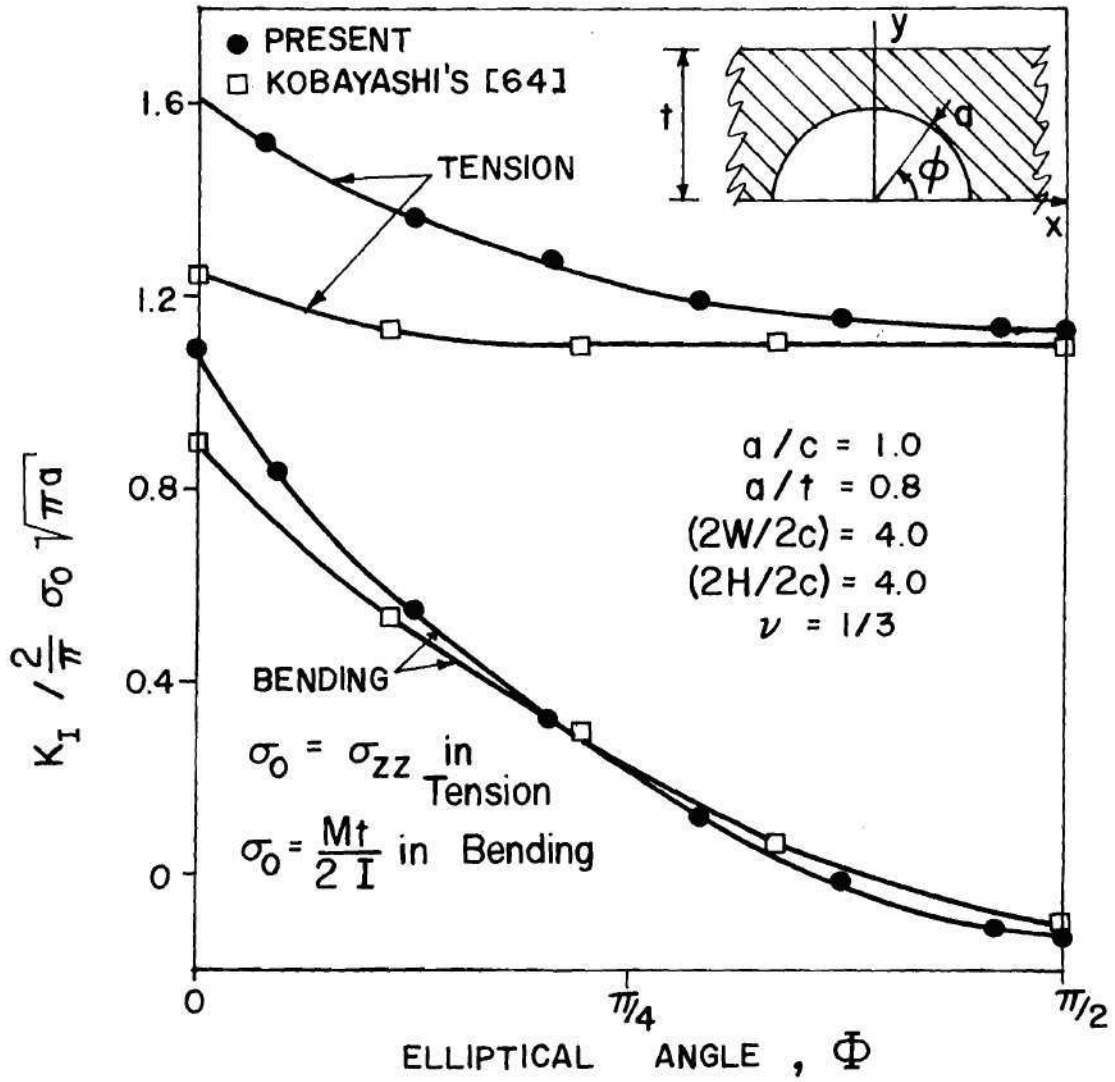

FIG. 56: Variation of Stress Intensity Factor for a Deep Semi-Circular Surface Crack in a Plate Subjected to Tension and Bending

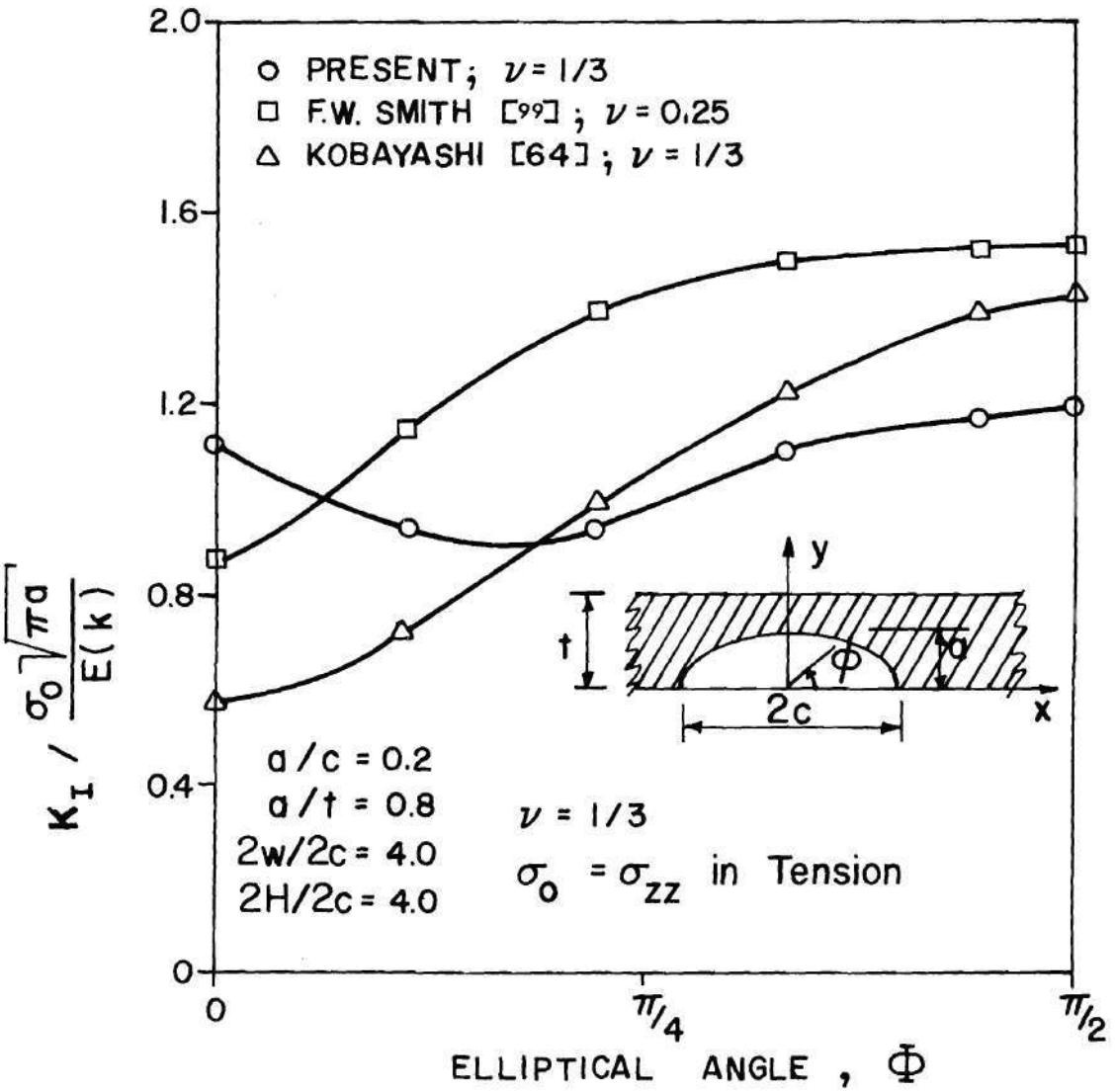

FIG. 57: Variation of Stress Intensity Factor for a Deep Semi-Elliptical Surface Crack in a Plate Subjected to Tension

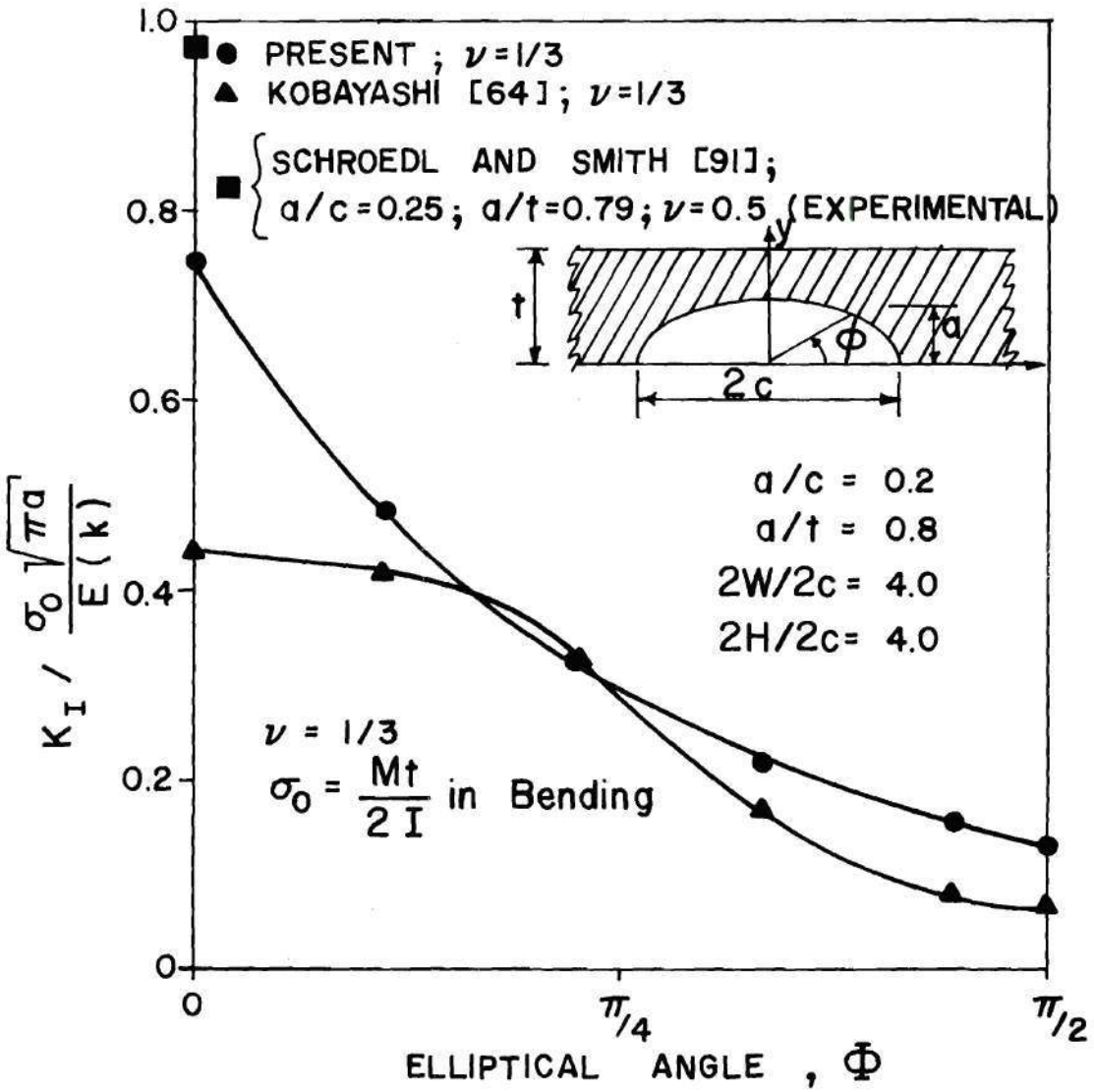

FIG. 58: Variation of Stress Intensity Factor for a Deep Semi-Elliptical Surface Crack in a Plate Subjected to Bending

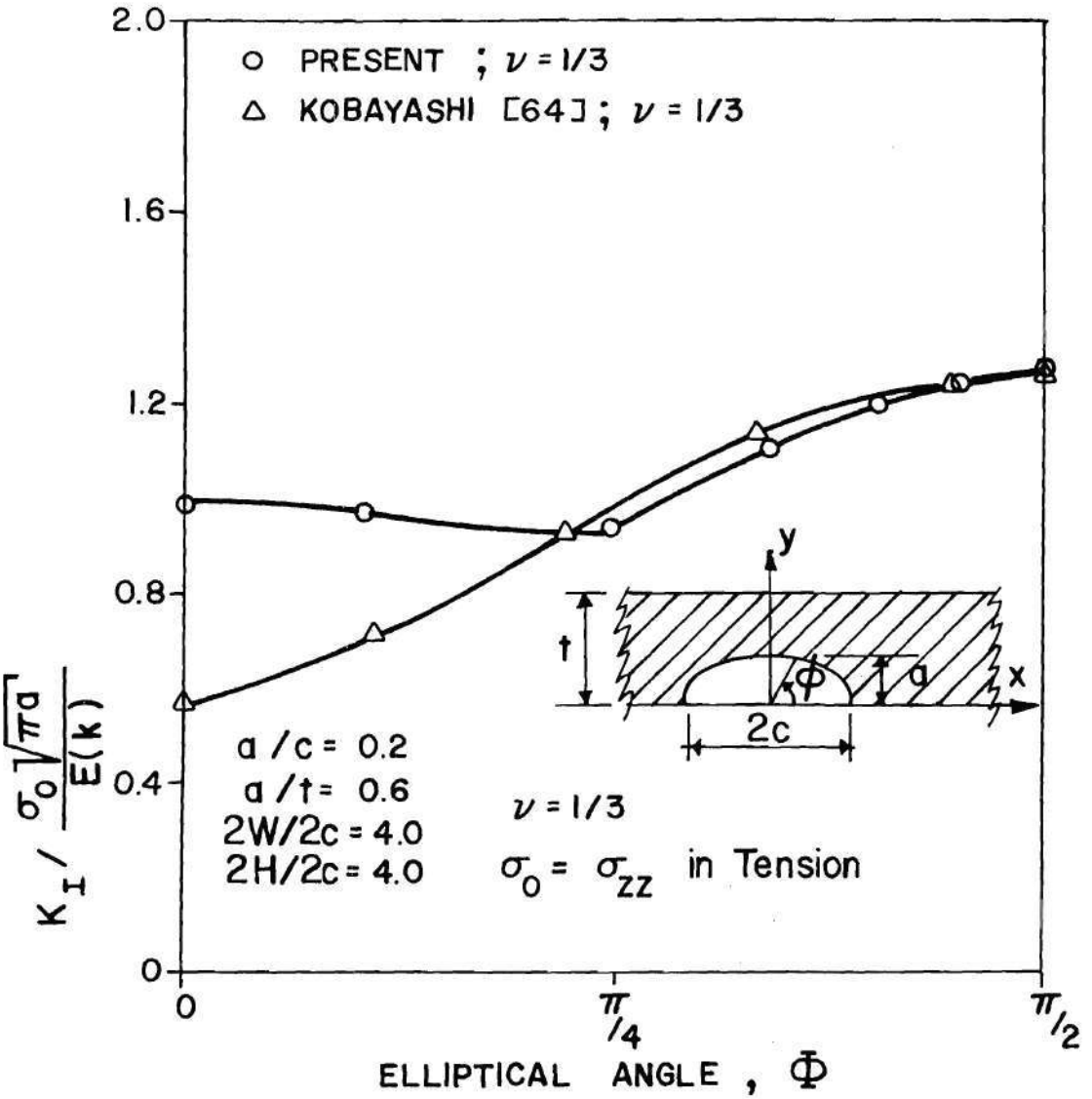

FIG. 59 : Variation of Stress Intensity Factor for a Semi-Elliptical Surface Crack in a Plate Subjected to Tension

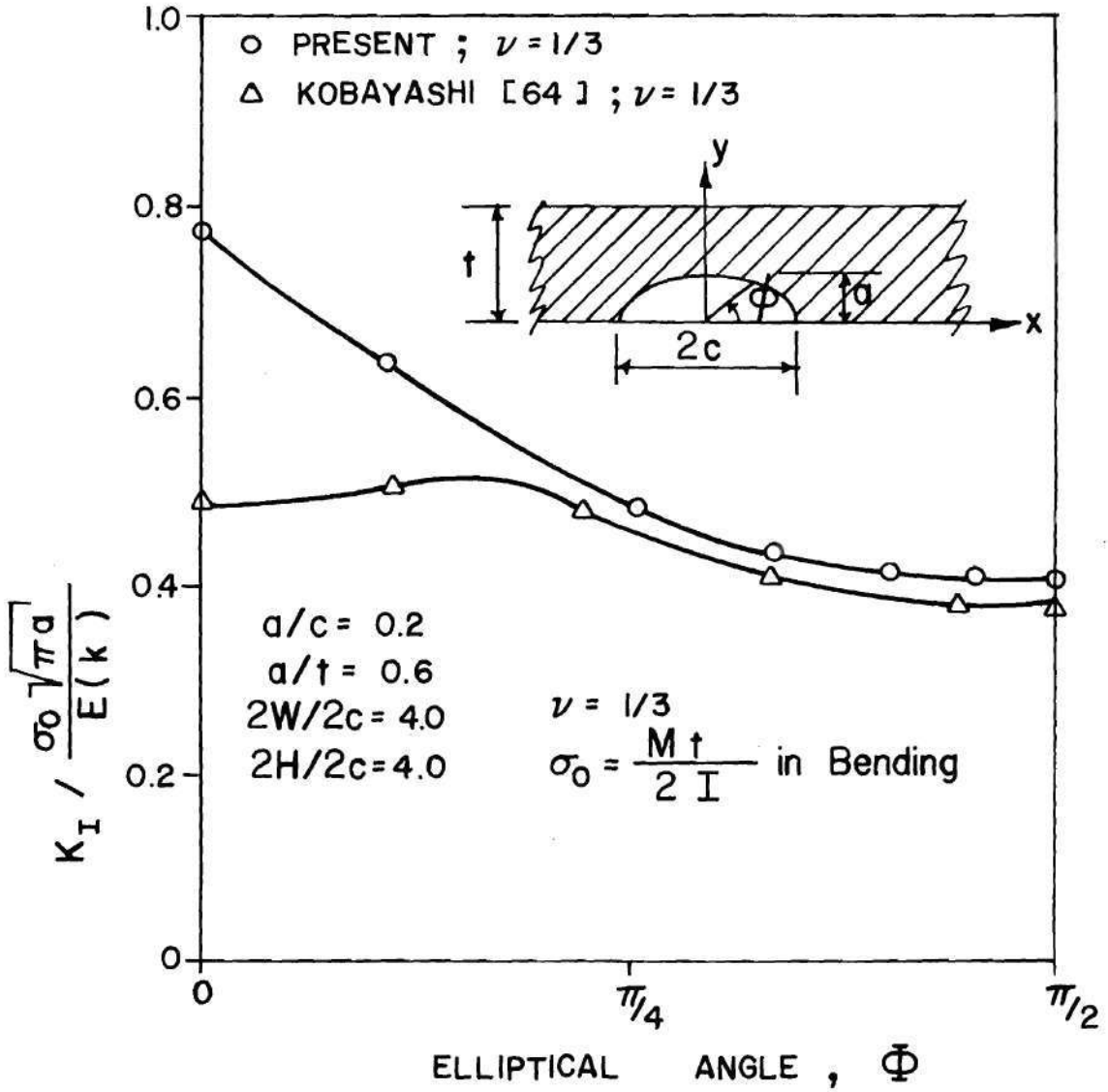

FIG. 60: Variation of Stress Intensity Factor for a Semi-Elliptical Surface Crack in a Plate Subjected to Bending

BIBLIOGRAPHY

1. Griffith, A. A., "Theory of Rupture", Proceedings of the First International Congress for Applied Mechanics, Delft, 1924, pp. 55-63.

2. Griffith, A. A., "The Phenomena of Rupture and Flows in Solids", Phil. Trans. Roy. Soc., London, Ser. A221, 1920, pp. 163-198.

3. Irwin, G. R., "Analysis of Stresses and Strains Near the End of a Crack Traversing a Plate", J. Appl. Mech., 24, 1957, pp. 361-364.

4. Rice, J. R., "Mathematical Analysis in Mechanics of Fracture", Fracture, II, edited by H. Liebowitz, Academic Press, 1968, pp. 192-308.

5. Sneddon, I. N., Proc. Roy. Soc. London, Series A187, 1946, p. 229.

6. Sneddon, I. N., Fourier Transforms, McGraw-Hill, New York

7. Williams, M. L., "On the Stress Distribution at the Base of a Stationary Crack", J. Appl. Mech., 1957, p. 24 - 109.

8. Kassir, M. K., and G. C. Sih, "Three-Diemnsional Stress Distribution Around Crack Under Arbitrary Loading", J. Appl. Mech., 33, 1966, pp. 601-611.

9. Sih, G. C., and H. Liebowitz, "Mathematical Theories of Brittle Fracture", Fracture, II, ed. by H. Liebowitz, Academic Press, 1968, pp. 67-190.

10. Irwin, G. R., "Fracture", Encyclopedia of Physics, VI, Springer, Heidelberg, 1958, pp. 551-590.

11. Irwin, G. R., "Structural Mechanics", Proc. of the 1st Sympos. on Naval Struc. Mech., Pergamon Press, New York, 1958, pp/ 557-591.

12. Eshelby, J. D., "The Continuum Theory of Lattice Defects", Solid State Physics (Ed. by F. Seitz and D. Turnbull), 3, Academic Press, New York, 1956, pp. 79-144.

13. Sih, G. C., Mechanics of Analysis and Solution of Crack Problems, I, Ed. by G. C. Sih, Noordhoff International Publ., Leydon, 1973, pp. XXI-XLV.

14. Burdekin, F. M., and D. E. W. Stone, "The Crack Opening Displacement Approach to Fracture Mechanics in Yielding Materials", J. of Strain Analysis, 1, No. 2, 1966, pp. 145-153.

15. Tada, H., P. C. Paris, and G. R. Irwin, The Stress Analysis of Cracks Handbook, Del Research Corporation, Hellertown, Pennsylvania, 1972.

16. Sih, G. C., Handbook of Stress-Intensity Factors, Lehigh University, 1973.

17. Gallagher, R. H., "Survey and Evaluation of the Finite Element Method in Fracture Mechanics Analysis", Proc. of First Intl. Conf. on Struc. Mech. in Reactor Tech., 6, Berlin, Part I, 1971, pp. 637-653.

18. Rowe, G. H., "Matrix Displacement Methods in Fracture Mechanics Analysis of Reactor Vessels", Nuclear Eng. and Design, 20, 1972, pp. 251-263.

19. Hilton, P. D., and G. C., Sih, "Application of Finite Element Method to the Calculation of Stress Intensity Factors", Methods of Analysis and Solutions of Crack Problems, ed. by G. C. Sih, Walters-Noordhoff, Groninger, The Netherlands, 1972, pp. 426-483.

20. Rice, J. R., and D. M. Tracey, "Computational Fracture Mechanics", Numerical and Computer Methods in Structural Mechanics, ed. by S. Fenves, et al., Academic Press, 1973, 585-623.

21. Oglesby, J. J., and O. Lomackey, "An Evaluation of Finite Element Methods for the Computation of Elastic Stress Intensity Factors", J. of Eng. for Industry, 95, 1973, pp. 177-183.

22. Pian, T. H. H., Crack Elements, Presented at the World Congress on Finite Element Methods in Structural Mechanics, Bournemouth, Dorset, England, 1975.

23. Benzley, S. E., and D. M. Parks, "Fracture Mechanics", Structure Mechanics Computer Programs, ed. by W. Pilkey et al., University of Maryland, Charlottesville, Maryland, 1974, pp. 81-102.

24. Christensen, R. H., and P. H. Denke, "Crack Strength and Crack Propagation Characteristics of High Strength Metals", Aero. Systems Div. Tech. Report 61-207, May 1961.

25. Denke, P. H., "Digital Analysis of Non-linear Structures by the Force Method", Matrix Methods of Structural Analysis, ed. by B. Fraeijs de Veubeke, Pergamon Press, 1964, pp. 317-342.

26. Watwood, V. B., "The Finite Element Method for Prediction of Crack Behavior", Nuclear Eng. and Design, 11, 1969. pp. 323-332.

27. Ando, Y., G. Yagawa, and K. Okabayashi, "The Application of the Finite Element Method to the Analysis of Fracture of Cylindrical Shells", Second Intl. Conf. on Structural Mechanics in Reactor Technology, Berlin, 3, Part G, paper G5/4, 1973.

28. Kobayashi, A. S., O. E. Maiden, B. J. Simon, and S. Iida, "Application of the Method of Finite Element Analysis to Two-Dimensional Problems in Fracture Mechanics", ONR Contract Nr 477 (39), NR 064-478, University of Washington, TR No. 5, 1968.

29. Chan, S. K., I. S. Tuba, and W. K. Wilson, "On the Finite Element Method in Linear Fracture Mechanics", Eng. Frac. Mech., 2, 1970, pp. 1-17.

30. Henshell, R. D., and K. G. Shaw, "Crack Tip Finite Elements are Unnecessary", University of Nottingham Report, 1973.

31. Miyata, H., S. Shida, and S. Kusumota, "A Simple Method of Evaluation of Stress Intensity Factor Using the Finite Element Method", Paper presented at the Symposium on Mechanical Behavior of Materials, Kyoto, August 21-24, 1974.

32. Dixon, J. R., and L. P. Pook, "Stress Intensity Factors Calculated Generally by the Finite Element Technique", Nature, 224, 1969, pp. 166-167.

33. Mowbray, D. F., "A Note on the Finite Element Method in Linear Fracture Mechanics", Eng. Frac. Mech., 2, 1970, pp. 173-176.

34. Anderson, G. P., V. L. Ruggles, and G. S. Stibor, "Use of Finite Element Computer Programs in Fracture Mechanics", Intl. J. of Fracture Mech., 7, 1971, pp. 63-76.

35. Parks, D. H., "A Stiffness Derivative Finite Element Technique for Determination of Elastic Crack Tip Stress Intensity Factors", Brown University Eng. Div. Tech. Rept. NASA NGL 40-002-080/13, May 1973.

36. Hellen, T. K., "On the Method of Virtual Crack Extension", Int. J. of Num. Meth. in Eng., 9, 1975, pp. 181-207.

37. Deverall, L., and G. H. Lindsay, "A Comparison of Numerical Methods for Determining Stress Intensity Factors", United Tech. Corp. Paper, 1969.

38. Tong, P. and T. H. H. Pian, "On the Convergence of the Finite Element Method for Problems with Singularity", Int. J. Solids Structures, 9, 1972, pp. 313-321.

39. Tracey, D. M., "Finite Elements for Determination of Crack Tip Elastic Stress Intensity Factors", Eng. Fracture Mech., 3, 1971, pp. 255-265.

40. Hilton, P., and J. W. Hutchinson, "Plastic Intensity Factors for Cracked Plates", J. of Eng. Frac. Mech., 3, 1971, pp. 435-451.

41. Walsh, P. F., "The Computation of Stress Intensity Factors by a Special Finite Element Technique", Int. J. of Solids and Structures, 7, 1971, pp. 1333-1342.

42. Atluri, S. N., A. S. Kobayashi, and M. Nakagaki, "Application of an Assumed Displacement Hybrid Finite Element Procedure to Two-Dimensional Problems in Fracture Mechanics", AIAA Paper No. 74-390, Presented at AIAA/ASME/SAE, 15th Structures, Structural Dynamics and Materials Conference, Las Vegas, Nevada, April 17-19, 1974.

43. Atluri, S. N., A. S. Kobayashi and M. Nakagaki, "An Assumed Displacement Hybrid Finite Element Method for Fracture Mechanics", Int. J. of Fracture, 11, 1975, pp. 257-271.

44. Pian, T. H. H., P. Tong, and C. H. Luk, "Elastic Crack Analysis by a Finite Element Method", Proc. of the 3rd Intl. Conf. on Matrix Methods in Structural Mechanics, Wright-Patterson AFB, October 19-21, 1971.

45. Wilson, W. K., "Crack Tip Finite Elements for Plane Elasticity", Westinghouse Research Lab., Tech. Rpt, 71-1E7-FMPWR-P2, 1971.

46. Byskov, I., "The Calculation of Stress Intensity Factors Using Finite Element Method with Cracked Elements", Int. J. of Frac. Mech., 6, 1970, pp. 159-167.

47. Rao, A. K., A. V. Krishnamurthy and I. S. Raju, "Special Finite Elements for the Analysis of Stress Concentrations and Singularities", Proc. First Intl. Conf. on Struc. Mech. in Reactor Tech., Berlin, 6, part M, 1971, pp. 391-408.

48. Aberson, J. A., and J. M. Anderson, "Cracked Finite Elements Proposed for NASTRAN", Third NASTRAN User's Colloquium, NASA TMX-2893, 1973, 531-550.

49. Tong, P., and T. H. H. Pian, "Application of Finite Element Method to Mixed-Mode Fracture", Presented at Soc. of Eng. Sci. 10th Anniversity Meeting. November 5-7, North Carolina State University, Raleigh, North Carolina, 1973.

50. Yamamota, Y., H. Tokuda, and Y. Sumi, "Finite Element Treatment of Singularities of Boundary Value Problems and its Application

to Analysis of Stress Intensity Factors", Theory and Practice in Finite Element Structural Analysis, ed. by Y. Yamada and R. H. Gallagher, University of Tokyo Press, 1973, pp. 75-90.

51. Yamamota, Y., and Y. Sumi, "Stress Intensity Factors of a Twisted Round Bar with a Circumferential Crack", Int. J. of Fracture, 10, 1974, pp. 269-270.

52. Yagawa, G., T. Nishioka, Y. Ando, and N. Ogura, "The Finite Element Calculation of Stress Intensity Factors Using Superposition", Presented at the 2nd ASME Pressure Vessel and Piping Conference, San Francisco, California, June 23-27, 1975.

53. Wilson, W. K., and D. G. Thompson, "On the Finite Element Method for Calculating Stress Intensity Factors for Cracked Plates in Bending", Eng. Fracture Mech. 3, 1971, pp. 97-102.

54. Miyamoto, H., "Application of Finite Element Method to Fracture Mechanics", Proc. of First Int. Conf. on Structural Mechanics in Reactor Tech. Berlin, 6, Part L, 1971, pp. 535-566.

55. Tracey, D. M., "3-D Elastic Singularity Element for Evaluation of K Along an Arbitrary Crack Front", Int. J. of Fracture, 9, 1973, pp. 340-343.

56. Tracey, D. M., "Finite Elements for Three-Dimensional Elastic Crack Analysis", Nuc. Eng. and Design, 26, 1974, pp. 282-290.

57. Bergan, P. G., and B. Aamodt, "Finite Element Analysis of Crack Propagation in Three-Dimensional Solids Under Cyclic Loading", Nuc. Eng. and Design, 29, 1974, pp. 180-188.

58. Aamodt, B., "Application of the Finite Element Method to Problems in Linear and Nonlinear Fracture Mechanics", Division of Struc. Mech. Rpt. No. 74-1, University of Trondheim, Norway, 1974.

59. Sih, G. C., P. D. Hilton, R. J. Hartranft, and B. V. Kiefer, "Three-Dimensional Stress Analysis of a Finite Slab Containing a Transverse Central Crack", Tech. Report No. N0014-67-A-0370-0012, Office of Naval Research, Arlington, Virginia, 1975.

60. Cruse, T. A., "Boundary-Integral Equation Method for Three-Dimensional Elastic Fracture Mechanics Analysis", Interim Report Air Force Office of Scientific Research, Arlington, Virginia, 1975.

61. Miyata, H., and S. Kusumoto, "A Method of Evaluation of Three-Dimensional Stress Intensity Factor Using the Finite Element Method", Paper presented at the JSME-ASME Joint Western Conference on Applied Mechanics, Honolulu, Hawaii, March 24-27, 1975.

62. Smith, F. W., A. F. Emery, and A. S. Kobayashi, "Stress Intensity Factors for Semi-circular Cracks", Trans. of ASME, J. of Appl. Mech., 34, 1967, pp. 953-959.

63. Kobayashi, A. S., N. Polvanich, A. F. Emery, and W. J. Love, "Stress Intensity Factor of a Surface Crack in a Pressurized Cylinder", Computational Fracture Mechanics, (edited by E. F. Rybicki and S. E. Benzley), ASME, 1975, pp. 121-132.

64. Kobayashi, A. S., N. Polvanish, A. F. Emery, and W. J. Love, "Surface Flaws in a Plate in Bending", Proceedings of 12th Annual Meeting of Society of Engineering Science, Austin, Texas, 1975, pp. 343-352.

65. Irons, B. M., "Engineering Application of Numerical Integration in Stiffness Method", AIAA Journal, 4, No. 11, 1966, pp. 2035-2037.

66. Zienkiewitz, O. C., B. M. Irons, J. Ergatoudis, S. Ahmad, and F. C. Scott, "Iso-Parametric and Associated Element Families for Two-and-Three-Dimensional Analysis", Finite Element Methods in Stress Analysis, ed. by I. Holand and K. Bell, TAPIR, 1969.

67. Nakagaki, M., "Linear Elastic Fracture Analysis by an Assumed Displacement Hybrid Finite Element Method", Ph.D. Thesis, Dept. of Mech. Eng., University of Washington, Seattle, 1974.

68. Sih, G. C., "Three-Dimensional Stress Problem for a Cracked Plate", Int. J. of Frac. Mech., 7, 1971, pp. 37-61.

69. Bucci, R. J., P. C. Paris, J. D. Landes, and J. R. Rice, "J-Integral Estimation Procedures", Fracture Toughness, Proc. of the 1971 National Symposium on Fracture Mechanics, Part II, ASTM STP 514, 1972, pp. 40-69.

70. Smith, F. W., and M. J. Alavi, "Stress Intensity Factors for a Penny Shaped Crack in a Half Space", Engineering Fracture Mechanics, Vol. 3, 1971, pp. 241-254.

71. Shah, R. C., and A. S. Kabayashi, "Stress Intensity Factors for an Elliptical Crack Approaching the Surface of a Semi-Infinite Solid", International Journal of Fracture, 9, No. 2, 1973, pp. 133-146.

72. Hartranft, R. J., and G. C. Sih, "Alternating Methods Applied to Edge and Surface Crack Problems", Chapter 4, Methods of Analysis and Solutions of Crack Problems, (edited by G. C. Sih) Noordhoff Publishing Co., Leyden, 1973.

73. Bowie, O. L., and C. E. Freese, "Elastic Analysis for Radial Cracks in a Circular Ring", Engineering Fracture Mechanics, 4,

No. 2, 1972, pp. 315-322.

74. Clifton, R. J., E. R. Simonson, A. F. Jones, and S. J. Green, "Determination of the Critical Stress-Intensity Factor K_{I_c} from Internally Pressurized Thick-Walled Vessels", SESA paper No. 2407A, May 1975, and to be published in Experimental Mechanics.

75. Underwood, J. H., "Stress Intensity Factors for Internally Pressurized Thick-Walled Cylinder", Stress Analysis and Growth of Crack, ASTM STP 513, 1972, pp. 59-70.

76. Kobayashi, A. S., "A Simple Procedure for Estimating Stress Intensity Factor in Region of High Stress Gradient", Significance of Defects in Welded Structures (edited by T. Kanazawa and A. S. Kobayashi), University of Tokyo Press, 1974, pp. 127-143.

77. Kobayashi, A. S., A. F. Emery, N. Polvanich, and W. J. Love, "Surface Flaw in a Pressurized and Thermally Shocked Hollow Cylinder", to be published in the Int. J. of Pressure Vessels and Pipings.

78. Kobayashi, A. S., A. F. Emery, N. Polvanich, and W. J. Love, "Inner and Outer Surface Cracks in Internally Pressurized Cylinders", to be presented at the Joint Conference on Pressure Vessels and Pipings and Petroleum Mechanical Engineering, Mexico City, September 1976 and published in ASME Transactions.

79. Blackburn, W. S., and T. K. Hellen, "Calculation of Stress Intensity Factors for Elliptical and Semi-Elliptical Cracks in Blocks and Cylinders", Central Electricity Generating Board Report No. RD/B/N3103, 1974.

80. Ayers, D. J., "Three-Dimensional Elastic Analysis of Semi-Elliptical Cracks to Thermal Shock", Computational Fracture Mechanics, (edited by E. R. Rybicki and S. E. Benzley), ASME, 1975, pp. 133-144.

81. Emery, A. F., and C. M. Segedin, "The Evaluation of Stress Intensity Factor for Cracks Subjected to Tension, Torsion and Flexion by an Efficient Numerical Technique", Journal of Basic Engineering, Trans. of ASME, 94, Series D, No. 2, 1972, pp. 387-393.

82. Liu, A. F., "Stress Intensity Factor for a Comer Flaw", Engineering Fracture Mechanics, 4, 1972, pp. 175-179.

83. Hsu, T. M., and A. F. Liu, "Stress Intensity Factors for Truncated Elliptical Cracks", Seventh National Symposium on Fracture Mechanics, College Park, Maryland, August 1973.

84. Shah, R. C., "Stress Intensity Factors for Through and Part-Through Cracks Originating at Fastener Holes", Eighth National Symposium on Fracture Mechanics, Brown University, August 1974.

85. Ganong, G. P., "Quarter-Elliptical Cracks Emanating from Holes in Plates", Ph.D. Thesis, Colorado State University, Fort Collins, Colorado, July 1975.

86. Hall, L. R., and R. W. Finger, "Investigation of Flaw Geometry and Loading Effects on Plane Strain Fracture in Metallic Structures", Technical Report NASA-CR-72659, Boeing Company, December 1971.

87. Hall, L. R., R. C. Shah, and W. L. Engstrom, "Fracture and Fatigue Crack Growth Behavior of Surface Flaws Originating at Fastener Holes", AFFDL-TR-74-47, Air Force Flight Dynamics Laboratory, 1974.

88. McGowan, J. J., and C. W. Smith, "Stress Intensity Factors for Deep Cracks Emanating from the Corner Formed by a Hole Intersecting a Plate Surface", Technical Report VPI-E-74-1, Virginia Polytechnic Institute and State University, January 1974.

89. Folias, E. S., "On the Three-Dimensional Theory of Cracked Plates", J. Appl. Mech., 42, No. 3, Sept. 1975, pp. 663-674.

90. Benthem, J. P., and W. T. Koiter, "Discussion on the Three-Dimensional Theory of Cracked Plates", J. Appl. Mech., 43, No. 2, June 1976, pp. 374-375.

91. Schroedl, M. A., and C. W. Smith, "Local Stresses Near Deep Surface Flaws under Cylindrical Bending Fields", Progress in Flaw Growth and Fracture Toughness Testing, edited by J. G. Kaufman, ASTM STP 536, 1973, pp. 45-63.

92. Shah, R. C., and A. S. Kobayashi, "Stress Intensity Factors for an Elliptical Crack Approaching the Surface of a Beam in Bending", Stress Analysis and Crack Growth, edited by H. T. Corten and J. P. Gallagher, ASTM STP 513, 1972, pp. 3-21.

93. Miyamoto, M., and T. Miyoshi, "Analysis of Stress Intensity Factor for Surface-Flawed Tension Plate", IUTAM Symposium, Liege, 1970.

94. Parmerter, R. R., "Stress Intensity Factors for Three-Dimensional Problems", AFRPL-TR-76-30, 1976.

95. Rice, J. R., and G. F. Rosengren, "Plane Strain Deformation Near a Crack Tip in a Power Law Hardening Material", J. Mech. and Physics of Solids, 16, 1968, pp. 1-12.

96. Hutchinson, J. W., "Plastic Stress and Strain Fields at a Crack Tip", J. Mech. and Physics of Solids, 16, 1968, pp. 337-347.

97. Zienkiewitz, O. C., The Finite Element Method in Engineering Science, McGraw-Hill, London, 1971.

98. Stroud, A. H., Approximate Calculation of Multiple Integrals, McGraw-Hill, New York, 1971.

99. Smith, F. W., and D. R. Sorensen, "Mixed Mode Stress Intensity Factors for Semi-Elliptical Surface Cracks", NASA-CR-134684, 1974.

100. Mondkar, D. P., and G. H. Powell, "Large Capacity Equation Solver for Structural Analysis", Computers and Structures, 4, 1974, pp. 669-728.

101. Love, A. E. H., A Treatise on Mathematical Theory of Elasticity, Dover Publications, 1944, pp. 88.

102. Gurtin, M. E., "The Linear Theory of Elasticity", Encyclopedia of Physics, Springer-Verlag, New York, 2, 1972.

VITA

K. Kathiresan was born at Bhavani in the State of Madras, India on January 15, 1949. He received his Bachelor of Engineering (Honours) degree in Mechanical Engineering from P.S.G. College of Technology, Coimbatore affiliated to University of Madras in June, 1971. He joined Indian Institute of Science, Bangalore, India, in August, 1971 as a graduate student and obtained the degree of Master of Engineering in Aeronautical Engineering in August 1973. He was enrolled as a doctoral student in the School of Engineering Science and Mechanics of Georgia Institute of Technology, Atlanta, Georgia since September 1973.